

THESE

En vue de l'obtention du : **DOCTORAT**

Structure de Recherche : **LaMCScI**

Discipline : **Physique**

Spécialité : **Physique informatique**

Soutenue le : **22 / 07 / 2020**

Présentée par:

Hicham BOUDA

**Electronic Structure and Computational Methods Applied to Some
Nanomaterial Compounds by Means of Monte Carlo Simulation and
Ab Initio Calculations**

JURY

LARBI LAANAB	<i>PES, Université Mohamed V-RABAT Faculté des Sciences</i>	<i>Président</i>
LAHOUCINE BAHMAD	<i>PES, Université Mohamed V-Rabat Faculté des Sciences</i>	<i>Directeur de Thèse</i>
RACHID MASROUR	<i>PH, Université Cadi Ayyad-Marrakech Ecole Nationale des Sciences appliquées-Safi</i>	<i>Co-directeur de Thèse</i>
ABDELILAH BENYOUSSEF	<i>PES, Académie Hassan II Des Sciences Et Techniques-RABAT</i>	<i>Rapporteur/Examineur</i>
HAMID EZ-ZAHRAOUI	<i>PES, Université Mohamed V-Rabat Faculté des sciences, Rabat</i>	<i>Rapporteur/Examineur</i>
MOURAD BOUGHRARA	<i>PH, Université Moulay Ismail- Meknès Faculté des sciences,</i>	<i>Rapporteur/Examineur</i>
ABDALAH EL KENZ	<i>PES, Université Mohamed V-Rabat Faculté des sciences, Rabat</i>	<i>Rapporteur/Examineur</i>

Année Universitaire :
2019-2020

Abstract

we used Monte Carlo simulation in order to investigate compensation and critical behaviours of some ferrimagnetic systems with mixed spins such as the mixed spins-(7/2,3), (7/2,3/2) and (7/2,5/2), we opted the Ising model because it is considered as the simplest model which enables to describe many real systems. We introduced Metropolis algorithm to calculate the canonical average of certain physical quantities, further, we examined the effect of single ion anisotropies on the magnetizations, and many ground-state diagrams have been established. We report multiple hysteresis loop behaviours such as double, triple and quintuple hysteresis cycles. Particularly, the superparamagnetic phase has been detected and several kinds of curves have been depicted, we have also, discussed the existence of compensation temperature for several cases. On the other hand, the structural electronic and magnetic properties of Ga doped delafossite $\text{CuFe}_{0.96}\text{Ga}_{0.04}\text{O}_2$ are investigated using first principle calculations and Monte Carlo simulation. The calculations are based on the density functional theory using Wien2k package within Full Potential Linearized Augmented Plane Wave method and spin-polarized generalized gradient approximation of the exchange-correlation functional of Perdew, Burke and Ernzerhof (PBE), PBE with an additional correction for on-site Colombian interactions (PBE + U). The simulated results show that an ideal Ga doped Delafossite is an antiferromagnetic, we have also explored the spin coupling interactions up to third nearest neighbours as well the coupling between adjacent layers in order to examine the magnetism and thermodynamical properties. Certain results have been compared to other literature works.

Mots-clefs : Monte Carlo simulation, ab initio, compensation temperature, Néel temperature, spin-7/2, magnétisme, Wien2k, single-ion anisotropie, superparamagnétisme, cycle d'hystérésis.

Résumé

On a utilisé la simulation Monte Carlo afin d'étudier la compensation et les comportements critiques de certains systèmes ferrimagnétiques à spins mixtes tels que les spins mixtes-(7/2,3), (7/2,3/2) et (7/2,5/2), on a choisi le modèle d'Ising car il est considéré comme le modèle le plus simple qui permet de décrire de nombreux systèmes réels. On a introduit l'algorithme Metropolis pour calculer la moyenne canonique de certaines grandeurs physiques, en outre, nous avons examiné l'effet des ions anisotropes sur les aimantations, de nombreux diagrammes de phase à l'état fondamental ont été établis. Nous avons observé plusieurs comportements de ces spins mixtes tels que : La température de compensation, plusieurs types de courbes ont été tracées. D'autre part, les propriétés électroniques et magnétiques structurales du composé delafossite $\text{CuFe}_{0.96}\text{Ga}_{0.04}\text{O}_2$ dopé par Ga ont été étudiées en utilisant les calculs ab initio et la simulation Monte Carlo. Ces calculs sont basés sur la théorie fonctionnelle de la densité en utilisant le code Wien2k, qui utilise aussi, la méthode des ondes planes augmentées linéaires à plein potentiel FPLAW et l'approximation du gradient généralisé polarisé en spin de la fonction d'échange-corrélation de Perdew, Burke et Ernzerhof (PBE), avec une correction supplémentaire pour les interactions coulombiennes des sites ($GGA + U$). Les résultats simulés montrent qu'un idéal Delafossite dopé par Ga est antiferromagnétique. De plus, nous avons exploré les interactions de couplage de spin jusqu'au troisième proches voisins ainsi que le couplage entre les couches adjacentes afin d'examiner le magnétisme et les propriétés thermodynamiques. De plus, on a rapporté les propriétés magnétiques de cet élément en utilisant la simulation Monte Carlo. Certains résultats ont été comparés avec d'autres travaux de littérature.

Mots-clefs: Monte Carlo simulation, ab initio calculation, compensation temperature, Néel temperature, spin-7/2, magnetism, Wien2k, single-ion anisotropy, superparamagnetism, hysteresis cycle.

Dedication

Firstly, all my thanks go to my God who gives me the power, knowledge, ability and opportunity to undertake this work and achieve and complete it satisfactorily.

To my friend's memory *Tarik BAHLAGUI*.

I dedicate my dissertation work to my family and many friends. A special feeling of gratitude to my loving parents, whose words of encouragement and push for tenacity ring in my ears. To all my sisters and brothers who have supported me and never left my side and are very special. I also dedicate this dissertation to many friends and my church family who have supported me throughout the process. This work will not exist without my wife; she was patient with me and she helps and encourages me, although the super-energy of my lovely son Abdellah and my little daughter Romayssae. I like to thank also, all my faithful friends, Yahya MKADMI, Abdeladim SEDDOUKI, Mounir CHERFI, Ismail ERRACHID, Abdel karim ANNA, Youssef AYYAD, Youssef BENKHATOU, Mohammed BOUAYAD, Driss, AJAKANE, Yassine AYACHI, Moustafa HAMANI, Soufiane BENDAHOUE, Moussa CHRAYTI, Rachid KERKRI, Aziz MBARKI, Mohsine TRIBAK, Abdelaziz MOUMEN, Mohammed OUHADI, Driss MAAZOUZ
....

Acknowledgement

This work has been made in laboratory of Matter Condensed and Interdisciplinary Sciences (LaMScI), Faculty of Science, Mohammed V University – Rabat, under the supervision of Prof LAHOUCINE BAHMAD.

I offer my sincerest gratitude to my supervisor, BAHMAD LAHOUCINE full professor in faculty of sciences Rabat, for his fruitful discussions and remarks.

My thanks go also to the co-supervisor RACHID MASROUR the ability professor in ENSA Safi Caddi ayyad University Marrakech, who has supported me throughout my thesis with their patience and knowledge whilst allowing me the room to work in my own way.

I would like also to express my thanks to the full Prof. LARBI LAANAB, from the Faculty of Science in Rabat, to accept to be the chairman of this thesis.

Also, my thanks go to my previous supervisor the professor ABDELILAH BENYOUSSEF, He inspired me, with his method of analysis, thanks to him searching has been made greatly, without them this thesis, would not have been completed or written. One simply could not wish for better or friendlier supervisors.

I'm grateful to the full professors of my laboratory, Professor EZ-ZAHRAOUI HAMID who accepted to report and examine this thesis and be members of the jury,

I would like to thank Prof. MOURAD BOUGHRARA, from the University of Moulay Ismail Meknès, Faculty of Science, for reporting and reviewing this PhD thesis.

I would like also to offer my thanks to full Prof. ABDALLAH ELKENZ for reporting and reviewing this thesis.

I'm grateful to all the other professors of my laboratory, Prof, assistant, SALMANI ELMEHDI, OMAR MOUNKACHI MOHAMMED LOULIDI.

I 'am also appreciative of all the help from colleagues in our research group at Laboratory of Condensed Matter and Interdisciplinary Sciences, Dr. M. Bhihi, Pr. H Zaari, Pr. El Benchafia, Pr., Dr. S. MAOULOUD, Dr. A. Rkhioui, Dr. N. Mamouni, Dr. M. Belakhel, Dr. H. Elmansouri. Pr Mourad Elyadari, Dr H. Bentour, Dr K. Sbai and Pr N. Habiballah, Dr. A. Elyousfi... my thanks go to all other students of my laboratory.

I am also, grateful to Professor Peter Blaha's team (Vienna, Austria) for providing me the license of Wien2K package and for fruitful discussions; my thanks go especially to the professor K. Schwarz.

Abstract

On the one hand in this thesis, we used Monte Carlo simulation in order to investigate compensation and critical behaviours of some ferrimagnetic systems with mixed spins such as the mixed spins- $(7/2,3)$, $(7/2,3/2)$ and $(7/2,5/2)$, we opted the Ising model because it is considered as the simplest model which enables to describe many real systems. We introduced Metropolis algorithm to calculate the canonical average of certain physical quantities, further, we examined the effect of single ion anisotropies on the magnetizations, and many ground-state diagrams have been established. We report multiple hysteresis loop behaviours such as double, triple and quintuple hysteresis cycles. Particularly, the superparamagnetic phase has been detected and several kinds of curves have been depicted, we have also, discussed the existence of compensation temperature for several cases. On the other hand, the structural electronic and magnetic properties of Ga doped delafossite $\text{CuFe}_{0.96}\text{Ga}_{0.04}\text{O}_2$ are investigated using first principle calculations and Monte Carlo simulation. The calculations are based on the density functional theory using Wien2k package within Full Potential Linearized Augmented Plane Wave method and spin-polarized generalized gradient approximation of the exchange-correlation functional of Perdew, Burke and Ernzerhof (PBE), PBE with an additional correction for on-site Colombian interactions (PBE + U). The simulated results show that an ideal Ga doped Delafossite is an antiferromagnetic, we have also explored the spin coupling interactions up to third nearest neighbours as well the coupling between adjacent layers in order to examine the magnetism and thermodynamical properties. Certain results have been compared to other literature works.

Mots-clefs: Monte Carlo simulation, ab initio calculation, compensation temperature, Néel temperature, spin- $7/2$, magnetism, Wien2k, single-ion anisotropy, superparamagnetism, hysteresis cycle.

Résumé

D'une part dans cette thèse, on a utilisé la simulation Monte Carlo afin d'étudier la compensation et les comportements critiques de certains systèmes ferrimagnétiques à spins mixtes tels que les spins mixtes- $(7/2,3)$, $(7/2,3/2)$ et $(7/2,5/2)$, on a choisi le modèle d'Ising car il est considéré comme le modèle le plus simple qui permet de décrire de nombreux systèmes réels. On a introduit l'algorithme Metropolis pour calculer la moyenne canonique de certaines grandeurs physiques, en outre, nous avons examiné l'effet des ions anisotropes sur les aimantations, de nombreux diagrammes de phase de l'état fondamental ont été établis. Nous avons observé plusieurs comportements de ces spins mixtes tels que : La température de compensation, La boucle d'hystérésis, la phase super-paramagnétique, les cycles d'hystérésis double, triple et quintuple, plusieurs types de courbes ont été tracées. D'autre part, les propriétés électroniques et magnétiques structurales du composé delafossite $\text{CuFe}_{0.96}\text{Ga}_{0.04}\text{O}_2$ dopé par Ga ont été étudiées en utilisant les calculs ab initio et la simulation Monte Carlo. Ces calculs sont basés sur la théorie fonctionnelle de la densité en utilisant le code Wien2k, qui utilise aussi, la méthode des ondes planes augmentées linéaires à plein potentiel FPLAW et l'approximation du gradient généralisé polarisé en spin de la fonction d'échange-corrélation de Perdew, Burke et Ernzerhof (PBE), avec une correction supplémentaire pour les interactions coulombiennes des sites ($GGA + U$). Les résultats simulés montrent qu'un idéal Delafossite dopé par Ga est antiferromagnétique. De plus, nous avons exploré les interactions de couplage de spin jusqu'au troisième proches voisins ainsi que le couplage entre les couches adjacentes afin d'examiner le magnétisme et les propriétés thermodynamiques. De plus, on a rapporté les propriétés magnétiques de cet élément en utilisant la simulation Monte Carlo. Certains résultats ont été comparés avec d'autres travaux de littérature.

Mots-clefs : Monte Carlo simulation, ab initio, compensation température, Néel température, spin- $7/2$, magnétisme, Wien2k, single-ion anisotropie, superparamagnétisme, cycle d'hystérésis.

List of publications

1. Bouda, H., Bahlagui, T., Masrour, R. et al. Eur. Phys. J. Plus (2019) 134: 543. <https://doi.org/10.1140/epjp/i2019-12955-8>. « Status: accepted»
2. Bouda, H., Bahlagui, T., Bahmad, L. *et al.* Hysteresis Cycle and Magnetization Behaviours of a Mixed-Spin (7/2, 3/2) Ferrimagnetic Ising Model: Monte Carlo Investigation. *J Supercond Nov Magn* **32**, 2539–2550 (2019) <https://doi:10.1007/s10948-018-4981-4> « status : accepted»
3. Bouda, H., Bahmad, L., Masrour, R. et al. *J Supercond Nov Magn* (2019) 32: 1837. <https://doi.org/10.1007/s10948-018-4894-2> « Status : accepted»
4. Bahlagui, T., Bouda, H., El Kenz, A., Bahmad, L., Benyoussef, A.: *Superl. Microstruct.* 110, 90 (2017) « status: accepted».
5. El Yousfi, H. Bouda, A. G. El Hachimi, M. A. Arshad, A. El Kenz, A. Benyoussef” Double Impurities Enhance Significantly Optical Properties of Rutile TiO₂ for Solar Cell Applications: First Principle Study”. ‘Status: revised form, Submitted to the journal of Optical Electronic Materials.’

“The Scientist must set in order. Science is built up with facts, as a house is with stones. But a collection of facts is no more a science than a heap of stones is a house.”

Henri Poincare, Science and Hypothesis List of Abbreviations

Table of Contents

Abstract.....	4
Résumé.....	5
List of publications.....	6
Dedication	1
Acknowledgement	2
List of tables	11
List of figures.....	12
List of abbreviations	14
GENERAL INTRODUCTION	16
Chapter 1	22
Theoretical background	22
1. Introduction.....	23
2. Classes of Magnetic Materials	23
2.1. Diamagnetism	23
2.2. Paramagnetism.....	24
2.3. Ferromagnetism	25
2.4. Antiferromagnetism	26
2.5. Ferrimagnetism	27
3. Exchange interactions.....	29
3.1. Super-exchange interactions	29
3.2. Double exchange.....	30
3.3. RKKY Interaction.....	31
4. Density functional theory	31
4.1. Schrödinger's equation	31
4.2. Born Oppenheimer Approximation	32
4.3. Hartree Fock Approximation	33
4.4. Density functional theory.....	35
4.5. Kohn and Sham equations:	36
4.6. Kohn-Sham equation resolution.....	37
Chapter 2	41
Numerical Methods.....	41
1. Introduction.....	42
2. Monte Carlo Simulation	42
3.1. Introduction.....	42
3.2. Ising Model	42

3.3.	Ergodicity.....	44
3.4.	Importance sampling and Markov chain.....	44
3.5.	Detailed Balance	45
3.6.	Observables Averaging.....	46
3.7.	Practical implementation of the Metropolis algorithm	47
3.8.	Other kind models of spins	48
2.8.1	Heisenberg Model.....	48
2.8.2	Potts Model	49
2.8.3	Blume-Emery-Griffiths Model	50
3.	Ab initio Calculations	51
3.1	Bloch theorem.....	51
3.2	The basic concepts of electronic structure calculations	51
3.3	Pseudopotential:.....	52
3.4	FLAPW	52
3.5	KKR Method.....	53
3.5.1	Green Function.....	53
3.5.2	Green Function and Dyson equation.....	54
3.5.3	Multiple scattering and the Green function of KKR.....	54
Chapter 3	57
Monte Carlo simulation of compensation behaviours for a mixed Spin-5/2 and spin-7/2 Ising system with crystal field interaction.....57		
1.	Introduction.....	58
2.	Simulation details.....	58
3.	Results and discussion	59
3.1.	The J model.....	59
3.2.	Effects of the exchange interactions J_S and J_σ	60
3.3.	Effects of the crystal fields Δ_S and Δ_σ	63
3.4.	Study of the case $J_S=0.25$ and $J_\sigma=4$ for different $(\Delta_S, \Delta_\sigma)$	66
4.	Conclusion	68
Chapter 4	69
Compensation Behaviours in a Ferrimagnetic Mixed Spin-7/2 And Spin-3: Monte Carlo Simulation..... 69		
1.	Introduction.....	70
2.	Model and Monte Carlo Details.....	70
3.	Results and Discussion.....	71
3.1.	Study of the $\Delta_{7/2}=\Delta_3=0$ Case.....	73
3.2.	Study of the $\Delta_{7/2}\neq 0, \Delta_3=0$ Case.....	73

3.3. Study of the $\Delta_3 \neq 0, \Delta_7/2 = 0$ Case.....	75
3.4. Study of the $\Delta_7/2 \neq 0, \Delta_3 \neq 0$ Case.....	78
4. Conclusion	80
Chapter 5	82
Hysteresis Cycle and Magnetization Behaviours of a Mixed–spin (7/2, 3/2) Ferrimagnetic Ising Model: Monte Carlo Investigation	82
1. Introduction:	83
2. Model and Monte Carlo Details.....	83
3. Results and discussion	84
3.1. Ground–state phase diagrams	84
3.2. Variation of the magnetization as a function of the crystal field	87
3.3. hysteresis loops under the effects of the temperature and the crystal fields	89
4. Conclusion	96
Chapter 6.....	97
Unexpected Magnetic Behaviours of Ga Doped $\text{CuFe}_{1-x}\text{Ga}_x\text{O}_2$ Delafossite, $x = 0.04$: First principle Calculation and Monte Carlo Simulation.....	97
1. Introduction.....	98
2. Computational methods	98
2.1. Ab initio calculations	98
2.2. Ising model and Monte Carlo simulations	99
3. Results and discussion	100
4. Conclusion	105
References.....	109

List of tables

Table.1 A summary of the different types of magnetic behaviours.

Table.2 Ground-state energies of the J - Δ S - $\Delta\sigma$ model, with $J=-1$ and $J_S=J\sigma=0$.

Table.3 Ground state energies of the J - Δ $7/2$ - Δ 3 model.

Table.4 Ground-state energies of the model J - Δ - h with $J = -1$.

Table.5 Ground-state energies of the model J - Δ $7/2$ - h when Δ $3/2 = 1$ with $J = -1$.

Table.6 Ground-state energies of the model J - Δ $3/2$ - h when Δ $7/2 = -1.5$ with $J = -1$.

Table.7 The calculated coupling interactions on doped Delafossite CuFeO_2 .

List of figures

Figure.1 Curves of the absolute value of the total magnetization $|M|$ as functions of temperature for several positive values of Δ_3 when $\Delta_{7/2} = 0$

Figure.2 Curves of the absolute value of the total magnetization $|M|$ as functions of temperature for several negative values of Δ_3 when $\Delta_{7/2} = 0$

Figure.3 Variation of the absolute value of the total magnetization $|M|$ for two opposite values of the crystal field Δ_3 when $\Delta_{7/2} = -1.1$

Figure.4 Thermal behaviours of the absolute value of the total magnetization $|M|$ for various negative values of the crystal field $\Delta_{7/2}$ when $\Delta_3 = -1$

Figure.5 Thermal behaviours of the absolute value of the total magnetization $|M|$ for various values of the crystal field $\Delta_{7/2}$ when $\Delta_3 = 1$

Figure.6 Thermal behaviours of the absolute value of the total magnetization $|M|$ for various values of the crystal field $\Delta_{7/2}$ when $\Delta_3 = 3$

Figure.7 Ground state–phase diagram of the mixed $(7/2, 3/2)$ Ising ferrimagnetic system for the model $J-\Delta-h$ for $J = -1$.

Figure.8 Ground state–phase diagram of the mixed $(7/2, 3/2)$ Ising ferrimagnetic system for the model $J-\frac{\Delta_7}{2}-h$ when $\Delta_{3/2} = 1$ for $J = -1$.

Figure.9 Ground state–phase diagram of the mixed $(7/2, 3/2)$ Ising ferrimagnetic system for the model $J-\Delta_{3/2}-h$ when $\Delta_{7/2} = -1.5$ for $J = -1$.

Figure.10 The total magnetization versus $\Delta = \Delta_{7/2} = \Delta_{3/2}$ for various h when $T = 2$.

Figure.11 The total magnetization versus $\Delta = \Delta_{7/2} = \Delta_{3/2}$ for various T .

Figure.12 Effect of the temperature on the hysteresis loops when $\Delta_{7/2} = \Delta_{3/2} = 0$ for M , $M_{7/2}$ and $M_{3/2}$. Hysteresis loops with various $\Delta = \Delta_{7/2} = \Delta_{3/2}$ when $T = 3$ for M , $M_{7/2}$ and $M_{3/2}$.

Figure.13 Hysteresis loops for various $\Delta_{7/2}$ when $T = 0.5$ and $\Delta_{3/2} = 1$ for M , $M_{7/2}$ and $M_{3/2}$

Figure.14 Hysteresis loops for various $\Delta_{3/2}$ when $T = 0.5$ and $\Delta_{7/2} = -1.5$ for M , $M_{7/2}$ and $M_{3/2}$.

Figure.15 Delafossite structure with hexagonal structure

Figure.16 Total DOS (a) and partial DOS (b) of CuFeO_2 .

Figure.17 Partial DOS of components for spin up (a) and spin down (b).

Figure.18 Total DOS of $\text{CuFe}_{0.96}\text{Ga}_{0.04}\text{O}_2$ delafossite.

Figure.19 Coupling interaction between next nearest neighbours.

Figure.20 Configurations of ordered spin states.

Figure.21 Thermal dependence of the magnetization M and Magnetic susceptibility χ in the absence of the single-ion anisotropy $\Delta = 0$.

Figure.22 Thermal dependence of the magnetization for three different values of the single-ion anisotropy $\Delta = -1, -2$ and -3 .

Figure.23 Magnetic susceptibility vs. the temperature for three different values of the single-ion anisotropy $\Delta = -1, -2$ and -3 .

List of abbreviations

MC: Monte Carlo.

DFT: Density functional theory.

T_N : Neel Temperature.

TC: Critical temperature.

Ψ : wave function.

T_e : Motion energy of electrons.

T_n : Motion energy of cores.

V_{n-n} : Potential energy of interaction between cores.

V_{e-n} : Potential energy of attraction between cores and electrons.

V_{e-e} : Potential energy of repulsion between electrons

$\rho(r)$: electronic density of r.

$V_{ext}(r)$: extern potential.

χ_m : the Susceptibility.

M: The magnetization.

F_{HF} : is the Hartree Fock operator.

$V_{eff}(r)$: effective potential.

H_{KS} the Hartree Fock Hamiltonian.

$E_{xc}[\rho]$: energy of exchange and correlation.

LDA: Local Density Approximation.

GGA: Gradient Generalized Approximation.

FLAPW: Full Potential Linearized Augmented Plane Wave.

APW: Augumented Plane Wave.

Pseudopotential: PP

$W(\alpha \rightarrow \beta)$: transition from the state α to β .

BZ: first zone of Brillion

G : Green Function

KKR: Kohn-Korringa -Rostoker

CPA: Coherent Potential Approximation.

VB: Valence Band

CB: Conduction Band.

DOS: Density of state.

P-DOS: Partial Density of state.

k : reciprocal lattice vector

R_n : direct lattice vector

GENERAL INTRODUCTION

In recent decades, Numerical Calculation methods have known a great interest, thanks to the enhancement of the power of computers and improvement of models and programming methods. That may lead to more understand about several experimental physical properties of compounds, such as the techniques of growth, the stability and various other properties. The formalization of the phenomenon can be achieved by means of mathematical models that have the advantage of providing results reflecting a stable evolution of the system over time. The steps of the simulation are executed as illustrated in the following flowchart:

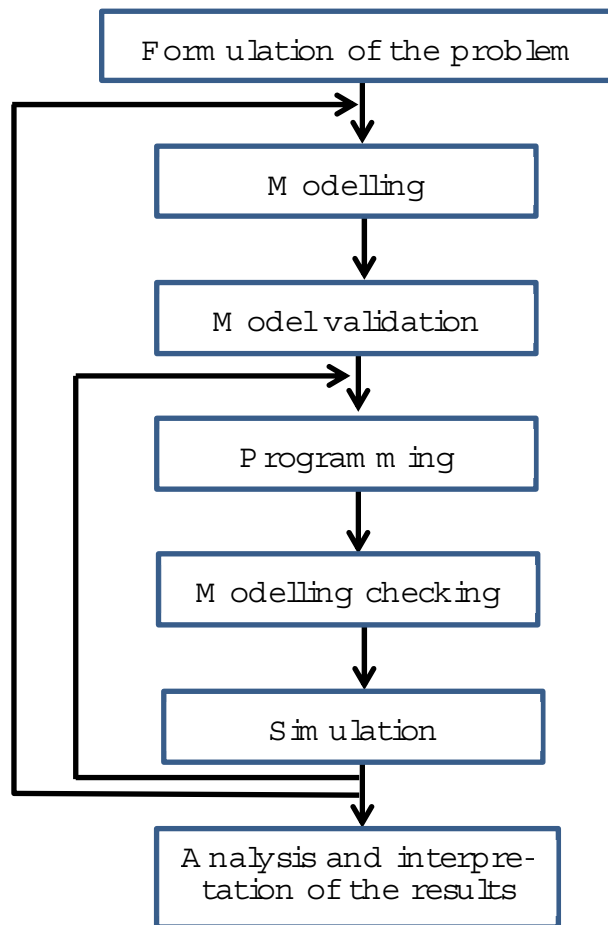


Figure 1.1: Flowchart of the different stages of simulation.

Thereby, obtaining accurate experimental results need new powerful algorithms and codes, which make this, part a crucial. There are several techniques for modelling and simulating materials, for instance, Monte Carlo Simulation, First principles calculation methods, molecular dynamic...etc. First principles calculations and Monte Carlo simulations play a key role to investigate many properties of materials. It allows us to determine several properties, for example calculating the density of state by employing ab initio calculations enable us to determine magnetic, optical, mechanical, thermoelectric properties...etc.

Furthermore, study of critical phenomena in Ferrimagnetic mixed-spin Ising systems has attracted considerable attention. These systems are of a great interest owing to their useful properties such as stable with spontaneous moments at room temperature; this makes these materials to be candidates for important technological applications [1-2]. For this aim, ferrimagnets, in which two sublattices have unequal magnetic moments regularly alternate and interact antiferromagnetically, seem to play a great role. Under appropriate conditions, ferrimagnets show a compensation point below the critical temperature at which the resultant moment vanishes because of the different temperature dependence of the sublattice magnetizations that compensate each other [3]. The existence of compensation temperatures in these materials makes them potential candidates for use in the area of thermo-magnetic data storage and magneto-optical recording media devices [4-7]. The ferrimagnetic order plays an important role in ferrimagnets, for this, investigation of ferrimagnetism in mixed systems with high spin value becomes a very active research field. This kind of materials has been intensively investigated both experimentally and theoretically. For instance, using density functional theory (DFT) within generalized gradient approximation (GGA) for exchange and correlation [8], it is found that the bimetallic cluster $GdMn_x$ ($x=2$ to 5), which is composed of the rare earth metal Gd and the transition metal Mn, is ferrimagnetically coupled. Also, the temperature dependence of the magnetization for $GdMn_2Ge_2$ exhibited ferrimagnetic coupling of Gd-Mn [10]. In addition, the heteronuclear complex $Gd_2Mn_3(CH_2C(CH_3)COO)_{12}(NC_6H_4-C_6H_4N)$ has been synthesized and the magnetic measurement showed antiferromagnetic behaviours between Mn(II) and Gd(III) with the spins values $5/2$ and $7/2$, respectively [11]. In addition, we can acquire ferrimagnetic mixed spin- $7/2$ and spin- 3 from doping, for example, monolayer compounds containing the gadolinium (Gd) element (Gd, Gadolinium oxide Gd_2O_3 , GdN, etc.) by terbium (Tb) [12-14], the electronic configurations for Gd : $[Xe]4f^75d^15s^2$ and Tb $[Xe]4f^85d^15s^2$, it satisfies that Gd holds spin- $7/2$ and spin- 3 for Tb which corresponds to the following possible values: $S = \pm \frac{7}{2}; \pm \frac{5}{2}; \pm \frac{3}{2}; \pm \frac{1}{2}$ and $\sigma = \pm 3; \pm 2; \pm 1; 0$, respectively; both the gadolinium oxide and gadolinium(II) nitride possess a cubic structure [12-16]. In regards to the mixed spin-($7/2, 3/2$) the hetero-complex $[Cr(CN)_4(\mu-CN)_2Gd(H_2O)_4-(bpy)]_n \cdot 4nH_2O \cdot 1.5nbpy$ has been synthesized successfully [17], it contains the Gd(III) and Cr(III) atoms which are coupled ferrimagnetically, it plays an important role on the enhancement of the density speed [18-20], the variations of the magnetization under the effects of both the temperature in the presence of an applied magnetic field of the gadolinium orthochromite $GdCrO_3$, in which the Cr^{3+} and Gd^{3+} moments hold antiparallel coupling, have been explored [21]. Furthermore, it is noteworthy that this system exhibits superparamagnetic phase for appropriate values of the

system parameters. This behaviour has been shown both theoretically [22-23] and experimentally [24-25]. Also, this phenomenon is exploited in diverse fields such as nanomedicine [26], relaxometry and magnetometry [27]. On the other hand, multiple loops are of considerable interest from technological perspective particularly in the area of multi-state memory devices [25, 28]. Otherwise, these compounds hold molecular magnetism which plays an important role on the quantum information storage applications and processing improvement.

In this thesis, using Monte Carlo method, we will firstly study a mixed ferrimagnetic Ising system on a square lattice in which the two inter-penetrating sublattices have spins $S=\pm 7/2$ and $\sigma=\mp 5/2$ to investigate the effects of the next-nearest neighbour interactions and the crystal field on the magnetic behaviours of the system especially on the compensation temperature. Secondly, we simulate the mixed ferrimagnetic Ising system spin-(7/2,3), aiming to describe the magnetization phenomena and to predict the impact of the variation of the crystal fields on the existence of the compensation temperature. Thirdly, we will show the effects of single-ion anisotropies and an external magnetic field on the magnetization of the mixed spin (7/2, 3/2) ferrimagnetic Ising system within. We will observe under certain values of the physical parameters, the hysteresis loop behaviours. Several ground-state phase diagrams will be presented.

On the other hand, we study the Magnetic Behaviours of Ga Doped $\text{CuFe}_{1-x}\text{Ga}_x\text{O}_2$ Delafossite which is a multiferroic material that has both ferroelectric and ferromagnetic properties. These compounds are of great interest due to the possibility of controlling the charge by a magnetic field or controlling the magnetism by an electric field. Recently, study of multiferroic delafossite has become quite interesting both experimentally [29–33] and theoretically [34–40] due to its wide-ranging technological applications in spintronics, multifunctional devices, information storage, sensors, electronics components, energy, catalysis, photocatalysis, nanomedicine, sensors, electrochemical devices and environmental applications [41–44]. Many studies have been carried out on delafossite structured compounds in order to clarify the origin of their physical properties [45–49]. The basic composition of delafossite family is ABO_2 where A-site cation can be occupied by Pt, Pd, Ag, or Cu ions nominally in a monovalent state and B-site cation can consist of most trivalent transition metals, group III for example, Cr, Co, Fe, Al, and Ni [49–50]. The crystal structure of delafossite was established earliest by Soller and Thompson [51], M.A. Sarabia et al. have synthesized CuFeO_2 from the reaction of Cu_2O and FeOOH , they reported the morphological and structural

properties using several techniques of characterization [52] also, L. Shi et al have prepared a single crystal samples of $\text{CuFe}_{1-x}\text{Ga}_x\text{O}_2$, with different values of x they detected an unusual magnetism on this compound because of its triangular lattice structure [53]. J. D. Song et al established that the thermal conductivities display extreme anomalies at temperature or field induced magnetic transitions, which indicate an intense spin–phonon coupling in Ga doped CuFeO_2 [54]. In recent publications CuFeO_2 and $\text{CuFe}_{1-x}\text{Ga}_x\text{O}_2$ films were grown successfully from stoichiometric mixtures of Cu_2O , Ga_2O_3 and Fe_2O_3 , it is concluded that both doped and undoped CuFeO_2 are capable of reducing CO_2 to CO photo-catalytically [55], similar properties have been observed by J. Gu et al, adding to that, they proved that doping CuFeO_2 with Mg enhances the conductivity of this material [56]. CuFeO_2 may be modelled by Heisenberg spin type [57] with frustrated systems where the spin lattice orders can be predicted from the first principles [58]. Different classes of magnetic ground states for various contributions of quenched random disorder and geometrical frustration are given in Ref. [59]. However, other references consider that CuFeO_2 exhibits an Ising-like collinear four- sublattice [60–63]; it is worth nothing that delafossite system contains a high anisotropy magnetic due to the difference along different axes [64]. Seki et al reported The magnetocaloric response for several kinds of magnetic order in triangular AMO_2MX_2 lattices [65], Such magnetic materials i.e. compounds containing high crystal field usually can be described by Ising model, the study achieved by T. Takagi et al examined the magnetic ordering of frustrated classical Ising spins with $S = 1/2$, they evaluated coupling interactions to the third next neighbours by means of Monte Carlo simulation [66].

Conceptually, DFT calculations made on the ground state, this means for $T=0$ K [67–68], in order to study compounds in temperature different to zero, molecular dynamic is a good choice, it is a computer simulation based on the integration of Newton’s equations of motion, it plays a key role to study thermal stability of such systems [69], T.F.T Cerqueira et al reported that several delafossite compounds are thermally stable particularly CuFeO_2 and CuGaO_2 structures [70–71]. The Stability of similar delafossite compounds has been discussed by other researchers [51, 72].

In [second part](#) of this work we aim to investigate the electronic structure of Ga doped CuFeO_2 delafossite, the calculations were performed by the density functional theory, using the Wien2k package which is considered as powerful Ab initio code of calculation of certain physical properties, with good reproducibility [73]. Furthermore, we reported the critical temperature and susceptibility using Monte Carlo simulation, the obtained values of exchange

interactions are used by Monte Carlo simulation to determine the Néel temperature for different values of single ion anisotropy.

The outline of this thesis is organized as follows:

In Chapter1, we introduce the necessary background for the understanding of numerical simulations, it starts by presenting, various classes of magnetic materials and exchange interactions in the following we discussed the fundament of density functional theory.

Chapter2, is devoted to computational methods used in this work we present in first time, we give the basic on Monte Carlo simulation by introducing several terms and models regarding to this method, on the other hand we discussed the fundamental on ab initio calculations.

Chapter 3, 4, 5 and 6 are devoted to discuss the main results obtained during this thesis

Chapter 1

Theoretical background

1. Introduction

Integrated circuits use the charges of electrons for data processing, while the storage of information in hard drives, for example, uses spin electronics. Recently, different types of spin polarization have been proposed in semiconductors: the spin introduced into magnetic atoms and the nuclear spin of the constituents of atoms. And they showed that a new function can be implemented by injecting the transport and the control of its spin states these results have emerged another field of semiconductors called Spintronic. The main problem remains the lack of suitable materials, for the construction of electronic object with quantum function, so there has the problem of very high sensitivity to external disturbances. For this, efforts have been devoted to the isolation of the chip from the outside, this by controlling its sensitivity to disturbance. In fact, study the magnetic properties of materials has taken off particularly in recent years in the field of nanomagnetism and spin electronics. Study of these properties is of fundamental interest and opens the door to a large number of applications: magnetic hard disks, magnetic memories (MRAM), magnetic field sensor, microwave sources or magnetic logic circuit.

On the other hand, at the atomic scale, if the relativistic effects are neglected, Schrödinger's equation is used to describe the quantum state of the material. To be able to solve this equation for systems made up of hundreds or thousands of atoms, approximations are necessary.

This chapter focuses on the concepts and the literature concerning magnetism, the next section presents different classes of magnetic materials and. Section 3 is devoted to show numerous types of exchange interactions. In the last section we discuss density functional theory (DFT), in its formulation given by Kohn and Sham (KS), this method is considered as the most commonly used quantum method to calculate the electronic structure of molecules and solids and several other properties. The main quantity of this method is the electron density, from which any other property of the system can be determined in a unique way, as demonstrated by Hohenberg and Kohn in 1964

2. Classes of Magnetic Materials

2.1. Diamagnetism

Characterized by a negative susceptibility with a low value of amplitude [74–75]. In the absence of magnetic field, this kind of materials are not magnetic, this may be explained to the reaction of matter versus the external magnetic field, however they acquired a slight induced magnetization opposite to the applied field. This slight magnetization is linearly dependent on the applied field and goes to zero when the field is removed.

It is a general property with a very small value of the susceptibility χ_m , independent of temperature and negative, it is described as following:

$$\chi_m = -\frac{ne^2\mu_0}{6m_e}\bar{r}^2 \tag{1.1}$$

Where n is the number of electrons by volume units of matter, \bar{r} is the correspondent average orbital radius and μ_0 is the vacuum permeability.

2.2. Paramagnetism

When we applied a magnetic field to a paramagnetic material, it required a slight magnetization [74–76], contrary to the diamagnetic substances; this magnetization is parallel to the applied field. Paramagnetic materials possess atoms with atomic magnetic moment but there is no interaction between the adjacent atomic moments as shown in Figure.2.2.

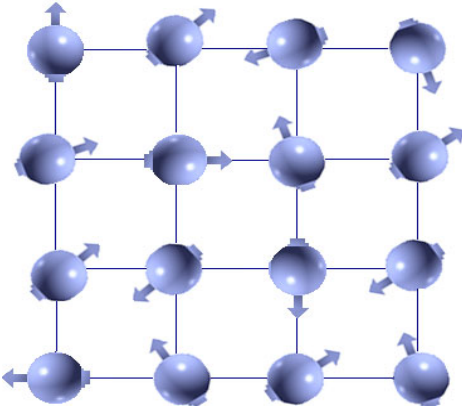


Figure.2.2 Paramagnetic ordering

Similar to the paramagnetic materials the magnetization is linearly dependent to the applied magnetic field and tends to zero when the field is removed. In these substances there is an important competition between thermal agitation and the effect of the orientation imposed by

the applied magnetic field \vec{B} manifested by a parallel magnetization to \vec{B} , hence, χ_m is positive intense and thermo-dependent, for several substances this relation can be expressed by the following relation.

$$\chi_m = C/T \quad (1.2)$$

Where C is the Curie constant the equ (1.2) above represents the Curie law, it can be applied to paramagnetic Gaz such as O₂, N₂, and for some diluted solutions of iron, chromium and cobalt.

However, for other paramagnetic substances obey to the following law:

$$\chi_m = \frac{C}{T - T_C} \quad (1.3)$$

Where T_C is the critical temperature, this law represents well, the Curie-Weiss law, it is only valid for temperatures higher than the critical temperature T_C .

It is also rarely possible that the susceptibility can be expressed by the following law:

$$\chi_m = \frac{C}{T + T_C} \quad (1.4)$$

2.3. Ferromagnetism

The ferromagnetism can be only possible when exchange interaction between neighbouring atoms leads to the parallel alignment of the atomic magnetic moment. In ferromagnetic compounds when we applied a magnetic field, a permanent magnetization appeared below a critical temperature, called the Curie temperature T_C , it is worth to note that heating the system above the Curie temperature disappears the spontaneous magnetization and the materials become paramagnetic, however, removing the applied field in this case, these materials possess an important spontaneous magnetization [77]. Generally these materials are constituted of micro-domains, where even if the external magnetic field is absent the electronic magnetic moments are organized as seen in Table.1, the total magnetization is a function of temperature; it is a maximum at 0 K, decreases as the temperature increases, and vanishes below the Curie temperature as shown in table1

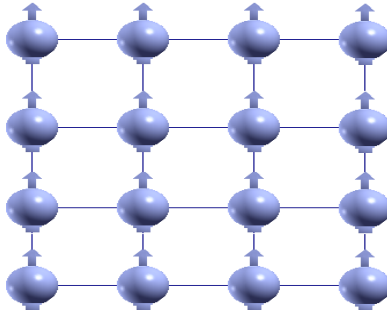


Figure3. Ferromagnetic order: the magnetic moments form a spontaneous magnetization.

2.4. Antiferromagnetism

Antiferromagnetic spin ordering was first verified experimentally in MnO by Shull and Smart [78] In Anti-ferromagnetic compounds, the magnetism of the system is identical, it is composed of two sublattices A and B with opposite direction as depicted in **figure.2**, thereby, the total magnetization of the system is null [74–75], and the material appears to behave in the same way as a paramagnetic material.

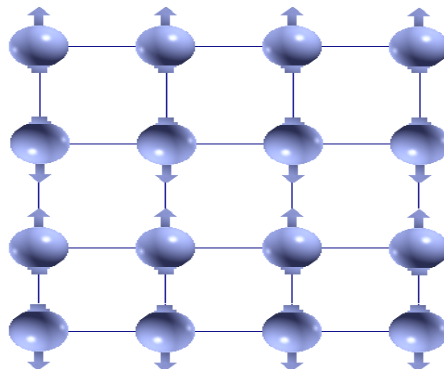


Figure.4 Antiferromagnetic ordering

controversy to the ferromagnetic case there is no spontaneous magnetization and the average magnetization of the system is null, however similar to ferromagnetic materials, these materials become paramagnetic above a transition temperature known as the Néel temperature, T_N .

$$M = M_A - M_B = 0 \tag{1.4}$$

Above Néel temperature the susceptibility varies to the following law

$$\chi_m = \frac{C}{T + T_C} \tag{1.5}$$

And below the Néel temperature the susceptibility increases with increasing the temperature. Then χ is maximal for $T = T_N$, which is one of properties of antiferromagnetic compounds.

In general terms, antiferromagnetic ordering may exist at sufficiently low temperatures, but vanishes at and above the Néel temperature, this nomenclature belongs to the French scientist Louis Néel, who had first identified this type of magnetic ordering [79]. Notably above the Néel temperature, the material is typically paramagnetic.

2.5. Ferrimagnetism

In ferrimagnetic compounds there are two sublattices ordered ferromagnetically, this kind of materials can be seen in several materials composed of two types of magnetic atoms, with different magnetic moments[76–77,80], It is therefore distinguished from both anti-ferromagnetism, for which the resulting magnetic moment is zero, and ferromagnetism, for which spontaneous magnetization results at the microscopic level from a parallel arrangement of magnetic moments as shown in Figure.3, further, Ferrimagnetism is only observed in compounds, which have more complex crystal structure than pure elements, typical examples include barium ferrite, $Ba_{0.6}Fe_2O_3$, magnetite Fe_3O_4 and maghemite Fe_2O_3 , $SrFe_{12}O_{19}$...etc . Because of the opposite directions the two sublattices, the total magnetization can be described as the difference in the two sublattice magnetizations, it is described by the following expression:

$$M = M_A - M_B \quad (1.4)$$

As result the spontaneous magnetization is different to zero and which can be an important. Consequently, such materials have a similar behavioursism to the ferromagnetic materials, however, comparing to the ferromagnetic elements they have a very slight magnetization in saturation.

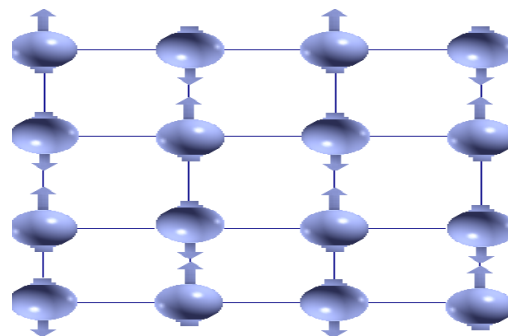


Figure5. Ferrimagnetic ordering

In summary the different classes of materials are represented in the following table

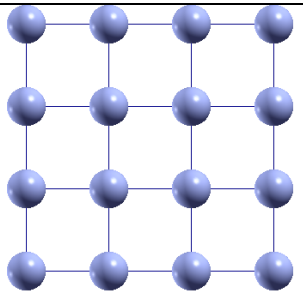
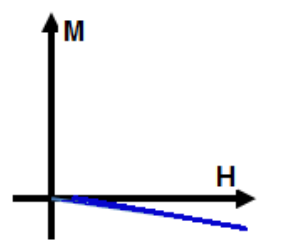
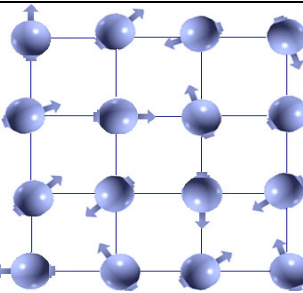
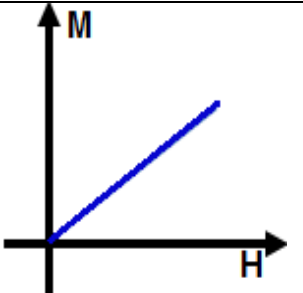
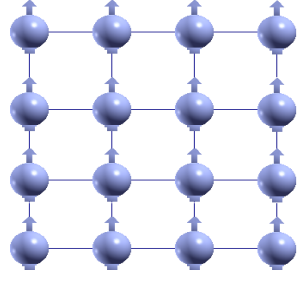
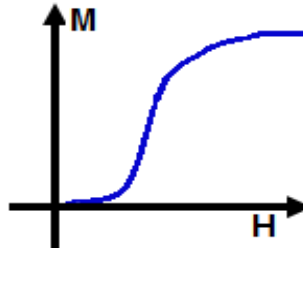
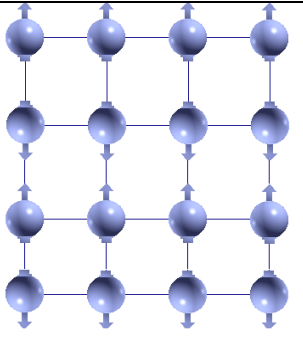
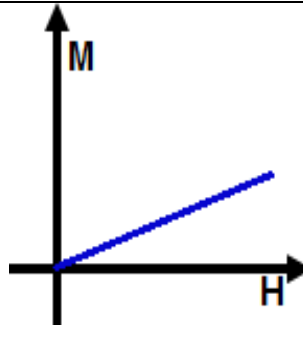
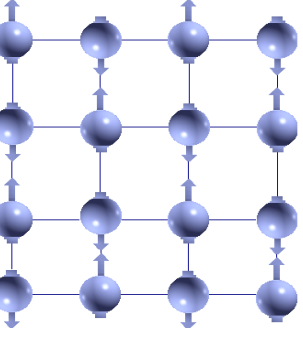
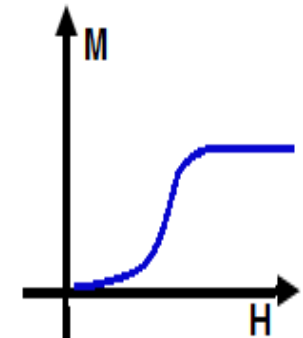
Type	Example	Atomic/Magnetic Behaviours		
Diamagnetism	Inert gases; many metals Au, Cu, Hg; non-metallic elements e.g. B, Si, P, S; many ions e.g. Na ⁺ , Cl ⁻ and their salts; diatomic molecules e.g. H ₂ , N ₂ ; H ₂ O; most organic compounds	Atoms have no magnetic moment. Susceptibility is small and negative, -10^{-6} to -10^{-5}		
paramagnetism	Some metals, e.g. Al; some diatomic gases, e.g. O ₂ , NO; ions of transition metals and rare earth metals, and their salts; rare earth oxides	Atoms have randomly oriented magnetic moments. Susceptibility is small and positive, 10^{-5} to 10^{-3}		
Ferromagnetism	Transition metals Fe, H, Co, Ni; rare earths with $64 \leq Z \leq 69$; alloys of ferromagnetic elements; some alloys of Mn, e.g. MnBi, Cu ₂ MnAl	Atoms have parallel aligned magnetic moments. Susceptibility is large (below TC)		
Antiferromagnetism	Transition metals Mn, Cr & many of their compound, e.g. MnO, CoO, NiO, Cr ₂ O ₃ , MnS, MnSe, CuCl ₂ .	Atoms have antiparallel aligned magnetic moments. Susceptibility is small and positive, $+10^{-5}$ to $+10^{-3}$		
Ferrimagnetism	Fe ₃ O ₄ (magnetite); γ-Fe ₂ O ₃ (maghemite); mixed oxides of iron and other elements such as Sr ferrite.	Atoms have mixed parallel and antiparallel aligned magnetic moments. Susceptibility is large (below TC)		

Table.1 A summary of the different types of magnetic behaviours.

3. Exchange interactions

With regard to exchange interactions between sites i and j , we take into account the fact that the kinetic energy of electrons is minimized by chemical bond formation. In general, the bonding orbital is favoured. The figure below shows the link between the sign of exchange and the recovery of orbitals for direct exchange interaction requires orbital recovery, many mechanisms exchange are indirect others are direct interactions.

3.1. Super-exchange interactions

Super-exchange is an indirect interaction that occurs between magnetic impurities through non-magnetic atoms, as in the case of transition metal oxides or compounds with a perovskite structure [85]. In this type of exchange, the charges are localized and the interaction strongly depends on the configurations of the 3d orbitals (e_g or t_{2g}), the number of electrons in play and the angle of bonding, which often gives rise to an antiferromagnetic coupling which follows the rules of Goodenough-Kanamori-Anderson [80-81]. Furthermore, on the insulator elements based on the d orbital, the super-exchange mechanism is very common when the magnetic ions are separated by non-magnetic ions. It involves an orbital p which hybridizes with d orbitals. Hence, the electron or the electrons of p orbitals delocalized on two d ions produce the indirect exchange interaction. In order to obtain a magnetic order. Fig 6 shows a diagram which gives the different cation-anion-cation configurations at 180° . In the case where the two cations have an orbital e_g half full pointing in the direction of the anion, the coupling is direct by Hund's rules and gives strong anti-ferromagnetism (Fig 6. (a)), Hence, super-exchange favours antiferromagnetism. The case where the two e_g orbitals are empty (Fig 6(b)) also gives anti-ferromagnetism, but weak. If the orbital overlap is strong enough, which means that the orbits of the two cations are sufficiently filled, each spin of the orbital p_x will interact with the electron of the orbital of the adjacent cation, forcing it to be antiparallel. As an example, is provided by the Mn^{3+} -ions with O^{2-} -ions centred on the bonds. Skipping of a hole from Mn^{3+} -ions trough O^{2-} to the next Mn^{3+} -ions (and return), Consequently, the spins of two atoms of the transition metals will have an antiparallel configuration. Such a mechanism leads to a strong antiferromagnetic coupling, this is super-exchange. But on the contrary, if the orbital coverage is very low or zero, the two cations will have parallel spins which leads to ferromagnetic coupling.

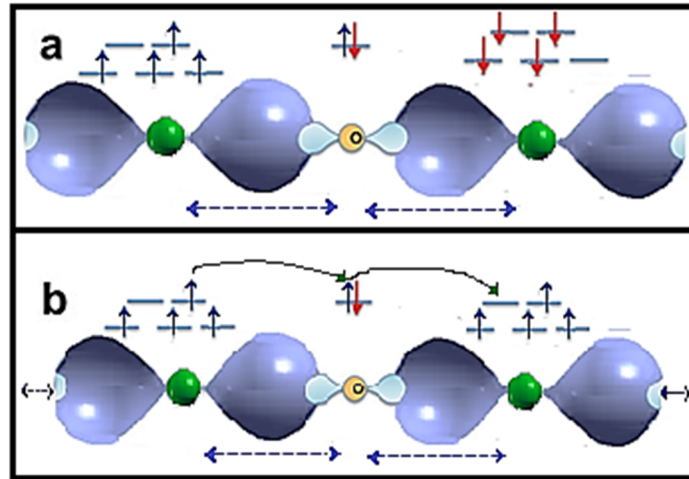


Figure.6 A schematic picture showing (a) super exchange interaction favouring AFM coupling (b) and double exchange interaction favouring FM coupling between the Mn ions, which is mediated via the O ion lying in between. The blue dotted line shows the Fe-O interatomic distance in both cases. The green connecting curved line shows the simultaneous charge transfer between Fe and O atoms.

3.2. Double exchange

The double exchange interaction is a ferromagnetic interaction which corresponds to the interaction between cations of the same species and of different valences, with exchange of a 3d layer electron via a non-magnetic atom, for example between Mn^{4+} and Mn^{3+} separated by an oxygen ion. It allows the system to gain energy by delocalizing the electron $e \uparrow g$ of the Mn^{3+} ion on the two Mn ions, compared to a configuration where the Mn^{3+} ion keeps its electron $e \uparrow g$. The jump is facilitated if the magnetic moments of the neighbouring manganese are aligned because the hopping can be done without emission of magnetic excitations. The model of double exchange has been introduced for the first time by the scientist C. Zener in 1951, he considered that ferromagnetism and electric conductivity are due to the interactions between the electrons of conduction band and the localized spins of d orbits of manganese. According to the Hund's rule, Zener also, considered that the ground state should be characterized by the alignment of the spins of localized electrons [83-84]. The electron should therefore move in this parallel localized spin environment in order to decrease the energy of the system, he studied the mechanism of Interactions as electronic transfer between the Manganese ions of the initial state ψ_i and the final state ψ_f via the oxygen ion, he invoked this interaction the double exchange as shown in **Figure.6.b**

3.3. RKKY Interaction

In metals the indirect exchange interaction RKKY (Ruderman-Kittel-Kasuya-Yoshida) is common for moments localized sites (especially for 4f orbital). The exchange interaction between magnetic moments is done via the electrons of conduction band which are randomly distributed [86-87]. Unlike the direct exchange interaction which requires the recovery of the electronic wave functions of the two local magnetic moments, the RKKY interaction does not require this recovery. This is, due to the intervention of electrons of the band conduction that it is likely to operate between two spins even are distant and that it is dominant in dilute magnetic alloys. Conceptually, the exchange interaction J_{ij} , which is a random variable, is assumed to be distributed confirming to a Gaussian curve with mean zero. The interaction is oscillating, it can be written in terms of the 4f spins localized on the ion, S_i and of the spins of the conduction electrons $\sigma(r)$:

$$E = - \sum_{R_i-r} J(R_i - r) S_i \sigma(r) \quad (1.6)$$

This interaction is positive and highly localized of the form $J(R_i - r) = J\delta(R_i - r)$ (intra-atomic exchange). Where R is the exchange interaction's distance.

4. Density functional theory

4.1. Schrödinger's equation

In the context of electronic structure calculations, in quantum mechanics, the physical state of an electron is described by the concept of the wave function, which can be defined as a function describing the probability of particle's quantum state as a function of position, momentum, time, and or spin. The most common symbols of the wave functions are denoted by the Greek letters Ψ or ψ (psi). One of the most fundamental tasks of quantum mechanics is then to solve a differential equation according to the electronic, nuclear and spin coordinates, it is the Schrödinger equation. Thereby determining physical properties of an N system comes back to the resolution of the wave function $\psi(r_1, \dots, r_N)$, where r_i represents the position of each electron i . The wave function $\psi(r_1, \dots, r_N)$ is solution of the electronic Schrödinger equation:

$$H\psi = E\psi \quad (1.7)$$

Where H is the Hamiltonian operator describing the contribution energy to the system, and E is the energy eigenvalue. The eq (1) applies to electrons traveling at non-relativistic speeds. It's

an equation that describes the evolution in the time of the wave function of an arbitrary quantum system, despite its simpler form, its analytical resolution is impossible, except in simple cases like the Hydrogen atom. For a system consisting of $2n$ electrons and nuclei without relativistic treatment, the Hamiltonian for a closed thin-film system is given as following:

$$H = - \sum_i^{2N_e} \frac{\hbar^2}{2m_e} \nabla_i^2 - \sum_\alpha^{N_\alpha} \frac{\hbar^2}{2M_\alpha} \nabla_\alpha^2 - \sum_\alpha^{2N_e} \sum_\alpha^{N_\alpha} \frac{Z_\alpha e^2}{|r_i - R_\alpha|} + \sum_i^{2N_e} \frac{e^2}{|r_i - r_j|} + \sum_{\alpha < \beta}^{N_\alpha} \frac{Z_\alpha Z_\beta}{|R_\alpha - R_\beta|} \quad (1.8)$$

$$T_e = - \sum_i^{2N_e} \frac{\hbar^2}{2m_e} \nabla_i^2 : \text{Electronic kinetic energy term.}$$

$$T_\alpha = - \sum_\alpha^{N_\alpha} \frac{\hbar^2}{2M_\alpha} \nabla_\alpha^2 : \text{Nuclear kinetic energy.}$$

$$V_{\text{noy-elc}} = \sum_\alpha^{2N_e} \sum_\alpha^{N_\alpha} \frac{Z_\alpha e^2}{|r_i - R_\alpha|} : \text{Potential energy of electrons in the nuclear fields.}$$

$$V_{\text{noy-noy}} = \sum_{\alpha < \beta}^{N_\alpha} \frac{Z_\alpha Z_\beta}{|R_\alpha - R_\beta|} : \text{The nuclear - nuclear repulsion.}$$

4.2. Born Oppenheimer Approximation

The first approximation introduced by Born Oppenheimer was in 1927 [88]. It consists of decoupling nuclei and electrons, the nuclei are infinitely heavy as compared to the electrons, therefore there is a strong separation of time scales between the electronic and nuclear motion. The Hamiltonian can be expressed separately on electronic contribution H_e and nuclear contribution H_N :

$$H = H_e + H_N \quad (1.9)$$

And the wave function can be written as product of two functions:

$$\psi(r, R) = \psi_R(r) \Phi(R) \quad (1.10)$$

Where $\Phi(R)$ is the nuclear wave function, $\psi_R(r)$ is the electronic wave function corresponding to a set of R positions of the frozen nuclei, r and R are the electronic and nuclear positions, respectively.

The eq (1.6) becomes:

$$H(\psi_R(r), \Phi(R)) = \psi(r)(T_N + V_{NN})\Phi(R) + \Phi(R)(T_e + V_{Ne} + V_{ee})\psi(r) \quad (1.11)$$

The eq (1.11) can be resolved in two steps:

First, we solve the electronic equation by assuming that the nuclei are fixed.

$$\Phi(R)(T_e + V_{Ne} + V_{ee})\psi(r) = E_e\Phi(r) \quad (1.12)$$

In this case we go from a problem of N electrons and M atoms, to a problem of N electrons feeling the potential V_{ext} of nuclei (exterior potential, $V_{ext} = V_{NN}$).

Then, the Born Oppenheimer approximation is limited to electronic components only.

$$H_e = T_e + V_{N-e} + V_{e-e} \quad (1.13)$$

T_e and V_{N-e} are mono-electronics, whereas V_{e-e} is bi-electronic which complicates the treatment of the wave function ψ_e .

4.3. Hartree Fock Approximation

The complexity of the Schrodinger equation is caused by the electron-electron interactions. One solution is to introduce molecular orbital (MO). This approximation suggests to decompose the multi-electronic wave function, $\psi(1,2, \dots, n_e)$ into a product of n_e mono-electronics spin-orbitals $\varphi_i(i)$ [89], assumed to be normalized and which each describe an electron. The simplest among them is the approximation of independent particles (Hartree) [90]. This situation physically corresponds to a model of independent particles, the multi-electronic wave function is expressed as follows.

$$\psi(1,2, \dots, n_e) = \varphi_1(1) * \varphi_2(2) * \varphi_3(3) \dots * \varphi_{n_e}(n_e) \quad (1.14)$$

Where each spin-orbital $\varphi_i(i)$ is the product of a space function and a spin function.

$$\varphi_i(r_i, s_i) = \chi_i(r_i)\eta_i(s_i) \quad (1.15)$$

Where r and s are the space and spin coordinate, respectively.

Hartree and fock have generalized the concept by demonstrating that the Pauli's principle of exclusion has been respected if we write the wave function in the form of discriminate constructed from n_e spin-orbitals.

$$\psi(1,2, \dots, n_e) = \frac{1}{\sqrt{n_e!}} \begin{vmatrix} \varphi_1(1) & \varphi_2(1) & \varphi_3(1) & \dots & \dots & \varphi_{n_e}(1) \\ \varphi_1(2) & \varphi_2(2) & \varphi_3(2) & \dots & \dots & \varphi_{n_e}(2) \\ \varphi_1(3) & \varphi_2(3) & \varphi_3(3) & \dots & \dots & \varphi_{n_e}(3) \\ \vdots & \vdots & \ddots & \ddots & \dots & \vdots \\ \vdots & \vdots & \ddots & \ddots & \dots & \vdots \\ \varphi_1(n_e) & \varphi_2(n_e) & \varphi_3(n_e) & \dots & \dots & \varphi_{n_e}(n_e) \end{vmatrix} \quad (1.16)$$

$$F\varphi_i(i) = \varepsilon_i\varphi_i(i) \quad (1.17)$$

Where F is the Hartree Fock operator for an electron defined by the following formula:

$$F(1) = T_e(1) + V_{N-e}(1) + \sum_i (J_i(1) - K_i(1)) \quad (1.18)$$

Where:

$J_i(1) = \int \varphi_i^*(2) \frac{1}{|r_1-r_2|} \varphi_j(2) dr_2$ represents the Colombian operator, it represents the average potential created by the other electrons.

And $K_i(1)\varphi_j(1) = \varphi_i(1) \int \varphi_i^*(2) \frac{1}{|r_1-r_2|} \varphi_j(2) dr_2$ is the exchange operator defined by its action on spin-orbital φ_j .

The eq (1.18) suggests that Fock operator is depending explicitly of its solutions, the resolution of this eq can be made by an iterative method.

The problem is to look for the best spin-orbitals conferring the lowest energy possible on the system, accordingly to the variational principle, this will be achieved by using the self-consistent method of Hartree Fock, that are solved by iterative methods, where the fock operator is updated at each iteration according to the spin-orbital's computed at the previous iteration. The calculation is considered complete when a convergence considered sufficient (on the energy, the wave function...) is reached.

The main problem of the Hartree-Fock theory is that it does not take into account the electronic interaction correlations and the correlation energy which is essential to realistic description of the molecular systems.

4.4. Density functional theory

The basic idea of the DFT is to seek to formulate the exact energy of the ground state of a molecular system from a functional of density electronic ρ . This system is composed of N electrons, at the position r_i subjected to the potential V_{ext} exerted by the nuclei with charge Z_i at position R_i , which the ground state of the system is not degenerated. The electronic density ρ is a functional of the external potential V_{ext} . In 1964 Hohenberg and Kohn [91] demonstrated by absurdity that the converse is also true, i.e. the external potential $V_{ext}(r)$, is with a constant is the unique functional of $\rho(r)$.

4.6.1. Hohenberg and Kohn Theorems:

The electronic density of a system with n electrons associated to the wave function $\Psi(r_1, r_2, \dots, r_n)$ for the electron 1 is given by the following expression:

$$\rho(r_1) = \int |\Psi(r_1, r_2, \dots, r_n)|^2 dr_2 dr_3 \dots dr_N \quad (1.19)$$

Where $\Psi(r_1, r_2, \dots, r_n)$ standardized to unity, is the wave function at the ground state. The DFT is based on two theorems by Hohenberg and Kohn [92] initially demonstrated for a non-degenerated ground state. The first establishes the existence of a functional of the density ρ and the second enunciated a variational principle by ratio to ρ . The one-to-one relationship between density ρ of the ground state and external potential V_{ext} is the foundation of the first theorem stated by Hohenberg and Kohn.

4.6.2. The first theorem of Hohenberg and Kohn:

The extern potential $V_{ext}(r)$ is an additive constant functional of $\rho(r)$. Consequently, as the Hamiltonian of the system is defined by $V_{ext}(r)$, the ground state energy is a functional of the unique $\rho(r)$.

So, if the electronic density $\rho(r)$ is known we can access to the number of electrons, the extern potential, and the total energy $E[\rho(r)]$, which can be formulated as follow:

$$E[\rho(r)] = F_{HK}[\rho] + \int \rho V_{ext} \quad (1.20)$$

$$E[\rho(r)] = T_{el}[\rho] + V_{el-el}[\rho] + V_{el-N}[\rho] \quad (1.21)$$

$$F_{\text{HK}}[\rho] = T_{\text{el}}[\rho] + V_{\text{el-el}}[\rho] \quad (1.22)$$

Where $F_{\text{HK}}[\rho]$ is the functional of Hohenberg-Kohn that includes the kinetic energy $T_{\text{el}}[\rho]$ and the inter –electronic interactions $V_{\text{el-el}}[\rho]$, however $V_{\text{el-el}}[\rho]$ represents the electron-nuclear interaction.

4.6.3. The second theory of Hohenberg-Kohn

The total energy functional of any multi-particle system has a minimum which corresponds to the density of the particle in the ground state.

This theorem is the basic of the variational principle expressed for $E[\rho(\mathbf{r})]$ the density functional energies. As the test density defines its own Hamiltonian and event its own test wave function. So, we have a correspondence between the variational principle in its wave function version and its electronic density version:

$$\begin{aligned} \langle \psi_{\text{test}} | H | \psi_{\text{test}} \rangle &= E[\rho_{\text{test}}] \geq E[\rho_{\text{ground}}] \\ &= \langle \psi_{\text{ground-state}} | H | \psi_{\text{ground-state}} \rangle \end{aligned} \quad (1.23)$$

4.5. Kohn and Sham equations:

In 1965, Kohn and Sham (KS) [93] proposed a new method in which the wave function ψ_{KS} describes n electrons system without interaction and subjected to an effective potential $V_{\text{eff}}(\mathbf{r})$. Each of these electrons is described by mono-electronic wave functions that verify:

$$\left[-\frac{1}{2} \nabla^2 + V_{\text{eff}}(\mathbf{r}) \right] \varphi_i = \epsilon_i \varphi_i \quad (1.24)$$

$$\text{Where } V_{\text{eff}}(\mathbf{r}) = V_{\text{ext}}(\mathbf{r}) + \int \frac{\rho(\mathbf{r}_j)}{|\mathbf{r}_i - \mathbf{r}_j|} d\mathbf{r} + V_{\text{xc}}(\mathbf{r}) \quad (1.25)$$

We cover all the particles, so the total Hamiltonian of this system is as follows:

$$H_{\text{KS}} = \sum_i^N -\frac{1}{2} \nabla_i^2 + \sum_i^N V_{\text{eff}}(\mathbf{r}_i) \quad (1.26)$$

The determination of the lowest n eigen values of the mono-electronic Hamiltonians of the equation (1.26) allows then to establish the formulation for the multi-electronic wave function of the system's ground state.

$$\Psi_{KS} = \frac{1}{\sqrt{n!}} \det[\varphi_1 \varphi_1 \dots \varphi_n] \quad (1.27)$$

The kinetic energy of the system is given by:

$$T_{KS}(\rho) = \langle \Psi_{KS} | \sum_i^N -\frac{1}{2} \nabla_i^2 | \Psi_{KS} \rangle \quad (1.28)$$

$$T_{KS}(\rho) = \sum_i^N \langle \varphi_i | -\frac{1}{2} \nabla_i^2 | \varphi_i \rangle \quad (1.29)$$

The electronic density associated is then:

$$\rho(\mathbf{r}) = \sum_i^N |\varphi_i(\mathbf{r}, S)|^2 \quad (1.30)$$

The equations. (1.26), (1.28), (1.29) are called the Kohn-Sham equations, they must be resolved by the self-consistent way since V_{eff} depends on the density. They show that one can always replace the problem to N-body of the electronic density of the unknown ground state, by an equivalent set of self-consistent equations.

From equation (1.21) we can write:

$$F_{HK}[\rho] = T_{KS}[\rho] + J[\rho] + E_{xc}[\rho] \quad (1.31)$$

Where
$$E_{xc}[\rho] = T[\rho] - T_{KS}[\rho] + V_{e-e}[\rho] + J[\rho] \quad (1.32)$$

Is the energy of exchange and correlation. By injecting (26) into (13) we obtain:

$$E_{HK}[\rho] = T_{KS}[\rho] + J[\rho] + E_{xc}[\rho] + \int \rho V_{ext}(\mathbf{r}) d\mathbf{r} \quad (1.39)$$

4.6. Kohn-Sham equation resolution

As we have already said, the Kohn-Sham equation should be solved by self-consistent way. The self-consistent solution is obtained by means of an iteration process as shown in figure (2.1). It is important to return here to the significance of the states of one electron ψ_i and their corresponding energies ϵ_i . Indeed, these energies have no physical meaning. With the same manner the eigenvectors of the eq 2.17 do not reflect any physical reality. However, it is quite common to interpret the energies as excited energies of the electron and also to use the state as the corresponding electron wave function. It has been shown that the Fermi energy of this system of particles is independent [94], i.e. the energy ϵ_n in the highest occupied state, is actually the output work of this system.

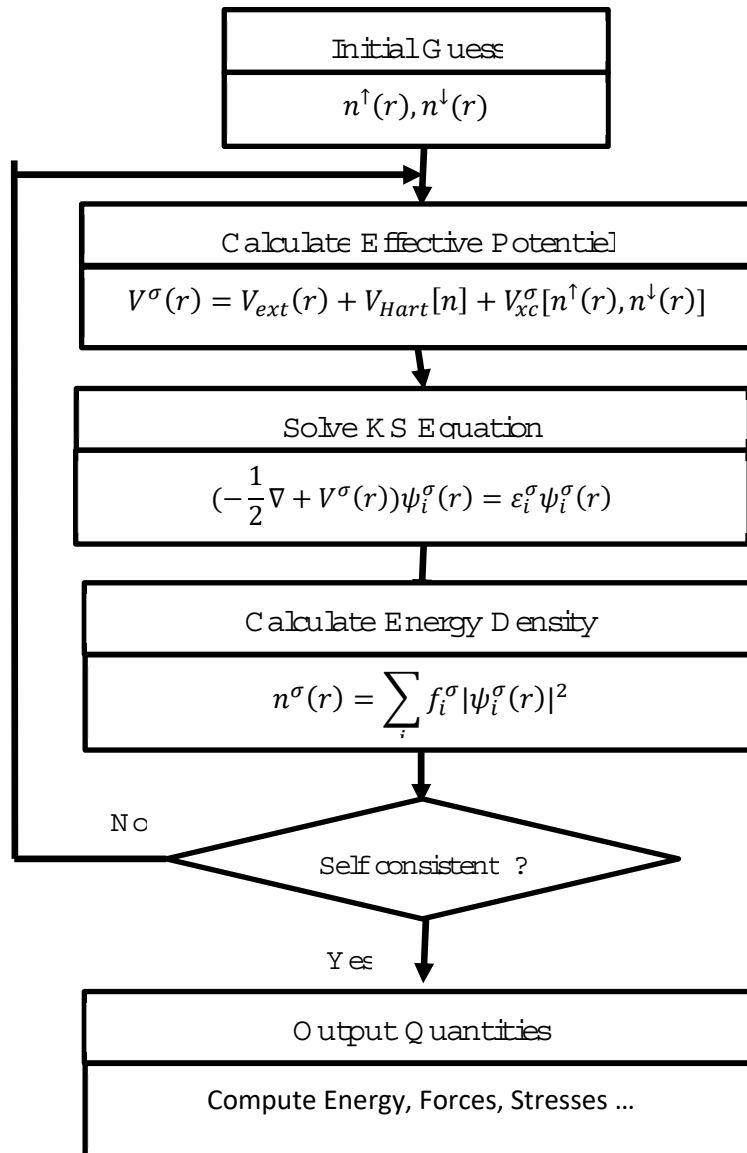


Figure 2.1 Self-consistent flowchart for solving the equations of Kohn-Sham.

The difficulty resides in the evaluation of the exchange-correlation energy $E_{xc}[\rho]$ whose exact expression is known only for a free electron gas.

4.6.1. Processing the exchange-correlation energy

In order that DFT and Kohn-Sham equations become useful in practice we need to propose a formulation of the exchange-correlation term which represents the smallest contribution of energy, see figure 2.2. And what's why, we have to go through different approximations.

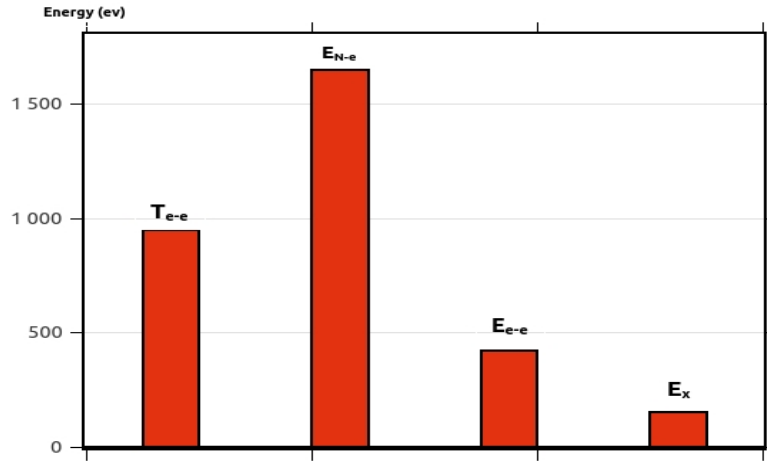


Figure 2.2 The contribution rate of each Energy.

1.1.1 Local density approximation

The local density approximation LDA is based on the known expression of the exchange-correlation energy of the homogenous gas of electrons. The basic assumptions of this approximation are given by the following equations:

$$E_{xc}^{LDA}[\rho] = \int \epsilon_{xc}(\rho(r))\rho(r)d^3r \quad (1.40)$$

Where ϵ_{xc} represents the exchange-correlation energy per particle, in the case of a homogenous gas. Finding this functional is not trivial, in fact it is the subject of many studies that determine the values of the exchange-correlation's functional. The first precise assessments were made in 1980 by D. Ceperly and B.J Alder [95], it is based on an interpolation of the results of very precise quantum Monte Carlo calculations on the uniform gas of electrons. Other approximations have obtained more successes such as that established by Vosko, Wilk and Nussair (VWN) [96], and also the Perdew approximation.

What is surprising in the LDA is the estimation of the energy of exchange-correlation of an inhomogeneous system using infinitesimal parts. The results of a homogeneous electron gas with a density equal to the local density of the inhomogeneous system. This method is reliable but it does not give very good results.

4.6.2. Local Spin Density Approximation (LSDA)

An extension of the LDA, which takes into account the contribution of spin polarization called Local Spin Density Approximation (LSDA). The exchange-correlation functional distinguishes the up and the down densities in the form:

$$E_{xc}^{LDA}[\rho_{\uparrow}, \rho_{\downarrow}] = \int \epsilon_{xc}(\rho_{\uparrow}(r), \rho_{\downarrow}(r)) \rho_{\uparrow}(r) \rho_{\downarrow}(r) d^3r \quad (1.41)$$

Where $\rho(r) = \rho_{\uparrow}(r) + \rho_{\downarrow}(r)$ (1.42)

Although it is very powerful at describing atoms or molecules, the LSDA is a formalism that can describe magnetism in solids. But the problem of the LDA is that it is not suitable to describe systems containing delocalized electrons.

4.6.3. Generalized Gradient Approximation (GGA)

The LDA tends to underestimate bond lengths and leads to too much cohesive energies. For this reason, Generalized Gradient Approximation GGA is preferred in these cases. GGA develops the expression of the exchange-correlation energy with respect to the first order of the gradient of the eq. 2.13, namely:

$$E_{xc}^{GGA}(\rho(r), |\nabla\rho(r)|) = \int \epsilon_{xc}^{GGA}(\rho(r), |\nabla\rho(r)|) \rho(r) d^3r \quad (1.43)$$

Where GGA is a function of the local density and the xc gradient of the local density. As in LDA there are different parameterizations of the GGA functional. The most used xc functional is Perdew, Burke and Ernzerhof [97].

Chapter 2

Numerical Methods

1. Introduction

Computational physics also, called computer simulations based conceptually on computer coding are of great interest to determine various physical properties and other complicated systems, computer simulations allow to represent the functioning of a system composed of different midpoint of activities, to highlight the characteristics of these systems and the interactions between them, to describe the circulation of different objects treated by these processes, thereby the use of this part may be a key role to more understand certain unclear and complex behavioursism of several properties of systems where analytical methods are not possible, furthermore these simulations may lead to customize the cost of the expensive experiments in laboratories and time consuming, simulating open the door to create new classes of materials.

2. Monte Carlo Simulation

3.1. Introduction

Monte Carlo Simulation is one of the most powerful class of stochastic methods used in computational physics by means of computer algorithms, unlike Molecular Dynamics, that allows calculating atomic trajectories by integrating the laws of classical mechanics to deduce the dynamic and thermodynamic properties of a particle assembly, the Monte Carlo method performs an exploration of the space of configurations accessible to the system subjected to particular thermodynamic conditions. This tool was emerged with the appearance of computer; it is generally based on probabilistic technique using random numbers which are generated during the simulation, it can solve a wide range of complicated problems where analytical solutions are not possible, that might be deterministic in several topics such as statistical physics, mathematics, medicine, Economy, sociology and various other domains.

3.2. Ising Model

The Ising model was first conceived by Wilhelm Lenz in 1920, who suggested it as a model of ferromagnet, on Ph.D. topic for his graduate student Ernst Ising who was able to resolve the problem exactly for 1D case and was published in 1925 [98], then, it was developed after by the Norwegian-born chemist Lars Onsager who earned in 1944 [99] the Nobel prize award in chemistry for his studies of nonequilibrium thermodynamics. This model is considered as the simplest one, it can be represented by magnetic dipole moments of atomic spins that can only possess two possible values +1 or -1, thus, it is an appropriate model which can treat and

examine the magnetic properties, Difference between this model and Heisenberg is that the first one consider the spins as scalars however the Heisenberg model consider it as operators (that means vectors in three dimensions which can point in all directions). The Ising model can be defined by a Hamiltonian for a system that is independent on the arrangement of variable spins on a lattice and it can be described by the following formula:

$$H = -J \sum_{\langle ij \rangle} S_i S_j - h \sum_i S_i \quad (2.1)$$

Where $\langle ij \rangle$ means that we sum over the nearest-neighbour pair of spins. And J is the coupling and h is the energy involved in the magnetization of the lattice invoked also the dimensionless. The partition function contains all of the essential information about the system under consideration because if we know it then, most thermodynamic quantities can be deduced from it. The partition function Can be calculated from the Hamiltonian as follow:

$$Z = \sum_{\langle i,j \rangle} e^{-E(\sigma)/T} \quad (2.2)$$

However, the thermal expectation value of a function $A(\sigma)$ can be expressed as follow:

$$\langle A \rangle = \frac{1}{Z} \sum_{\sigma} A(\sigma) e^{-E(\sigma)/T} \quad (2.3)$$

Where the summation is running over all spin states σ of the system. Z represents the partition function, here for simplicity we consider $K_B = 1$ is the Boltzmann's constant. In the ground state ($T \rightarrow 0$), for ferromagnetic couplings (i.e $J < 0$) there are only two contributing spin configurations; all spins are up or the inverse. For antiferromagnetic couplings (i.e $J > 0$) are also two lowest-energy configurations if the lattice is bipartite, i.e., if the system can be subdivided into two sublattices such that all interacting pairs $\langle i, j \rangle$ have one member on each sublattice.

The probability to find the system on state α at time t during the simulation is a set of the weight $P_{\alpha}(t)$ of this state in the real system. Following it is necessary to create a dynamic of choice to this kind of simulations which means the rule to pass from state to other trough the simulation. every particular state of the system is also determined by the partition function. So, the master equation for the evolution of $P_{\alpha}(t)$ in terms of the rates $W(\alpha \rightarrow \beta)$ is given as following:

$$\frac{dP_\alpha}{dt} = \sum_{\beta} [P_\beta(t)W(\alpha \rightarrow \beta) - P_\alpha(t)W(\alpha \rightarrow \beta)] \quad (2.4)$$

The term dP_α/dt of this equation represents the rate at which the system is undergoing transitions into state α the second term is the rate at which it is undergoing transitions out of α into other states β . The probabilities $dP_\alpha(t)$ must also obey the sum rule

$W(\alpha \rightarrow \beta)$ are chosen of manner that the solution which guide to the equilibrium are proportional to the Boltzmann factor. Therefore, the probability that the system is in the state α , is described as follow:

$$P_\alpha = \frac{e^{-E_\alpha/T}}{Z} \quad (2.5)$$

3.3. Ergodicity

The main idea of ergodicity condition is that all states of the system can be visited that means that the system can from a given state through the Markov chain, reach to any state of the system after a long sufficiently time. For instance, if transition probability is not possible from a given state is null, thus, the ergodicity is broken. The different states are not equiprobable which means they do not have all the same probability, however the probability that the system pass from a state to other is not null and all configurations are possible.

3.4. Importance sampling and Markov chain

At low temperature when we have large N , simulating the system using MC becomes complicated because we can sample only very small fraction and the system is dominated by configurations with large ordered domains which are more complicated to be generated within a random sampling, to overcome this the configuration. Monte Carlo thermic consist to choose a sample which contains the dominant states, this operation is invoked the importance sampling.

Conceptually, Monte Carlo method employs the Markov chain to generate the random numbers. Transition from current state “ α ” to another state “ β ” is related only to the first one (the “ α ” configuration). Then, this implies that transition, which can follow the probability, $W(\alpha \rightarrow \beta)$ is almost local in time. We can define a Markov chain as follows:

$$\{ \dots \xrightarrow{W} \{\sigma_i\} \xrightarrow{W} \{\sigma_i\}' \xrightarrow{W} \{\sigma_i\}'' \xrightarrow{W} \dots \} \quad (2.6)$$

Where W is the transition probability from a configuration " $\alpha \equiv \{\sigma_i\}$ " to a configuration " $\beta \equiv \{\sigma_i\}'$ ". This probability must respect the following conditions:

$$W(\{\sigma_i\} \rightarrow W(\{\sigma_i\}') \geq 0 \text{ for all } \{\sigma_i\}, \{\sigma_i\}' \quad (2.7)$$

$$\sum_{\{\sigma_i\}'} W(\{\sigma_i\} \rightarrow W(\{\sigma_i\}') = 1 \text{ for all } \{\sigma_i\} \quad (2.8)$$

$$\sum_{\{\sigma_i\}} W(\{\sigma_i\} \rightarrow W(\{\sigma_i\}') P_\alpha(\{\sigma_i\}) = P_\alpha(\{\sigma_i\}') \text{ for all } \{\sigma_i\}' \quad (2.9)$$

Monte Carlo Simulations process is based on the generation of a Markov chain which can be generated by a succession of Markov process of states, this process is chosen to respect the Boltzmann's probability. This process which Leads to the equilibrium is known also as the coming to the equilibrium this invocation reflects that the simulation describes correctly the evolution of a real system. Thus, a simple choice for W fulfilling the necessary conditions is given in terms of the energy change $\Delta E = H(\{\sigma_i\}') - H(\{\sigma_i\})$, as proposed by Metropolis.

It is worthy to note that in order to reach the Markov process, it is necessary that two supplementary conditions must be achieved. The ergodicity and the detailed balance.

3.5. Detailed Balance

In the ergodicity we have seen that all spin configurations are taken into the account in the calculations and thus they are generated by their correct Boltzmann probabilities. However, in order for the spin configurations to follow the Boltzmann probability distribution and not any other distribution, the algorithm must obey the detailed balance conditions. Conceptually, it can be defined as follow: each process is equilibrated by its reverse process. Thus, the system is in equilibrium and the transition rate from a state to the same state are equals, this can be expressed as follow:

$$\sum_{\beta} P_\alpha W(\alpha \rightarrow \beta) = \sum_{\alpha} P_\beta W(\beta \rightarrow \alpha) \quad (2.10)$$

Using eq (2.9), this eq can be simplified to

$$P_\alpha = \sum_{\alpha} P_\beta W(\beta \rightarrow \alpha) \quad (2.11)$$

Because of the Markov dynamic's process, for each transition probabilities that subjected to the above eq can be considered as an equilibrium state, however fulfilling this equation do not guarantees to get equilibrium from any state of the system.

We note that it is ubiquitous that the Markov process enter in limited cycle which mean that the system does not reach the equilibrium, to overcome this problem, the flowing condition is imposed.

$$P_\alpha W(\alpha \rightarrow \beta) = P_\beta W(\beta \rightarrow \alpha) \quad (2.12)$$

The eq (2.12) represents the balance detailed condition, it can exclude the evolution to the limited cycle. The detailed balance is respected on real systems, furthermore, if we look that the distrubition responsible on the equilibrium is the Boltzmann distribution, then

$$\frac{W(\alpha \rightarrow \beta)}{W(\beta \rightarrow \alpha)} = \frac{P_\beta}{P_\alpha} = e^{-\Delta E/T} \quad (2.13)$$

Where $\Delta E = E_\beta - E_\alpha$ represents the energy difference between the energy in the state β and the state α respectively.

3.6. Observables Averaging

The observables of particular interest are $\langle E \rangle$, $\langle E^2 \rangle$, $\langle M \rangle$, and $\langle M^2 \rangle$.

These are calculated in the following way,

$$M = \frac{1}{N} \sum_i^N M(i) \quad (2.14)$$

According to the Hamiltonian of the system, the energy can be described as following:

$$\langle E \rangle = \left\langle \frac{1}{2} \sum_i^N H_i \right\rangle = \frac{1}{2} \left\langle -J \sum_{\langle i,j \rangle}^N S_i S_j \right\rangle \quad (2.15)$$

The factor of a half is introduced in order to account for the spins being counted twice. Equation (2.15) is used in a similar way to determine $\langle E^2 \rangle$ At the Curie temperature we expect a marked fluctuation in these quantities. A good candidate to illustrate this fluctuation would be the variance $\Delta(A^2) = \langle A^2 \rangle - \langle A \rangle^2$ This leads us to the logical conclusion of calculating the heat capacity, C , and the susceptibility, χ :

$$C = \frac{\partial E}{\partial T} = \frac{(\Delta E)^2}{T} = \frac{\langle \Delta E \rangle^2 - \langle \Delta E^2 \rangle}{T^2} \quad (2.16)$$

$$\chi = \frac{\partial M}{\partial T} = \frac{(\Delta M)^2}{T} = \frac{\langle \Delta M \rangle^2 - \langle \Delta M^2 \rangle}{T} \quad (2.17)$$

3.7. Practical implementation of the Metropolis algorithm

The main idea behind Monte Carlo simulation is to test different configurations of spins that we will reject or accept according to their weight in the Boltzmann statistics. In Monte Carlo calculations, the dynamic behaviour of an atomic system for example, following random modifications imposed on the system: spin interacting, modification of the dihedral angles, displacement of the atoms, etc. The succession of random modifications imposed on an initial three-dimensional structure forms a set of configurations. The sampling procedure can be described as follows: by means of a random number generator, a randomly selected atom is moved in any direction and the energy of the new configuration obtained after that displacement is calculated. If this energy is lower than the previous configuration, that means the energy has been minimized which lead to the equilibrium, thus, the new configuration is accepted. If, on the other hand, the energy of the new configuration is greater than that of the old one, the Metropolis algorithm makes it possible to decide whether the new configuration should be retained or not.

The probability that the new configuration is kept depends on its Boltzmann factor, which is $B = e^{-E/T}$, In other words, a number μ of the random interval $[0, 1]$ is compared with the Boltzmann factor B . If μ is less than B , the new configuration is accepted. Otherwise, it will be rejected and the old configuration is again subjected to another elementary disturbance. The set of configurations retained is thus progressively constructed and forms a Markov chain. This is a natural way of searching for conformational space. The resulting structures may be the starting point for future minimization. The Metropolis algorithm can be summarized as follows:

- ✓ The initialization step: construct an initial energy E_α
- ✓ Do a random change of this initial state by e.g., flipping an individual spin α to a new state β energy with the energy E_β . Calculate then $\Delta E = E_\beta - E_\alpha$
- ✓ If $\Delta E \leq 0$ accept the new configuration.
- ✓ If $\Delta E > 0$, calculate the value $W = e^{-\beta \Delta E}$
- ✓ Generate a random number r and compare it the computed value W ,
If $r \leq W$ accept the flip, else go back to the previous configuration.
- ✓ Compute the averaging observables in the sums, $\sum A_s W_s$.
- ✓ Repeat the above steps in order to have a large enough number of microstates
- ✓ For a given number of MC cycles, compute then expectation values.

The Metropolis Flowchart can be represented as depicted in the following figure

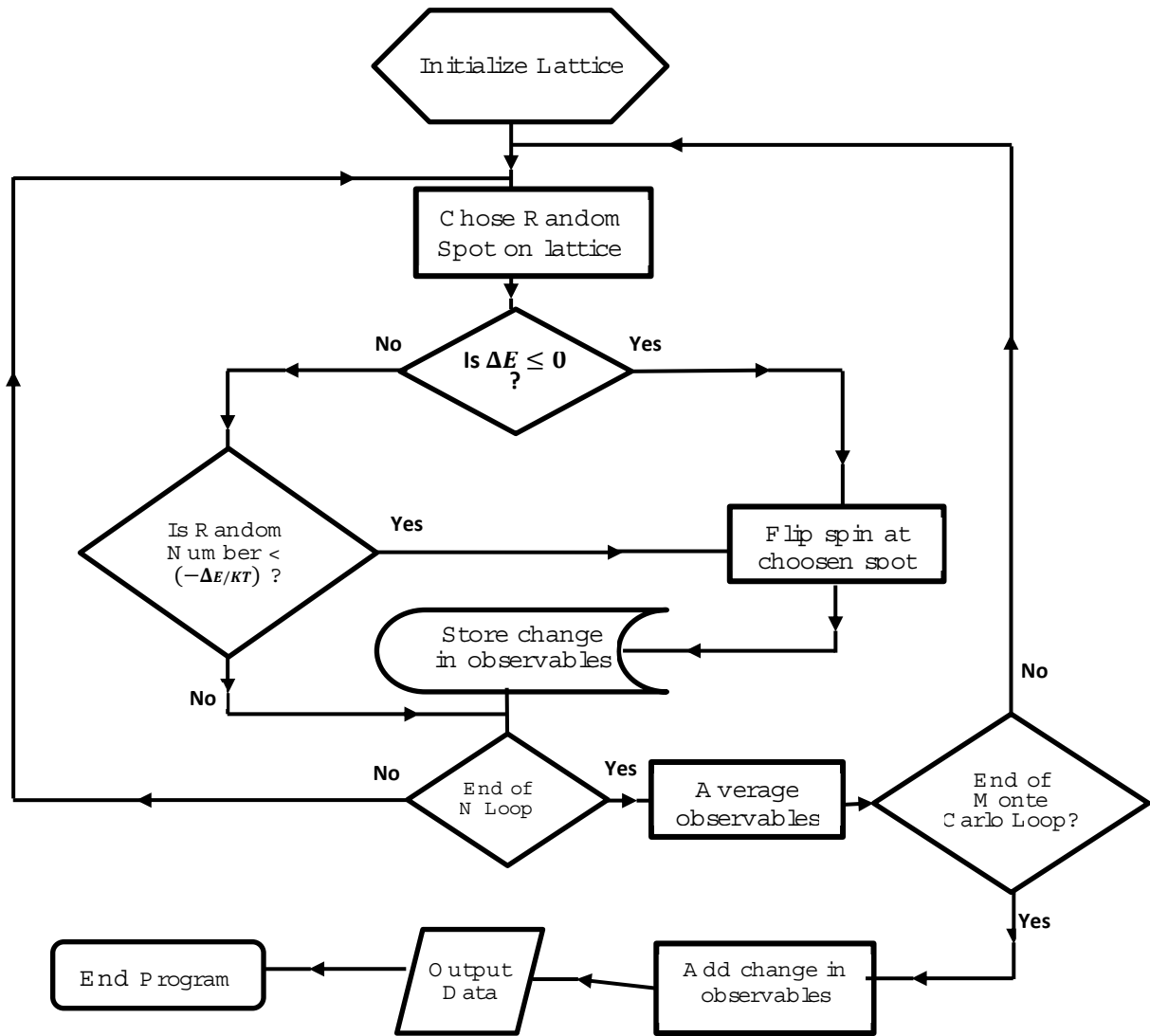


Figure Metropolis Flowchart.

3.8. Other kind models of spins

2.8.1 Heisenberg Model

The Heisenberg model, introduced by Werner Heisenberg in 1928, it is a statistical mechanical model used to describe the interaction between neighbouring spins which leads to long range ferromagnetic order [100] This model usually, allows to study magnetic properties of magnetic systems, their critical points and phase transitions. One writes the Hamiltonian of such model as follows

$$H = -J \sum_{\langle i,j \rangle} \vec{S}_1 \vec{S}_2 \quad (2.18)$$

Where J is the exchange coupling between spins at site i and j , and $\langle i, j \rangle$ design the sum over all nearest neighbours spin pair.

$$\vec{S}_i \vec{S}_j = S_i^x S_j^x + S_i^y S_j^y + S_i^z S_j^z \quad (2.19)$$

If we take on consideration the applied extern field \vec{h} on to the system, the expression of the Hamiltonian becomes

$$H = -J \sum_{\langle i, j \rangle} S_i^x S_j^x + S_i^y S_j^y + S_i^z S_j^z - \vec{h} \cdot \sum_{i=1}^N \vec{S}_i \quad (2.20)$$

$$\vec{h} \cdot \vec{S}_i = S_i^x h_x + S_i^y h_y + S_i^z h_z \quad (2.21)$$

Then

$$H = -J \sum_{\langle i, j \rangle} S_i^x S_j^x + S_i^y S_j^y + S_i^z S_j^z - \sum_{j=1}^N S_i^x h_x + S_i^y h_y + S_i^z h_z \quad (2.22)$$

Which is the XYZ model, \vec{S}_i vectors represent Pauli spin matrices. In the case of the spin- 1/2 these matrices are given by

$$S^x = \begin{bmatrix} 0 & 1 \\ 1 & 0 \end{bmatrix}, S^y = \begin{bmatrix} 0 & -i \\ i & 0 \end{bmatrix}, S^z = \begin{bmatrix} 1 & 0 \\ 0 & -1 \end{bmatrix} \quad (2.23)$$

2.8.2 Potts Model

In statistical physics, the Potts model is a generalization of the Ising model. It is a model of interaction of spins on a crystal lattice. This model makes it possible to understand the behaviour of ferromagnetic materials. It is also used to explain certain phenomena relating to solid state physics such as phase transitions and the magnetic properties of periodic layered structures. The Potts model is similar to the Ising model, except that the spin if on each site of the network can take more than two different discrete values [101]. Usually these values are represented by positive integers from 1, and the Potts model with q states is one in which each spin can have integer values. $\sigma_i = 1 \dots q$. The Hamiltonian can be expressed as following:

$$H = -K \sum_{\langle i, j \rangle} \delta_{\sigma_i, \sigma_j} \quad (2.24)$$

The delta function insures that only when neighbouring spins, defined by σ , are equal will the energy be lowered. The sign of the K coefficient determines ferromagnetism versus anti-ferromagnetism, it is easy to verify that the Potts model with $q=2$ is reduced to the Ising model.

2.8.3 Blume-Emery-Griffiths Model

The Blume-Emery-Griffiths (BEG) model is a spin-1 Ising model. It was originally inspired by the experimental observation that the continuous superfluid transition in He^4 with He^3 impurity becomes a first order transition into normal (He^3) and superfluid (He^4) phase separation above some critical He^3 concentration, the first analytical solution using mean field approximation was introduced in 1971 by Blume, Emery and Griffiths in order to explain the phase separation and superfluidity in the He^3 - He^4 mixtures [102]. This model was proposed to describe a system with three states per spin. It has two terms, the first takes the form:

$$H = -J \sum_{\langle i,j \rangle} S_i S_j \quad (2.25)$$

where the spin variable takes the value $S_i = -1, 0, 1$, $\sum_{\langle i,j \rangle}$ denotes a summation over all nearest-neighbours (NN) and J denotes the bilinear spin interaction which allows the appearance of the ferromagnetic order which is interpreted as a superfluid, such identification is purely phenomenological, when the concentration of He^3 atoms is zero the Hamiltonian H becomes an Hamiltonian for Ising ferromagnet. The presence of He^3 atoms is similar to an introduction of nonmagnetic impurities which affects the transition temperature T_c and the superfluidity when the concentration is sufficiently large because the mixture can support superfluid ordering by breaking into two phases (phase separation). To modulate this phase separation, they added a second term which describes the anisotropic interaction between the different entities which is presented by the generalized Hamiltonian:

$$H = -J \sum_{\langle i,j \rangle} S_i S_j - K \sum_{\langle i,j \rangle} S_i^2 S_j^2 + D \sum_i S_i^2 + h \sum_i S_i \quad (2.26)$$

J and K are respectively, the bilinear interaction and the biquadratic interaction. D and h are the crystal field and the magnetic field respectively.

3. Ab initio Calculations

3.1 Bloch theorem

In a crystal the nuclear positions and the electronic density are periodic, i.e. $f(\mathbf{r} + \mathbf{T}(n_1, n_2, n_3 \dots)) = f(\mathbf{r})$ for each translation of the Bravais lattice.

$$\mathbf{T}(n) = \mathbf{T}(n_1, n_2, n_3 \dots) = n_1 \mathbf{a}_1 + n_2 \mathbf{a}_2 + n_3 \mathbf{a}_3 + \dots \quad (2.27)$$

Using the translation properties on a translation operator, and the conditions on the boundary of the Born-Von-Karman (BVK), we therefore have the statement of Bloch's theorem [103]: The eigen functions of the Hamiltonian H to an electron in periodic potential $V(\rho(\mathbf{r}))$ have the shape of the product of plane wave for a function $U(\mathbf{r})$ having the periodicity of the lattice:

$$\psi(\mathbf{r}) = e^{i\mathbf{k}\mathbf{r}}U(\mathbf{r}) \quad (2.28)$$

The vector \mathbf{k} which characterizing the eigenvalues of the translation operator has therefore:

$$\psi(\mathbf{r}) = e^{i\mathbf{k}\mathbf{r}}U_{\mathbf{k}}(\mathbf{r}) \quad (2.29)$$

A wave vector obeying Bloch's theorem can be characterized by an infinite number of wave vectors $k_1, k_2, k_3 \dots$ such that:

$$k_i - k_j = G \quad (2.30)$$

Therefore one can restrict reciprocal space to the smallest and simplest domain, which is usually the first zone of Brillouin

3.2 The basic concepts of electronic structure calculations

We can summarize the essential steps for electronic structure calculations in the figure 2.3 below:

Figure 2.3 Representative diagram of the basic calculation methods of the DFT.

3.3 Pseudopotential:

As the size of the atoms increases, the calculations become more expensive, so the DFT, becomes useless and to overcome this problem we use a pseudo-potential.

The most studied physicochemical properties in molecular systems involve only valence electrons. It is therefore not to explicitly treat the core electrons and replace their effects on the valence electrons by a fictitious potential, commonly called pseudo-potential.

The core electrons have two effects on the valence electrons: they give classical electrostatic and exchange-correlation contributions to the energies of valence layers and they prevent them from penetrating the core, during the minimization of the electronic energy. But to describe the rapid oscillations of the wave function in the core region, All Electron calculations require a large number of plane waves. To render the calculations realizable, two approximations are made: firstly, we consider the electrons inside a certain radius of the nuclei of the atoms, called the cut-off radius r_c , as “frozen”, in a second step, the electrons inside this sphere are replaced by a so-called pseudo-potential operator whose function is to reproduce their action on the valence electrons by reducing the number of parameters to be optimized during the electronic minimization calculations. The valence electrons are thus described by a series of pseudo-functions [104]. The valence pseudo-functions have a behaviour “softer” and “easier” to describe the core region, but, from the cut-off radius they have the same behaviours as the valence electrons of the real atom.

3.4 FLAPW

The resolution of the Schrödinger equation can be done by projecting the electronic wave function on a set of bases of spatial functions, which amounts to transforming the problem of finding eigenvalues [105-106]. The wave function developed on these basic functions is as follows:

$$\psi_{k,v} = \sum_i C_{k,v}^i \varphi_i \quad (2.31)$$

Where k and v , denote the quantum numbers related to the wave function, i.e. the Bloch k wave vector and the band index v in the case of crystal, the index i allows to sum on all the basic functions φ_i . Using the plane wave as a basic function we have:

$$\varphi_G(\mathbf{r}) = \frac{1}{\sqrt{V}} e^{i\mathbf{G}\cdot\mathbf{r}} \quad (2.32)$$

The index \mathbf{I} corresponds to the wave vector \mathbf{G} of the plane wave, chosen in reciprocal space so as to ensure translational symmetry. The \mathbf{k} -dependence of Bloch waves is then contained in the Hamiltonian. The plane waves are orthogonal and normalized. There for, the Kohn-Sham equation can be written in the following matrix form:

$$(H_k^{GG'} - \epsilon_{k,v}) C_{k,v}^{G'} = 0 \quad (2.33)$$

Where $H_k^{GG'}$ are the elements of the Hamiltonian matrix of the Kohn-Sham equation. Making this equation in matrix form proves usefulness of numerical calculations.

3.5 KKR Method

The Kohn-Korringa -Rostoker (KKR) method is the method that allows to solve the Schrodinger equation without going through the determination of the values and eigenvectors of the Hamiltonian of the system [107]

3.5.1 Green Function

Mathematically: Either \hat{A} a differential operator. The Green function $G(\mathbf{r}, \mathbf{r}')$ [108] is the solution of the following equation:

$$\hat{A} G(\mathbf{r}, \mathbf{r}') = \delta(\mathbf{r} - \mathbf{r}') \quad (2.34)$$

If $G(\mathbf{r}, \mathbf{r}')$ is known it is possible to solve all the partial differential equations of the form:

$$\hat{A} \phi(\mathbf{r}) = f(\mathbf{r}) \quad (2.35)$$

Indeed, the solution of this equation is as follow:

$$\phi(\mathbf{r}) = \int G(\mathbf{r}, \mathbf{r}') f(\mathbf{r}') d\mathbf{r}' \quad (2.36)$$

To simplify, we work in reciprocal space and to define the uniqueness of a solution we apply the boundary conditions.

However, in solid state physics, the Green function is called the function which is determined by the solution of the following Schrodinger equation:

$$(-\partial_r^2 + V(r) - E)G(r, r'; E) = -\delta(r - r') \quad (2.37)$$

In this equation we assumed that $\frac{\hbar^2}{2m} = 1$

The relationship between Green's function and the wave function is as follows

$$G(r, r'; E + i\varepsilon) = \sum \frac{\psi_\alpha(r)\psi_\alpha^*(r')}{E + i\varepsilon - E_\alpha} \quad (2.38)$$

This function allows to calculate the following quantities:

Density of state $\rho(E)$ localized on an atom is given by:

$$\rho(E) = -\frac{1}{\pi} \text{Im} \int_{\Omega_{ws}} G(r, r, E) dr \quad (2.39)$$

The charge density $\rho(r)$ localised on an atom is given by the following:

$$n(r) = -\frac{1}{\pi} \text{Im} \int_{-\infty}^{E_f} G(r, r, E) dE \quad (2.40)$$

3.5.2 Green Function and Dyson equation

$$G(r, r'; E) = G_0(r, r'; E) + G_0(r, r'; E)\Delta V(r)G(r, r'; E) \quad (2.41)$$

Which give:

$$G(r, r'; E) = [1 + G_0(r, r'; E)\Delta V(r)]^{-1} G_0(r, r'; E) \quad (2.42)$$

3.5.3 Multiple scattering and the Green function of KKR

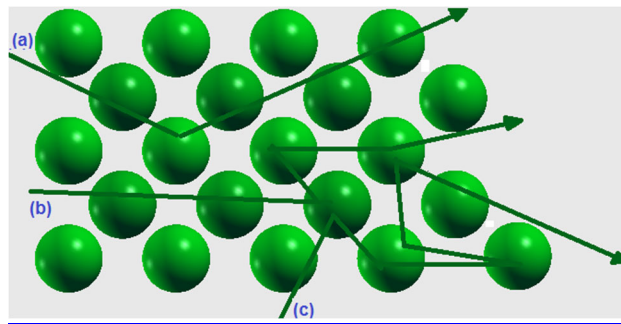


Figure1: Model of multiple scattering: an electron in motion between atoms

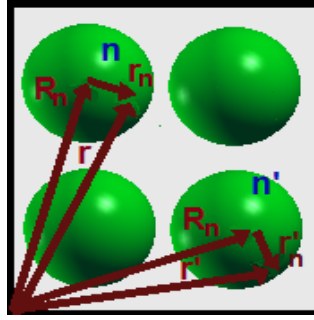


Figure2: Muffin tin model: The potential is Spherical on the atomic sphere,

When calculating G on a site where $r = r'$ and $n = n'$ [109]; it takes the following form:

$$G^\alpha(\vec{r}, \vec{r}, \varepsilon) = \sum_{LL} \left[z_l^\alpha(r, \varepsilon) \tau_{li}^\alpha Z_l^\alpha(\vec{r}, \varepsilon) - Z_l^\alpha(\vec{r}, \varepsilon) j_l^\alpha(\vec{r}, \varepsilon) \right] \quad (2.43)$$

$z^\alpha(\vec{r}, \varepsilon)$, $J^\alpha(\vec{r}, \varepsilon)$ and τ^α are successively the regular solution, the irregular solution and the path operator on the site

$$\tau^\alpha(E) = \frac{1}{N} \sum_{k \in \text{BZ}} \left[\frac{1}{t_\alpha^{-1} - B(k, \varepsilon)} \right] \text{With } B(\varepsilon, k) = \sum_n \exp(ikR_n) B(\varepsilon, k) \quad (2.44)$$

$$t_l^\alpha = -\frac{1}{\sqrt{E}} \exp(i\delta_l^\alpha) \sin \delta_l^\alpha \text{ Where } \delta_l^\alpha \text{ represents the phase shift}$$

$$L = l, m$$

$B(E, k)$ is the complex function of the crystal structure

k : reciprocal lattice vector

R_n : direct lattice vector

To study the electronic and magnetic structure of chemically disordered alloys, the Coherent Potential Approximation (CPA) is used. It consists of replacing τ^α by τ^{CP} .

The condition of the CPA is written on a site shared by different types of atoms:

$$\tau^{CP} = \sum_{\alpha} c_{\alpha} \tau^{\alpha} \quad (2.45)$$

Each type of atom is characterized by the index α and its occupancy rate c_{α}

$$\tau^{\alpha} = \left[1 + (t_{\alpha}^{-1} - t_{cp}^{-1}) \tau^{CP} \right]^{-1} \quad (2.46)$$

At the end of each cycle, we calculate τ^{CP} and t^{CP} , we deduce τ^α and t^α

Generally, one can calculate the density of state on a given site from the operator $\tau^\alpha(\mathcal{E})$.

$$n(\mathbf{\epsilon}) = -\frac{1}{\pi} \sum_L F_l(\mathbf{\epsilon}) \text{Im} \tau_{LL}^{00}(\mathbf{\epsilon}) \quad (2.47)$$

$$\text{Where } F_{l'}(\mathcal{E}) = \int_{\Omega} Z_{l'}(\mathcal{E}, r) Z_{l'}(\mathcal{E}, r) d^3 r \quad (2.48)$$

Chapter 3

Monte Carlo simulation of compensation behaviours for a mixed Spin- $5/2$ and spin- $7/2$ Ising system with crystal field interaction

1. Introduction

During the last few years, the study of critical phenomena in mixed–spin Ising systems has attracted considerable attention. These systems are of a great interest owing to their useful properties. For this aim, ferrimagnets, in which two sublattices have unequal magnetic moments regularly alternate and interact antiferromagnetically, seem to play a great role. Under appropriate conditions, ferrimagnets show a compensation point below the critical temperature at which the resultant moment vanishes because of the different temperature dependence of the sublattice magnetizations that compensate each other. In this chapter we use Monte Carlo simulation to study the magnetization of the mixed spin–5/2 and spin–7/2 Ising ferrimagnetic model on a square lattice with periodic boundary conditions. The total magnetization and the magnetizations of the two sublattices under the effects of exchange interactions and the crystal field anisotropy are studied. The ground–state diagrams are constructed. We obtained different types for the thermal dependence of magnetization. Compensation points where the global magnetization of the system vanishes have been detected for appropriate values of the system parameters.

The outline of this chapter is organized as follows: In section 2, we introduce the model and give the details of our simulation. In section 3, we present our numerical results and discuss the ground–state phase diagrams and magnetization. Finally, we summarize the main results of our study in section 4.

2. Simulation details

We study a 2D Ising model with spins $S=\pm 7/2, \pm 5/2, \pm 3/2, \pm 1/2$ and $\sigma=\mp 5/2, \mp 3/2, \mp 1/2$, located in alternating sites of a square lattice. The nearest neighbours are the S and the σ spins. However, the spins of the same type (S – S or σ – σ) are next–nearest neighbours. The Hamiltonian of the system being studied with spin–7/2 and spin–5/2 including first and second neighbour interactions and crystal field is given by the formula:

$$H = -J \sum_{\langle i,j \rangle} S_i \sigma_j - J_S \sum_{[i,j]} S_i S_j - J_\sigma \sum_{[i,j]} \sigma_i \sigma_j - \Delta_S \sum_i S_i^2 - \Delta_\sigma \sum_i \sigma_i^2 \quad (3.1)$$

Where $\langle i,j \rangle$ and $[i,j]$ denote summations over all nearest–neighbour and all next nearest–neighbour pairs of spins, respectively. J , $J_S(>0)$ and $J_\sigma(>0)$ are the bilinear exchange

interactions between spins S- σ , S-S and σ - σ , respectively. Δ_s and Δ_σ are the crystal-fields acting on the spins S and σ , respectively. All the calculations were performed with $J=-1$.

The system contains $N=L*L=10^4$ spins with L is the number of spins along each square axis. We use a single spin-flip algorithm and the Monte Carlo method to simulate the Hamiltonian described by (1). In each spin-flip attempt, a spin was randomly chosen from the possible projections with a uniform distribution, the probability of a particular configuration is proportional to the Boltzmann factor. The flips are accepted or rejected according to the Metropolis approximation [110]. Data were generated with 10^5 Monte Carlo steps per spin after discarding the first 10^4 steps per site for equilibrium. The periodic boundary conditions on the square lattice are taken into account. Our program calculates the sublattice magnetizations per site defined by:

$$M_S = \frac{2}{N} \left\langle \sum_{i=1}^{N/2} S_i \right\rangle \quad (3.2)$$

And

$$M_\sigma = \frac{2}{N} \left\langle \sum_{j=1}^{N/2} \sigma_j \right\rangle \quad (3.3)$$

The total magnetization is given by: $M=(M_s+M_\sigma)/2$. At the critical temperature T_c , $M(T_c)=M_s(T_c)=M_\sigma(T_c)=0$. By means of a Monte Carlo simulation, we explore the finite-temperature behaviours of the magnetization.

3. Results and discussion

In this section, we show and discuss some simulation results for the ferrimagnetic mixed spin- $7/2$ and spin- $5/2$ Ising model and the ground-state diagrams in the planes (J_s, J_σ) and (Δ_s, Δ_σ).

3.1. The J model

First, let us consider the case $J_s=J_\sigma=\Delta_s=\Delta_\sigma=0$. The ground-state diagram is given in Fig. 1. This diagram is similar to those for the mixed spins (2, 5/2) [111] and (3/2, 5/2) [112]. The

saturation values of the sublattice magnetizations are $|M_S(T=0)|=7/2$ and $|M_\sigma(T=0)|=5/2$. In these conditions, this model cannot display compensation behaviours.

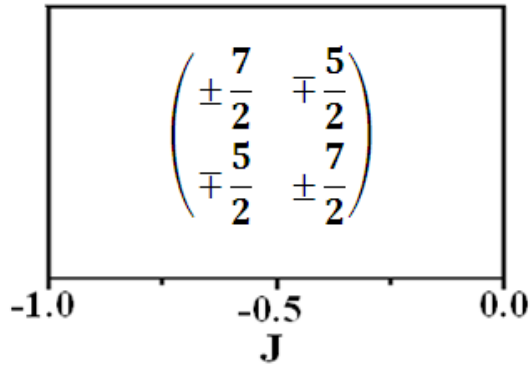


Fig. 1. The ground–state diagram for the J–model

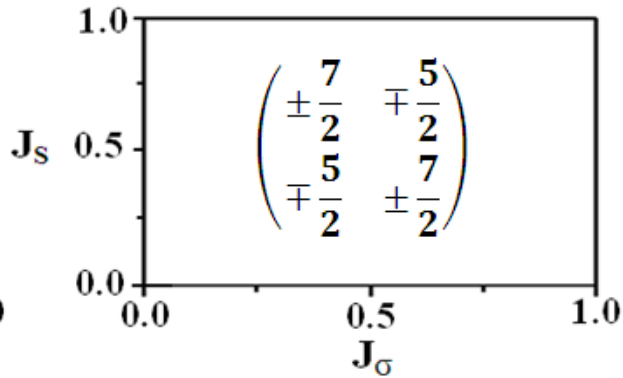


Fig. 2. The ground–state diagram in the plane (J_s, J_σ) when $\Delta_S=\Delta_\sigma=0$

Now we consider the case where the crystal field anisotropies are neglected ($\Delta_S=\Delta_\sigma=0$). We consider only the nearest and the next–nearest exchange interactions. We keep J_s fixed and vary J_σ and vice versa in order to study the effect of each exchange interactions J_s and J_σ . The Hamiltonian describing the system in this case is:

$$H = -J \sum_{\langle i,j \rangle} S_i \sigma_j - J_s \sum_{[i,j]} S_i S_j - J_\sigma \sum_{[i,j]} \sigma_i \sigma_j \quad (3.4)$$

The ground–state phase diagram is depicted in Fig. 2. At $T=0$, the saturation values of the sublattice magnetizations are $|M_S|=7/2$ and $|M_\sigma|=5/2$ for any values of J_s and J_σ . The topology of this diagram is similar to those obtained in Refs. [111-112] for $J_s > 0$ and $J_\sigma > 0$.

3.2.1. Effects of J_s for $J_\sigma=7.0$

To analyse the effect of J_s , we take $J_\sigma=7.0$ and vary J_s at $T>0$. To perform this, we carry out the partial $|M_S|$, $|M_\sigma|$ and total M magnetizations of our system. For some ferromagnetic exchange interaction values of J_s , the $-\sigma$ sublattice keeps magnetic order more than the S –sublattice at relatively higher temperatures. In Fig. 3, we plot the thermal behaviours of $|M_S|$, $|M_\sigma|$ and M for $J_s=1$ and 4 with $J_\sigma=7$. From Fig. 3(A), it can be seen that, as the temperature increases, the sublattice magnetization curves both decrease monotonically from the saturation values $|M_S|=3.5$ and $|M_\sigma|=2.5$ at $T=0$ as predicted in Fig. 2. Thus, $|M(T=0)|=0.5$. It is clear that there exists a crossing point between $|M_S|$ and $|M_\sigma|$ below T_c , for the value $J_s=1$. This point is called compensation temperature (T_{comp}), is defined by the two conditions: $M_S(T_{\text{comp}})=-M_\sigma(T_{\text{comp}})$ and $T_{\text{comp}}<T$, at which the sublattice magnetizations cancel each other,

giving rise to zero total magnetization: $M(T_{\text{comp}})=(M_S+M_\sigma)/2=0$ (Fig. 3(A)). When $T>T_{\text{comp}}$, $|M_S|$ and $|M_\sigma|$ begin to be disordered but the order remains a little for σ —spins because $|M_\sigma| > |M_S|$. Then, $|M_S|$, $|M_\sigma|$ and M all decay to zero at T_C . By contrast, Fig. 3(B) illustrates that the sublattice magnetizations do not cross at any point small than T_C and all curves go to zero at T_C , which implies that the compensation does not occur for $J_S=4$. This can be explained by the fact that $|M_\sigma|$ decreases faster than $|M_S|$ and σ —spins loss order more than S —spins as temperature increases.

Fig. 4 displays the variations of the total magnetization curves when $J_\sigma=7.0$ as functions of temperature. Fig. 4(A) demonstrates that there are compensation points for the selected values of J_S . Also, it is evident that J_S has an important influence on T_{comp} , but there is a slight effect on T_C . In fact, on increasing J_S , T_{comp} increases linearly as illustrated in Fig. 5 where the progress of T_{comp} as a function of J_S for several J_σ is plotted. However, T_C seems insensitive to the variation of J_S . As a result, the difference T_C-T_{comp} becomes smaller as J_σ increases, until T_{comp} disappears. Additionally, Fig. 5 shows clearly that, for a given value of J_σ , there is a maximum value of J_S above which compensation does not appear. Fig. 4(B) presents some examples of J_S values for which the system cannot exhibit compensation behaviours because the total magnetizations vanish only at T_C . Also, T_C is an increasing function of J_σ in absence of compensation. Our results in this case are similar to the ones obtained in Refs. [113]. It is worthy to note that J_S has no effect on the saturation value of the total magnetization at $T=0$ which is $M=0.5$.

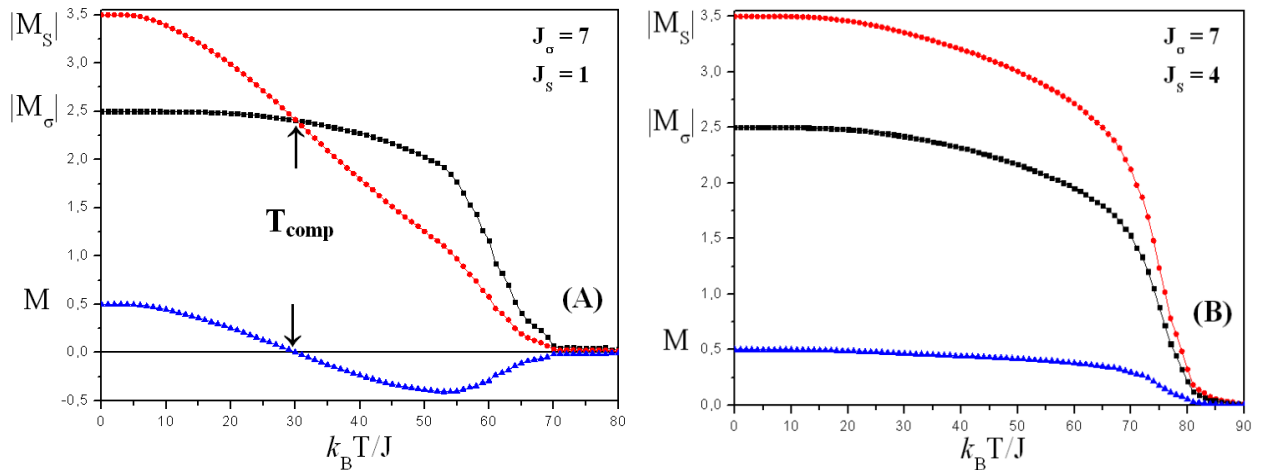


Fig. 3. Variations of the total magnetization M and the absolute values of the sublattice magnetizations $|M_S|$, $|M_\sigma|$ as functions of the temperature with $J_\sigma=7$ (A) for $J_S=1$ and (B) for $J_S=4$.

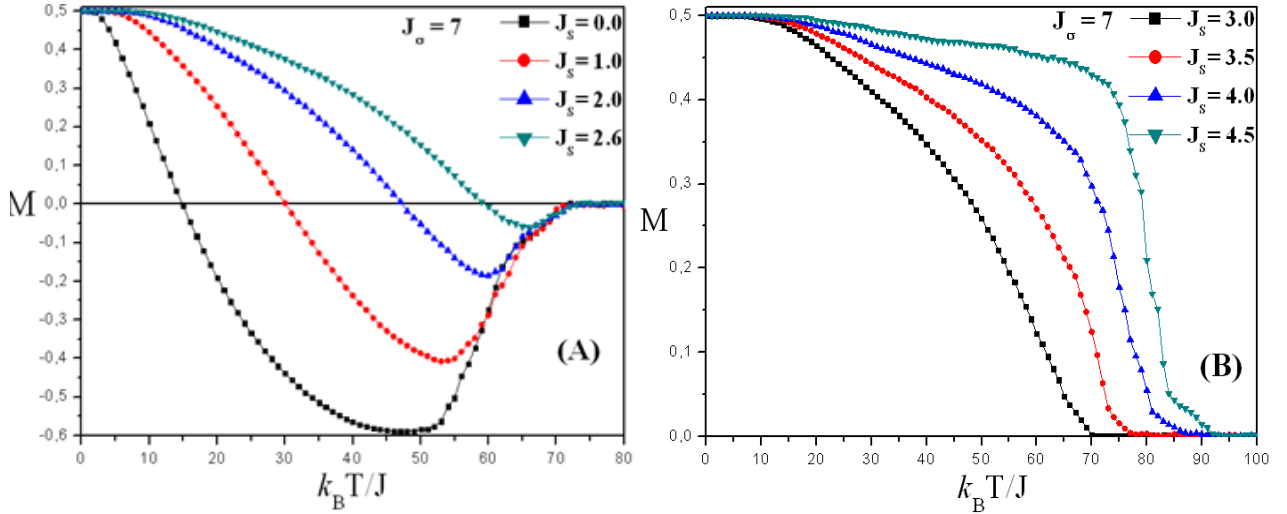


Fig. 4. Variation of the total magnetization M as a function of the temperature with $J_\sigma=7$

(A) for $J_s=0, 1, 2, 2.6$ and (B) for $J_s=3, 3.5, 4, 4.5$.

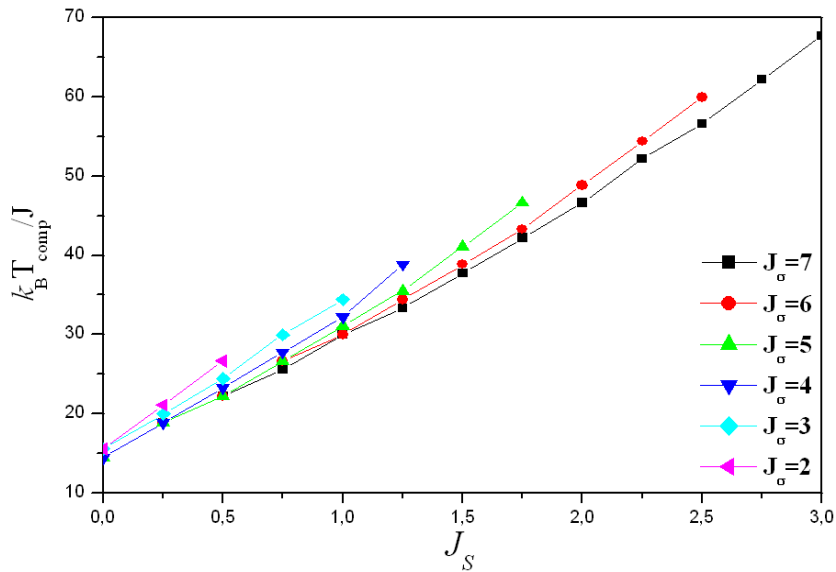


Fig. 5. T_{comp} as a function of J_s for various J_σ .

3.2.2. Effects of J_σ for $J_s=0.25$

To study the effect of J_σ at $T>0$, we vary J_σ for $J_s=0.25$. Fig. 6 evidences the thermal variations of the total magnetization M for different values of J_σ . From Fig. 6(A), we remark, as the temperature increases, that each curve decreases from the value 0.5 at $T=0$ to zero before T_c is reached until a negative minimum and then increases to zero at T_c . So, the system exhibits compensation points for $J_\sigma=3, 4, 5$ and 6 . By contrast, T_{comp} cannot exist when $J_\sigma=0, 0.5, 1$ and 1.5 because all M curves vanish only at T_c (Fig. 6(B)). From Fig. 6, we note that J_σ has a

minimum value below which compensation phenomenon does not occur. This minimum is also observed in other Refs. [113–114]. Furthermore, all the curves coincide until T_{comp} which means that T_{comp} remains almost constant, but the influence of J_{σ} on T_C is considerable. T_C increases with increasing values of J_{σ} . So, the difference $T_C - T_{\text{comp}}$ becomes bigger contrary to the effect of J_S at a fixed value of J_{σ} in the previous subsection. All these results can be compared with those of Refs. [113]. The effect of J_{σ} on magnetization at $T=0$ is similar to that of J_S in the precedent case.

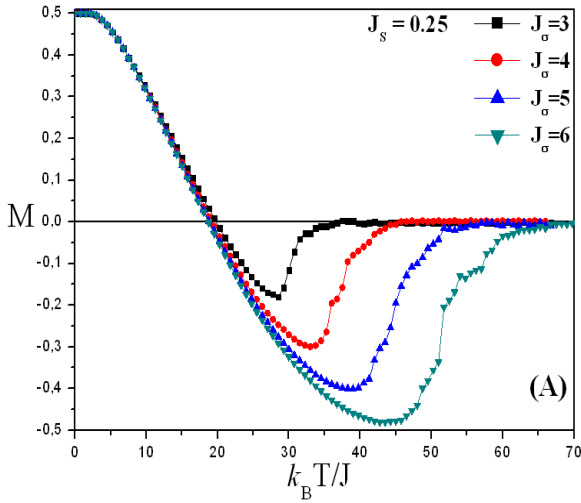


Fig.(A)

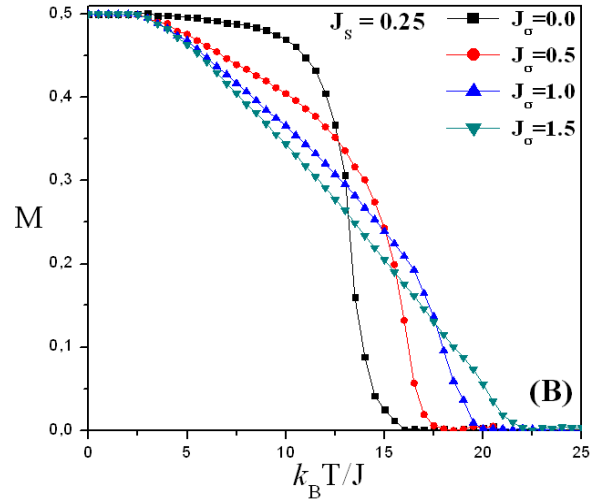


Fig.(B)

Fig. 6. Variation of the total magnetization M as a function of the temperature with $J_S=0.25$ **(A)** for $J_{\sigma} = 3, 4, 5, 6$ and **(B)** for $J_{\sigma} = 0, 0.5, 1, 1.5$.

3.3. Effects of the crystal fields Δ_S and Δ_{σ}

In this section, we are going to outline the influence of the crystal fields on the total and the partial magnetizations behaviours of the system. Now, we take the crystal field into account and neglect the next–nearest exchange interactions ($J_S=J_{\sigma}=0$). The crystal field anisotropies can take both negative and positive values. In this case, the Hamiltonian is given by the formula:

$$H = -J \sum_{\langle i,j \rangle} S_i \sigma_j - \Delta_S \sum_i S_i^2 - \Delta_{\sigma} \sum_i \sigma_i^2 \quad (3.5)$$

The phase diagram at $T=0$ K enables us to interpret the results of the phase diagrams at finite temperature. The ground-state phase diagram in the plane $(\Delta_s, \Delta_\sigma)$ is determined from (2) by comparing the energies of the different configurations as depicted in Fig. 7. At $T=0$, one can see six phases with four saturation values of the total magnetization 1, 0, 0.5 and -0.5 . The corresponding energies are shown in Table 1. We mention that the straight lines represent the region where two spin configurations can coexist. Also, there are several points where more than two phases can coexist. Also, we remark that the minimization and the maximization of the spin value depend on the value and the sign of the crystal fields $(\Delta_s, \Delta_\sigma)$.

In Fig. 8, we showed the behaviours of the total and sublattice magnetizations as functions of the temperature for several values of $(\Delta_s, \Delta_\sigma)$ in the case $J_s=J_\sigma=0$. From Fig. 8(A), we note that the crystal-fields Δ_s and Δ_σ have a considerable effect on the spin configurations at $T=0$ because M has four saturation values which are 1, 0, 0.5 and -0.5 . This result can be explained from the sublattice magnetizations in Fig. 8(B). Effectively, $M(T=0)=1$ comes from $M_s(T=0)=7/2$ and $M_\sigma(T=0)=-3/2$ for $(\Delta_s=2, \Delta_\sigma=-3.57)$. However, $M(T=0.5)=0.5$, because the two couples $(\Delta_s=2, \Delta_\sigma=-3.57)$ and $(\Delta_s=1, \Delta_\sigma=1)$ correspond to the spin configurations $(7/2, -5/2)$ and $(5/2, -3/2)$, respectively. Also, for $(\Delta_s=-2, \Delta_\sigma=1)$ and $(\Delta_s=-3, \Delta_\sigma=-2)$, we have $M(T=0)=0.5$ due to the spin configurations $(5/2, -5/2)$ and $(1/2, -1/2)$. In addition, $M(T=0.5)=-0.5$ is for $(\Delta_s=-4, \Delta_\sigma=0)$ because $M_s(T=0)=3/2$ and $M_\sigma(T=0)=-5/2$. This is in good agreement with the results given by Fig. 7. On the other hand, the curves $|M_s|$, $|M_\sigma|$ and M all vanish at different values of temperature in transition depending on the value of $(\Delta_s, \Delta_\sigma)$. Consequently, the effects of crystal-fields are important on T_C , on the spin configurations in the ground state and on the shapes of the magnetic curves. Similar effects are observed in Refs. [114].

The case $(\Delta_s=-3, \Delta_\sigma=-2)$ corresponds at $T=0$ to the antiferromagnetic phase $(1/2, -1/2)$. Thus, $|M_s|=|M_\sigma|=1/2$ and the total magnetization M is zero for all temperature values (Fig. 8(A)). For $\Delta_s=-2$ and $\Delta_\sigma=1$, the corresponding curve starts, at $T=0$, from $M=0$ which comes from the fact that the spin projection values are $M_s(T=0)=5/2$ and $M_\sigma(T=0)=-5/2$. Also, one can see that the total magnetization curve is L-type as described in the Néel theory. This type is also obtained in Ref. [115 W. Wang, D. Lv, F. Zhang, J. Bi, J. Chen. *J. Magn. Magn. Mater.* 385 (2015) 16.]. Moreover, other magnetization curve types are obtained in the thermal variation of M . In fact, Q-type and P-type are for $(\Delta_s=1, \Delta_\sigma=1)$ and $(\Delta_s=-4, \Delta_\sigma=0)$, respectively. However, the behaviours obtained for $(\Delta_s=2, \Delta_\sigma=-3.57)$ has not been predicted in Ref. [Néel] but was also found by Refs. [115]. In addition, the total magnetization shows a small hump for $(\Delta_s=-1.1, \Delta_\sigma=-3.5)$ at low temperatures. That hump can be explained from Fig. 8 (B) where one can

see that M_s increases a little then decreases with the increase of $k_B T/J$ but M_σ seems constant, under the effect of Δ_s .

Fig. 8 indicates that this model cannot exhibit any compensation point for the selected values of $(\Delta_s, \Delta_\sigma)$ when $J_s=J_\sigma=0$. Therefore, the existence of interactions between pairs of the next-nearest neighbours J_s and J_σ may be necessary to the appearance of compensation temperature as reported in Refs. [116-118].

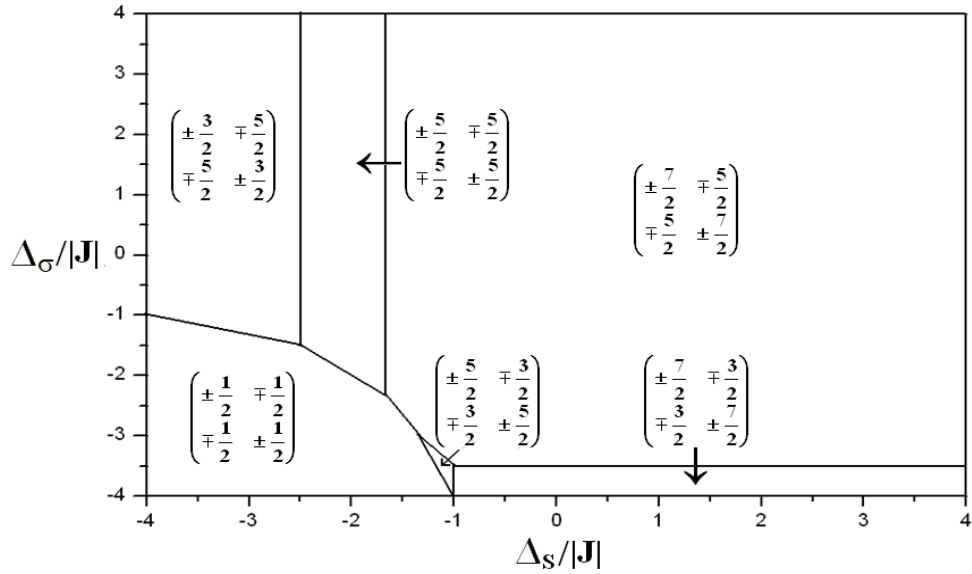


Fig. 7. Ground-state phase diagram of the model for $J_s=J_\sigma=0$.

Table 1

Ground-state energies of the J - Δ_s - Δ_σ model, with $J=-1$ and $J_s=J_\sigma=0$.

Ground state	Energy	Ground state	Energy
$\begin{pmatrix} \pm \frac{7}{2} & \mp \frac{5}{2} \\ \mp \frac{5}{2} & \pm \frac{7}{2} \end{pmatrix}$	$-70 J -24.5\Delta_s-12.5\Delta_\sigma$	$\begin{pmatrix} \pm \frac{5}{2} & \mp \frac{5}{2} \\ \mp \frac{5}{2} & \pm \frac{5}{2} \end{pmatrix}$	$-50 J -12.5\Delta_s-12.5\Delta_\sigma$
$\begin{pmatrix} \pm \frac{7}{2} & \mp \frac{3}{2} \\ \mp \frac{3}{2} & \pm \frac{7}{2} \end{pmatrix}$	$-42 J -24.5\Delta_s-4.5\Delta_\sigma$	$\begin{pmatrix} \pm \frac{3}{2} & \mp \frac{5}{2} \\ \mp \frac{5}{2} & \pm \frac{3}{2} \end{pmatrix}$	$-30 J -4.5\Delta_s-12.5\Delta_\sigma$
$\begin{pmatrix} \pm \frac{5}{2} & \mp \frac{3}{2} \\ \mp \frac{3}{2} & \pm \frac{5}{2} \end{pmatrix}$	$-30 J -12.5\Delta_s-4.5\Delta_\sigma$	$\begin{pmatrix} \pm \frac{1}{2} & \mp \frac{1}{2} \\ \mp \frac{1}{2} & \pm \frac{1}{2} \end{pmatrix}$	$-2 J -0.5\Delta_s-0.5\Delta_\sigma$

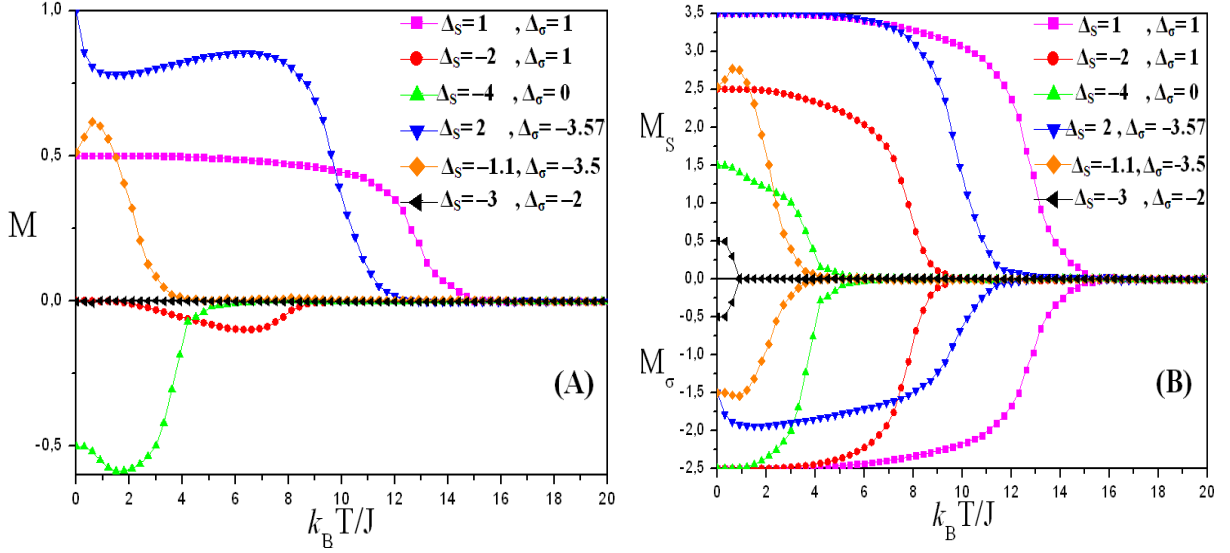


Fig. 8. Variations of (A) the total magnetization M and (B) the sublattice magnetizations M_S, M_σ as functions of the temperature for different values of $(\Delta_S, \Delta_\sigma)$.

3.4. Study of the case $J_S=0.25$ and $J_\sigma=4$ for different $(\Delta_S, \Delta_\sigma)$

Now, our purpose is to investigate the effects of both the next-nearest exchange interactions and the anisotropies on compensation phenomenon in the case $J_S=0.25$ and $J_\sigma=4$ varying the values of $(\Delta_S, \Delta_\sigma)$.

In Fig. 9, we presented the temperature dependence of the sublattice magnetizations $|M_S|, |M_\sigma|$ and the total magnetization M when $\Delta_S=\Delta_\sigma=1$ and $(\Delta_S=-1, \Delta_\sigma=-3.5)$. It can be seen that the sublattice magnetization curves monotonically decrease from the saturation values $|M_S|=3.5$ and $|M_\sigma|=2.5$ at $T=0$ as the temperature increases, vanishing at the critical temperature T_C . With T increasing, $|M_\sigma|$ decreases more slowly than $|M_S|$. Therefore, the sublattice magnetizations cancel each other at a certain temperature below T_C , giving rise to zero total magnetization at that temperature, which is a compensation point. For $(\Delta_S=1, \Delta_\sigma=1)$ and $(\Delta_S=-1.1, \Delta_\sigma=-3.5)$, the model has no compensation point (T_{comp}) when $J_S=J_\sigma=0$ (Fig. 8), but this point exists if we take $J_S=0.25$ and $J_\sigma=4$ (Fig. 9). Consequently, T_{comp} is due to the existence of interactions between pairs of next-nearest neighbours. This result supports the ones reached in Refs. [116-118].

In Fig. 10(A), we plotted the total magnetization per spin versus temperature for two values of $(\Delta_S, \Delta_\sigma)$ when $J_S=0.25$ and $J_\sigma=4$. The upper curve is for $(\Delta_S=1, \Delta_\sigma=-14)$ which corresponds to $S=\pm 7/2$ and $\sigma=\mp 3/2$ at $T=0$ then the total magnetization is $M=1$. The lower curve is obtained for $S=\pm 1/2$ and $\sigma=\mp 5/2$ at $T=0$ then $M=-1$ when $(\Delta_S=-10, \Delta_\sigma=1)$. There is no compensation point

for the two selected values of $(\Delta_S, \Delta_\sigma)$, because the sublattice magnetizations do not intercept at any point smaller than T_C (Fig. 10(B)). So, the total magnetization M vanishes only at T_C as shown in Fig. 10(A). However, the system has T_{comp} for the same values ($J_S=0.25, J_\sigma=4$) in absence of crystal fields ($\Delta_S=\Delta_\sigma=0$) (Fig. 5). As a result, even if spins of the σ -sublattice are more coupled than those of the S -sublattice because of $J_\sigma > J_S$, this model can show compensation (Fig. 9) or not (Fig. 10) depending on the values of both Δ_S and Δ_σ . That is to say, for a given couple (J_S, J_σ) , there are some values of $(\Delta_S, \Delta_\sigma)$ for which compensation points appear and for some other couples $(\Delta_S, \Delta_\sigma)$ there is no compensation temperature. It is noteworthy that the condition for the occurrence of compensation is that the exchange interaction J_σ , at a fixed value of J_S , should exceed a minimum value in the two cases $(\Delta_S=-10, \Delta_\sigma=1)$ and $(\Delta_S=1, \Delta_\sigma=-14)$. This result is the same as that of Ref. [119].

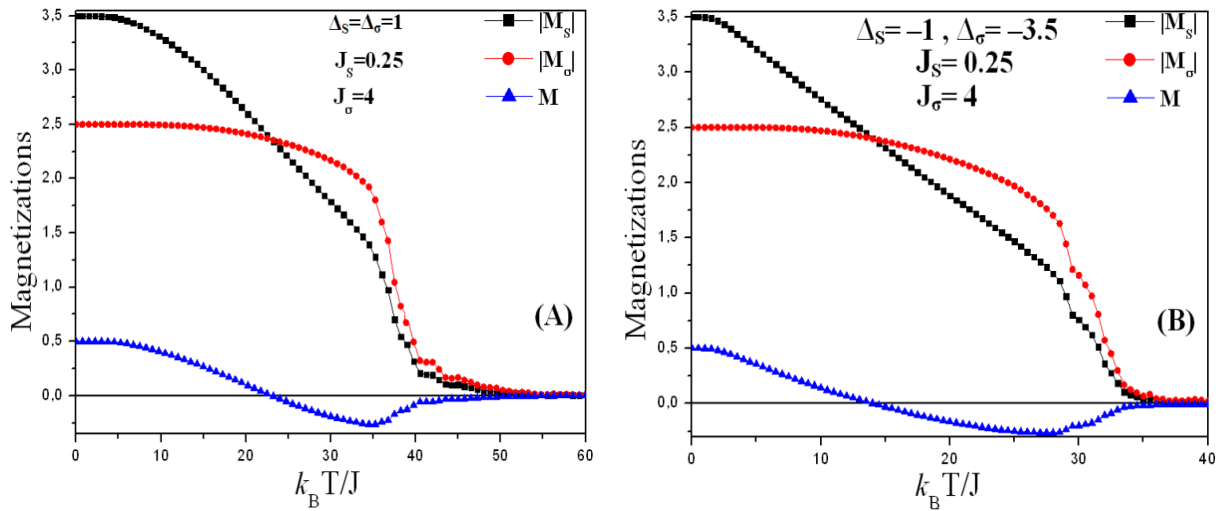


Fig. 9. The temperature dependence of the total magnetization M and absolute values of the sublattice magnetizations $|M_S|$ and $|M_\sigma|$ with $J_S=0.25$ and $J_\sigma=4$

(A) for $\Delta_S=\Delta_\sigma=1$ and **(B)** for $\Delta_S=-1, \Delta_\sigma=-3.5$

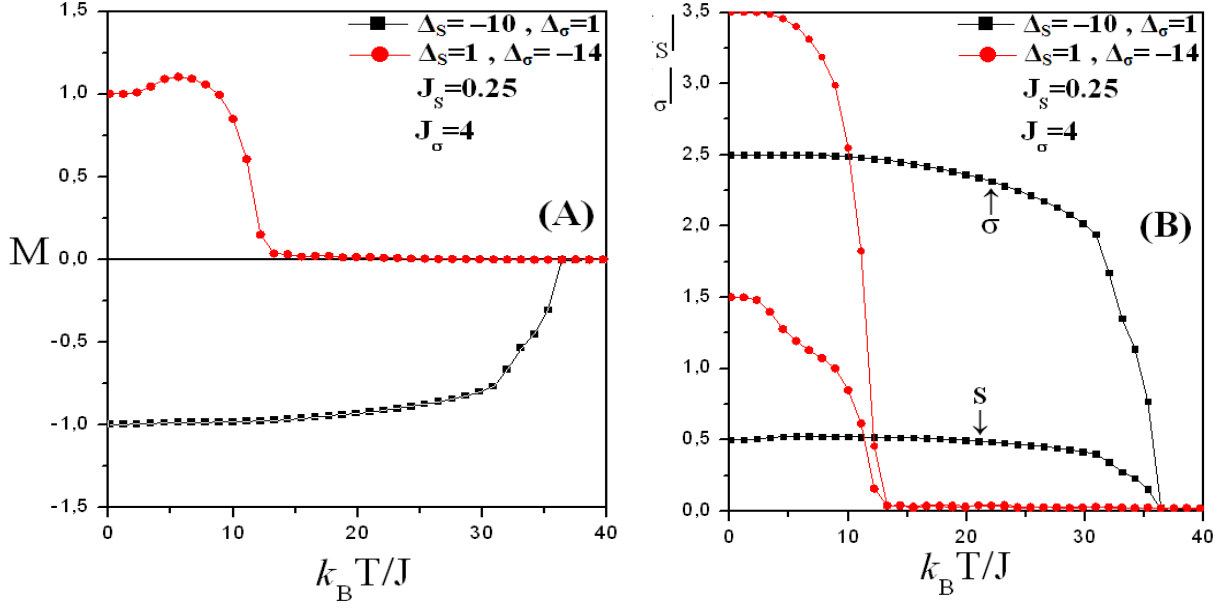


Fig. 10. The thermal variations of **(A)** the total magnetization M and **(B)** the absolute values of the sublattice magnetizations $|M_S|$ and $|M_\sigma|$ for $(\Delta_S = -10, \Delta_\sigma = 1)$ and $(\Delta_S = 1, \Delta_\sigma = -14)$ with $J_S = 0.25$ and $J_\sigma = 4$.

4. Conclusion

We have applied Monte Carlo simulation to study a mixed Ising antiferromagnetic nearest-neighbour interactions with crystal field on a square lattice, where spins $S=7/2$ alternate with spins $\sigma=5/2$, modeled by the Hamiltonian (1). We carried out the finite-temperature phase diagrams of M , $|M_S|$ and $|M_\sigma|$ for several combinations of the parameters J_S , J_σ , Δ_S and Δ_σ . We found that the system has compensation temperatures (T_{comp}) for appropriate values of J_S , J_σ in absence of any crystal field. In fact, for each value of J_S , there are several values of J_σ for which T_{comp} exist and vice versa. In addition, we have also examined the effect of J_S and J_σ on the compensation temperature. At a fixed value of J_σ , T_{comp} increases linearly with the increase of J_S . While, for a fixed value of J_S , T_{comp} is almost insensitive to the variations of J_σ . On the other hand, in the case where Δ_S and Δ_σ are taken into account with only nearest-neighbour interaction, the model Δ_S - Δ_σ cannot show compensation point for some selected values of $(\Delta_S, \Delta_\sigma)$. However, the compensation phenomenon may occur for some $(\Delta_S, \Delta_\sigma)$ with appropriate values of next-nearest neighbours (J_S, J_σ) . So, we can conclude that J_S and J_σ play an important role in the appearance of the compensation phenomenon. As a result, we can say that the system in presence of crystal fields exhibits or not the compensation behaviours depending on the competition between the exchange interactions and the crystal field. It is worthy to note that different types of magnetization curves are obtained.

Chapter 4

Compensation Behaviours in a Ferrimagnetic Mixed Spin– 7/2 And Spin–3: Monte Carlo Simulation

1. Introduction

The ferrimagnetic systems have been extensively investigated because of their fascinating properties. In this chapter, the mixed spin-7/2 and spin-3 Ising system with periodic boundary conditions on a square lattice has been studied using the Monte Carlo simulation within the Metropolis algorithm; the Hamiltonian of the system includes the interaction between the first nearest neighbours and the crystal fields $\Delta_{7/2}$ and Δ_3 generated by the spin-7/2 and spin-3, respectively. The ground state phase diagram of the system for the $J-\Delta_{7/2}-\Delta_3$ model ($J = -1$) has been established. On the other hand, the impact of the single-ion anisotropies on the compensation temperature has been shown. Several topologies of the total magnetization have been found for this system.

The outline of this work is organized as follows: in the next section we introduce the model and give the details of our simulation. In Sect 3, we present our numerical results and discuss the ground-state phase diagram and magnetizations. Finally, we conclude the obtained results of the studied system in Sect 4.

2. Model and Monte Carlo Details

The studied mixed spin-7/2 and spin-3 ferrimagnetic Ising system is governed by the following Hamiltonian:

$$H = -J \sum_{\langle i,j \rangle} S_i \sigma_j - \Delta_{7/2} \sum_i S_i^2 - \Delta_3 \sum_i \sigma_i^2 \quad (4.1)$$

For the first sum, $\langle i,j \rangle$ denote the first nearest neighbours, the other sums run over all sites, S and σ sublattices generated by spin-7/2 and spin-3 respectively. J is the exchange interaction and $\Delta_{7/2}$ and Δ_3 are the crystal field interactions generated by the spin S and σ respectively, we normalized all calculations by considering ($J = -1.0$).

The Hamiltonian (1) was simulated by standard importance sampling. In each spin-flip attempt, a spin was randomly chosen with a uniform distribution, the probability of a particular configuration is proportional to the Boltzmann factor. The flips are accepted or rejected by the Metropolis approximation [metropolis]. Data were generated with 10^5 Monte Carlo steps per spin after discarding the first 10^4 steps per site for equilibrium. We consider periodic boundary conditions.

Our program calculates the sublattice magnetizations and the total magnetization defined as follow:

$$M_{7/2} = \frac{2}{L_S} \left\langle \sum S_i \right\rangle \quad (4.2)$$

$$M_3 = \frac{2}{L_\sigma} \left\langle \sum \sigma_j \right\rangle \quad (4.3)$$

$$M = (M_{7/2} + M_3)/2 \quad (4.4)$$

Where $LS = 100$ and $L\sigma = 100$ are the numbers of spin along the sublattice generated by spin S and σ , respectively.

3. Results and Discussion

To understand the influence of the crystal fields on the existence of compensation phenomenon, it is necessary to investigate the total and sublattice magnetizations variations of the system as functions of temperature for different values of the crystal field interactions using the Monte Carlo simulation. Critical temperature (T_C) is defined as the temperature where the total magnetization and all sublattice magnetizations vanish. The appearance of a compensation point is due to the fact that, the magnetic moments of the sublattices compensate the other completely. Then, the compensation temperature can be determined by seeking the condition $|M_{7/2}(T_{comp})| = |M_3(T_{comp})|$ and $\text{sign}(M_{7/2}(T_{comp})) = -\text{sign}(M_3(T_{comp}))$. Graphically, we know the compensation when the sublattice magnetizations cross at $T < T_C$. To perform this, we simulate the variations of $|M|$, $|M_3|$ and $|M_{7/2}|$. **Table 1** presents the ground state phase energies for the $J-A_{7/2}-A_3$ model, **Figure 1** displays the ground-state phase diagram for the Hamiltonian in formula (1); it contains 12 possible configurations. The regions where two phases can coexist are represented by the straight lines. There are several points where more than two phases can coexist. The information given by this diagram at $T=0K$ enables us to interpret the obtained results at finite temperature, from this; we can locate regions where the system may present considerable magnetic behaviours.

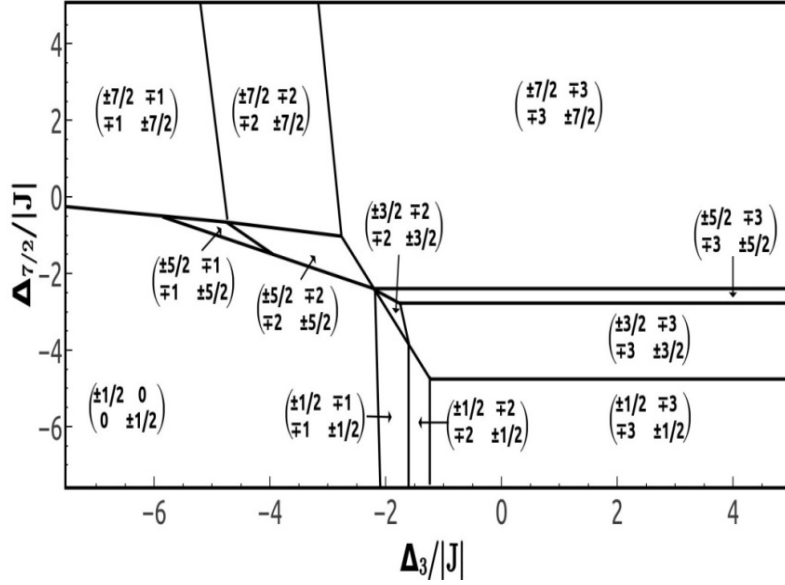


Fig. 1 The ground-state phase diagram for the J - $\Delta_{7/2}$ - Δ_3 model ($J = -1$)

Ground-state	Energy	Ground-state	Energy
$\begin{pmatrix} \pm \frac{7}{2} & \mp 3 \\ \mp 3 & \pm \frac{7}{2} \end{pmatrix}$	$-84 J - 24.5\Delta_{7/2} - 18\Delta_3$	$\begin{pmatrix} \pm \frac{7}{2} & \mp 2 \\ \mp 2 & \pm \frac{7}{2} \end{pmatrix}$	$-56 J - 24.5\Delta_{7/2} - 8\Delta_3$
$\begin{pmatrix} \pm \frac{7}{2} & \mp 1 \\ \mp 1 & \pm \frac{7}{2} \end{pmatrix}$	$-28 J - 24.5\Delta_{7/2} - 2\Delta_3$	$\begin{pmatrix} \pm \frac{5}{2} & \mp 3 \\ \mp 3 & \pm \frac{5}{2} \end{pmatrix}$	$-60 J - 12.5\Delta_{7/2} - 18\Delta_3$
$\begin{pmatrix} \pm \frac{5}{2} & \mp 2 \\ \mp 2 & \pm \frac{5}{2} \end{pmatrix}$	$-40 J - 12.5\Delta_{7/2} - 8\Delta_3$	$\begin{pmatrix} \pm \frac{5}{2} & \mp 1 \\ \mp 1 & \pm \frac{5}{2} \end{pmatrix}$	$-20 J - 12.5\Delta_{7/2} - 2\Delta_3$
$\begin{pmatrix} \pm \frac{3}{2} & \mp 3 \\ \mp 3 & \pm \frac{3}{2} \end{pmatrix}$	$-36 J - 4.5\Delta_{7/2} - 18\Delta_3$	$\begin{pmatrix} \pm \frac{3}{2} & \mp 2 \\ \mp 2 & \pm \frac{3}{2} \end{pmatrix}$	$-24 J - 4.5\Delta_{7/2} - 8\Delta_3$
$\begin{pmatrix} \pm \frac{1}{2} & \mp 3 \\ \mp 3 & \pm \frac{1}{2} \end{pmatrix}$	$-12 J - 0.5\Delta_{7/2} - 18\Delta_3$	$\begin{pmatrix} \pm \frac{1}{2} & \mp 2 \\ \mp 2 & \pm \frac{1}{2} \end{pmatrix}$	$-8 J - 0.5\Delta_{7/2} - 8\Delta_3$
$\begin{pmatrix} \pm \frac{1}{2} & \mp 1 \\ \mp 1 & \pm \frac{1}{2} \end{pmatrix}$	$-4 J - 0.5\Delta_{7/2} - 2\Delta_3$	$\begin{pmatrix} \pm \frac{1}{2} & 0 \\ 0 & \pm \frac{1}{2} \end{pmatrix}$	$-0.5\Delta_{7/2}$

Table.1. Ground state energies of the $J-\Delta_{7/2}-\Delta_3$ model.

In order to understand more the importance of the single ion anisotropy in occurring compensation phenomenon, we subdivide our study in four cases ($\Delta_3=0, \Delta_{7/2}=0$), ($\Delta_3=0, \Delta_{7/2}\neq 0$), ($\Delta_{7/2}=0, \Delta_3\neq 0$) and ($\Delta_{7/2}\neq 0, \Delta_3\neq 0$).

3.1. Study of the $\Delta_{7/2}=\Delta_3=0$ Case

Firstly we analyze our model out of any crystal field's effect. **Figure 2** presents the variations of the absolute values of total $|M|$ and sublattice magnetizations $|M_{7/2}|$ and $|M_3|$ versus the temperature in the absence of anisotropic interaction. From this figure, it is clear that sublattice $|M_{7/2}|$ and $|M_3|$ magnetizations start from the saturation values 3.5 and 3 at $T=0K$ respectively, as predicted in the ground-state phase diagram shown in **Figure 1**. In addition, all the curves decrease monotonically as the temperature increases and tend to zero its value at T_c . The total magnetization behaves like a Q-type, as described in the Néel classification [Néel]. So, the system exhibits no compensation temperatures at $T\neq 0K$, because there is no crossing point under the critical temperature between the sublattice curves of magnetization, as clearly shown in **Fig.2**.

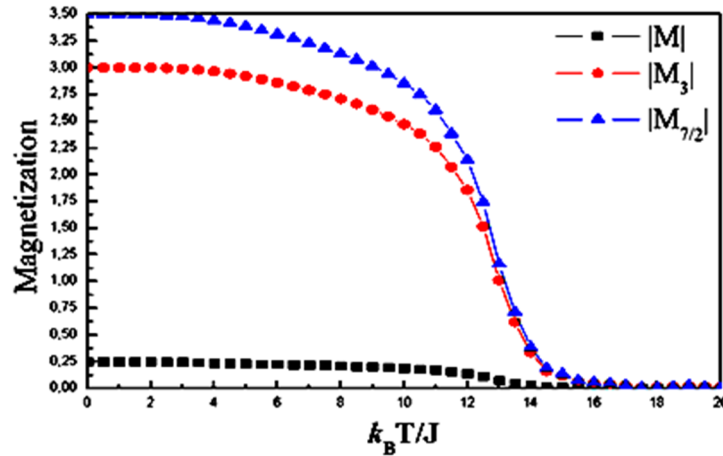


Fig. 2 Magnetic moments variation with the temperature for the spin—7/2 sublattice $|M_{7/2}|$, the spin—3 sublattice $|M_3|$, and the total moment $|M|$ when $\Delta_{7/2}=\Delta_3=0$

3.2. Study of the $\Delta_{7/2}\neq 0, \Delta_3=0$ Case

Figure 3 shows that the absolute values of magnetizations are equal at a point under the T_c . Actually, the curve $|M_{7/2}|$ decreases rapidly from its value 3.5 at $T=0$ until intersecting with $|M_3|$ that maintains the order until the crossing point, while the temperature increases.

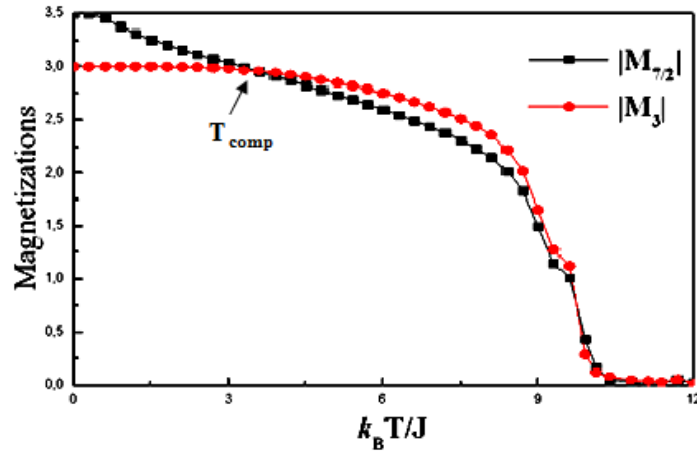


Fig. 3 Thermal behaviours of the sublattice magnetizations $|M_{7/2}|$ and $|M_3|$ for $\Delta_{7/2} = -1.7$ when $\Delta_3 = 0$

Figure 4 displays that the total magnetization vanishes at the same point, which means that the system exhibits a compensation temperature for $\Delta_{7/2} = -1.7$ when $\Delta_3 = 0$. **Fig.5** presents the total magnetization's curves for different negative values of $\Delta_{7/2}$ when $\Delta_3 = 0$. The system exhibits compensation temperatures for all the values $\Delta_{7/2} = -1.25, -1.5, -1.7, -1.8$ and -1.99 except for $\Delta_{7/2} = -1$ where no compensation behaviours is observed. The effect of the presence of the crystal field $\Delta_{7/2}$ is important on T_{comp} which increases with decreasing values of $\Delta_{7/2}$. In addition, when $\Delta_3 = 0$, the total magnetization corresponding to the values $-1.25, -1.5, -1.7, -1.8, -1.99$ of $\Delta_{7/2}$ present N-type, in contrast for $\Delta_{7/2} = -1$, the curve behaves like a Q-type.

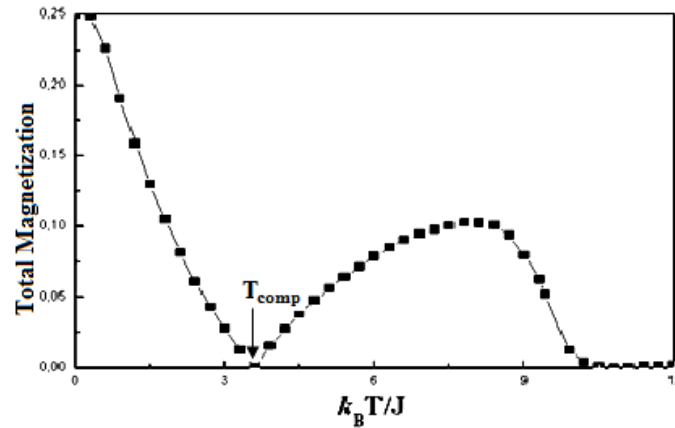


Fig. 4 Thermal behaviours of the absolute value of the total magnetization $|M|$ for $\Delta_{7/2} = -1.7$ when $\Delta_3 = 0$

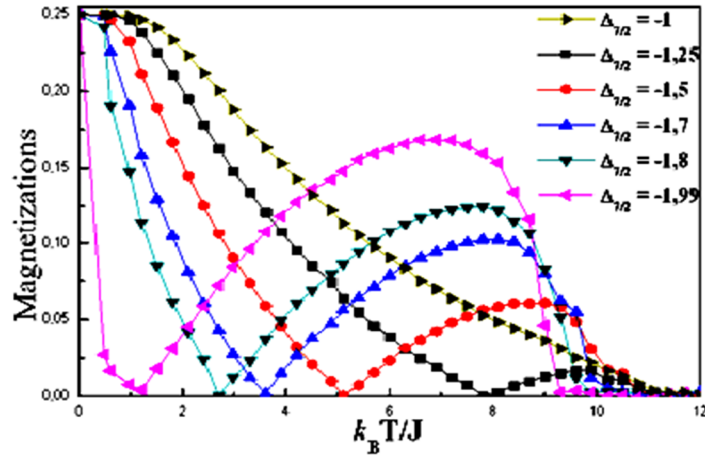


Fig. 5 The behaviours of the absolute value of the total magnetization $|M|$ for various negative values of the crystal field $\Delta_{7/2}$ when $\Delta_3 = 0$

Figure 6, indicates that there is no compensation point where the magnetic curves are depicted for different positive values of $\Delta_{7/2}$ with $\Delta_3 = 0$. The total magnetizations do not vanish at any point below T_C and decay to zero continuously at the critical point. The P-type curves are for $\Delta_{7/2} = 0.5, 1, 1.5, 2$ and 2.5 whereas the Q-type is for $\Delta_{7/2} = 0.1$.

It is worth noting that the condition for appearance of T_{comp} when $\Delta_3 = 0$ is that $\Delta_{7/2}$ should be below certain maximal values, because the system can't show the compensation behaviours for any positive value of $\Delta_{7/2}$ as understood from **Fig.6**. Thus, this maximal value of $\Delta_{7/2}$ is negative.

Briefly, for $\Delta_{7/2} = -1$, no compensation and no cross-point is detected for these values.

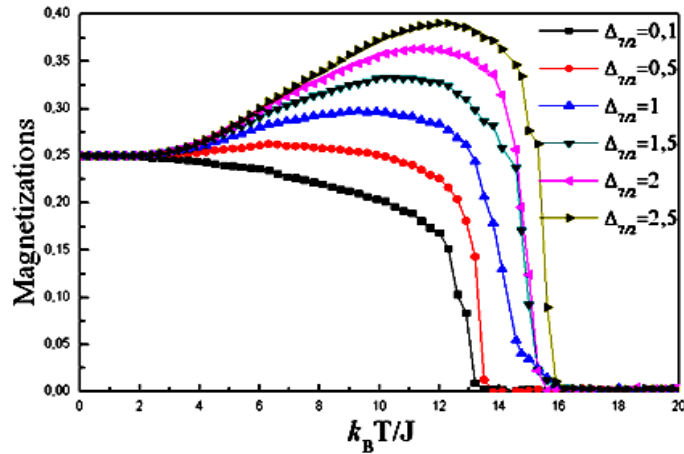


Fig. 6 Thermal behaviours of the absolute value of the total magnetization $|M|$ for various positive values of the crystal field $\Delta_{7/2}$ when $\Delta_3 = 0$.

3.3. Study of the $\Delta_3 \neq 0, \Delta_{7/2} = 0$ Case

In this case we do not take into account the crystal field $\Delta_{7/2}$ ($\Delta_{7/2} = 0$), to clarify the effects of the crystal field interaction Δ_3 only, which acts on the spins-3. **Figure 7** shows the temperature dependence of $|M|$ for $\Delta_3 = -4, 4.25$ when $\Delta_{7/2} = 0$. In the first case ($\Delta_3 = -4$) there is no compensation point and the two curves of magnetization do not cross at any point as shown in **Fig.8a** but tend simply to zero at T_c . However, for the second case ($\Delta_3 = 4.25$), the total magnetization vanishes at the point $T_{\text{comp}} < T_c$ (**Fig.7**) and the sublattice magnetizations intersect at the same point (**Fig.8(a)**) which is caused by the existence of the compensation temperature. One can see this point more clearly in **Fig.8b**, where the two curves cross effectively at T_{comp} .

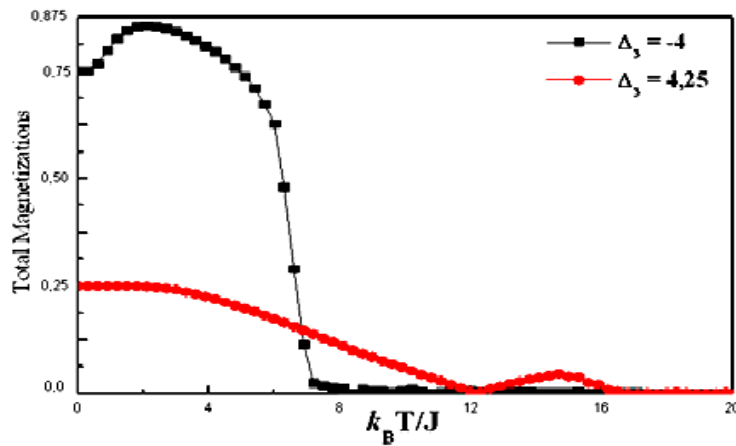


Fig. 7 The absolute value of the total magnetization $|M|$ versus temperature for $\Delta_3 = -4$ and $\Delta_3 = 4.25$ when $\Delta_{7/2} = 0$.

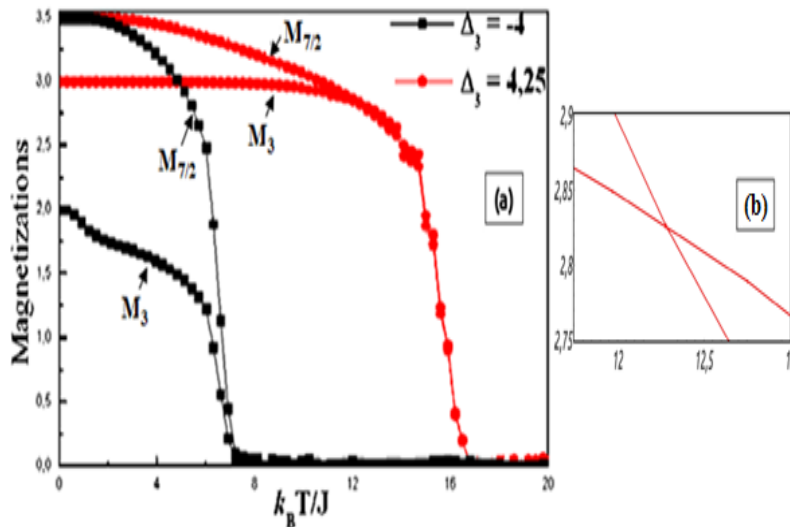


Fig. 8a Thermal behaviours of the sublattice magnetizations $|M_{7/2}|, |M_3|$ for $\Delta_3 = -4$ and $\Delta_3 = 4.25$ when $\Delta_{7/2} = 0$. **b** The crossing point between the magnetizations $|M_{7/2}|$ and $|M_3|$ curves

Figure 9 plots the temperature dependence of the total magnetization $|M|$ for several positive values of Δ_3 ($= 3.5, 3.75, 4, 4.25, 4.5$) when $\Delta_{7/2} = 0$. The studied system presents compensation

in all the previous cases and the curves behave following the N-type. There is no considerable influence on T_{comp} of the crystal field, when T_{comp} exists. Consequently, T_{comp} remains almost unchanged when $\Delta_{7/2} = 0$. As result, the compensation phenomenon is independent on the value of Δ_3 when $\Delta_{7/2} = 0$. The condition to obtain compensation point when $\Delta_{7/2} = 0$, is that the crystal field Δ_3 should be beyond a certain positive values, because, all the negative values of Δ_3 do not show compensation behaviours as understood from Fig.10. It demonstrates different curves of total magnetization for several negative values of Δ_3 ($=-0.1, -0.5, -1, -2, -3, -4, -5$) when $\Delta_{7/2} = 0$. The reason behind this is that negative crystal field tends to reduce the spin-3 value below $|M_3(T=0)| = 3$ but the spin-7/2 tries to maintain the saturation value $|M_{7/2}(T=0)| = 3.5$ at relatively high temperatures since $\Delta_{7/2} = 0$.

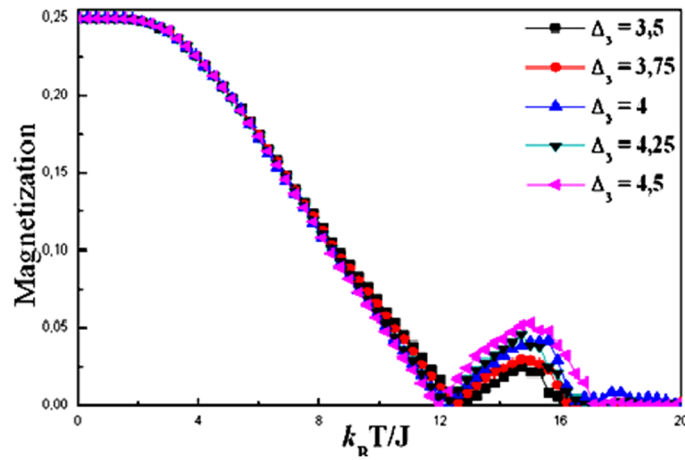


Fig. 9 Curves of the absolute value of the total magnetization $|M|$ as functions of temperature for several positive values of Δ_3 when $\Delta_{7/2} = 0$

Regarding the topological types of the total magnetization, one can see in Fig.10 that the system exhibits the Q-, P-, and S-type. From this, the Q-type is obtained for $\Delta_3 = -0.1$; the curves corresponding to $\Delta_3 = -0.5, -1, -2$ and -4 are P-type. On the other hand, The S-type is obtained for both values -3 and -5 of Δ_3 . As result, all negative values of Δ_3 when $\Delta_{7/2} = 0$ denote no compensation point.

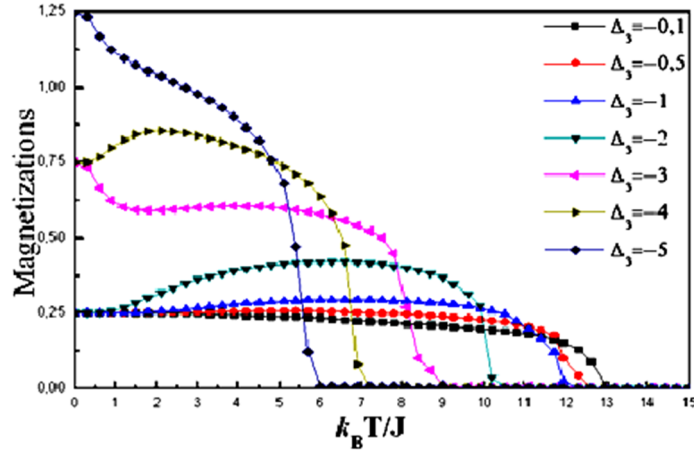


Fig. 10 Curves of the absolute value of the total magnetization $|M|$ as functions of temperature for several negative values of Δ_3 when $\Delta_{7/2} = 0$

3.4. Study of the $\Delta_{7/2} \neq 0, \Delta_3 \neq 0$ Case

In this subsection, we investigate the magnetization behaviours of the system in the presence of both crystal field interactions Δ_3 and $\Delta_{7/2}$, in order to evaluate their influences together on the magnetic properties of our system (in particular on compensation); the total magnetizations $|M|$ versus temperature are constructed for two opposite values of the crystal field Δ_3 at the fixed value $\Delta_{7/2} = -1.1$ as shown in the [Fig.11](#).

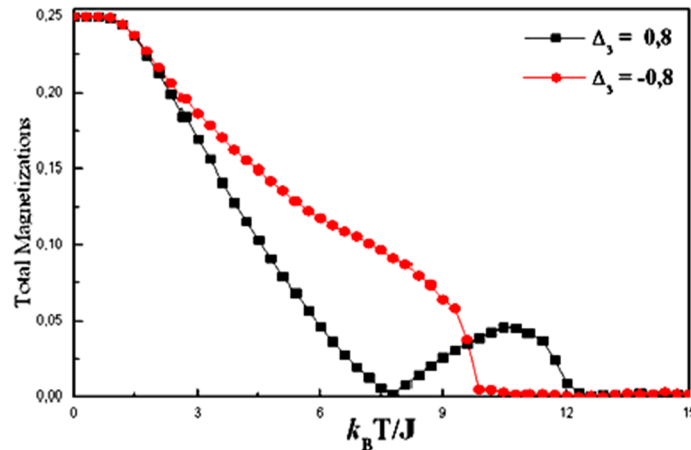


Fig. 11 Variation of the absolute value of the total magnetization $|M|$ for two opposite values of the crystal field Δ_3 when $\Delta_{7/2} = -1.1$

From this figure, the magnetization for $\Delta_3 = -0.8$ decreases continuously with the increasing of reduced temperature and vanishes at T_C . For the other case $\Delta_3 = 0.8$, the total magnetic moment behaves N-type curve. So, the model exhibits compensation for $\Delta_{7/2} = -1.1$ and $\Delta_3 = 0.8$ but not for $\Delta_{7/2} = -1.1$ and $\Delta_3 = -0.8$; hence the sign of the crystal field may be important to give birth to T_{comp} for various values of $(\Delta_3, \Delta_{7/2})$. [Figure 12](#) illustrates three types of $|M|$ curves, Q-, P- and L-type. The effect of the $(\Delta_3, \Delta_{7/2})$ values on T_C depends on the signs of Δ_3 and $\Delta_{7/2}$, For $\Delta_{7/2}$

$\langle 0T_{\text{comp}} \rangle$ takes different values, when $\Delta_3 < 0$ ($= -1.0$) the $|M|$ curves almost tend to zero at the same value of T_C , however, for $\Delta_3 > 0$ ($= 1.0, 3.0$), T_C takes different values as shown in **Figures 13** and **14**; it follows that both sign and crystal field values govern the T_C .

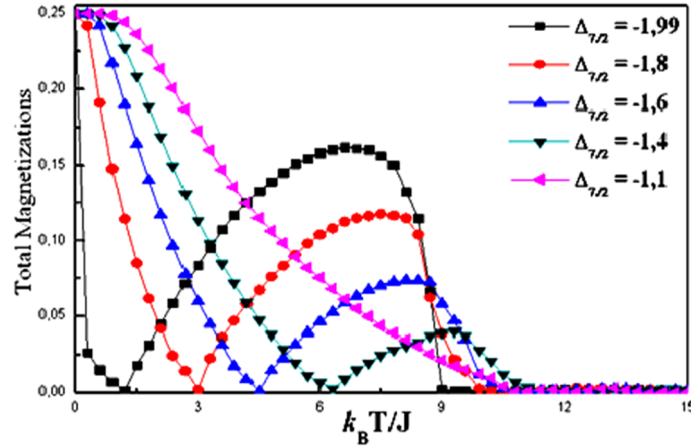


Fig. 12 Thermal behaviours of the absolute value of the total magnetization $|M|$ for various negative values of the crystal field $\Delta_{7/2}$ when $\Delta_3 = -1$

The system can display richer types of $|M|$ curves, as shown in **Figs.13** and **14**, for various values of $\Delta_{7/2}$. The $|M|$ curves present Q-type ($\Delta_3 = 1, \Delta_{7/2} = -0.1, -1.3$), ($\Delta_3 = 3, \Delta_{7/2} = 0.6$) and N-type ($\Delta_3 = 1, \Delta_{7/2} = -1, -1.5$), ($\Delta_3 = 3, \Delta_{7/2} = -1, -0.75$), $|M|$ presents L-type for ($\Delta_3 = 3, 1, -1, \Delta_{7/2} = -1.99$); similar curve behaviours have been observed for different mixed spin systems [119-122].

So, we conclude that the single ion anisotropies do not have the same effect on the total magnetization curves. Compensation temperatures are also obtained in other works [123-126] despite taking into account only the nearest-neighbour interaction in the Hamiltonian. However, some references indicate that no compensation point occurs if next-nearest-neighbour couplings are not considered [127-128].

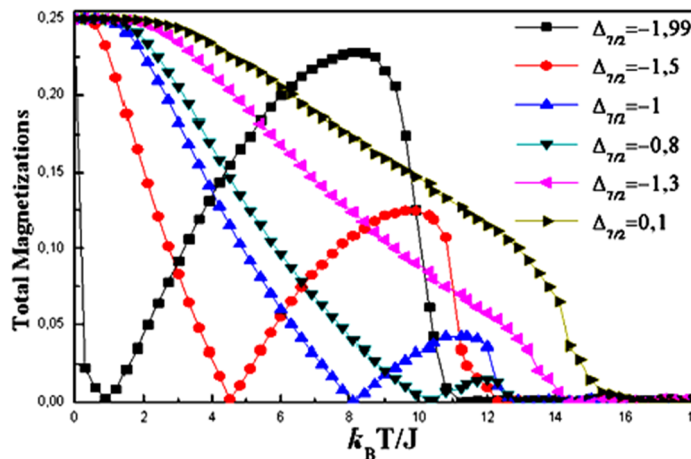


Fig.13 Thermal behaviours of the absolute value of the total magnetization $|M|$ for various values of the crystal field $\Delta_{7/2}$ when $\Delta_3 = 1$

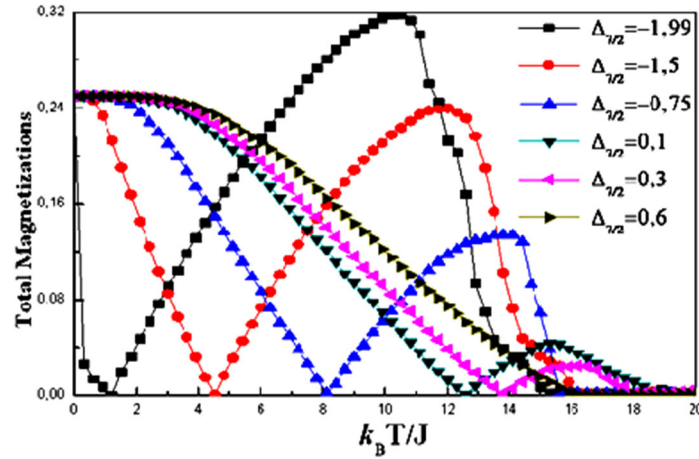


Fig. 14 Thermal behaviours of the absolute value of the total magnetization $|M|$ for various values of the crystal field $\Delta_{7/2}$ when $\Delta_3 = 3$

4. Conclusion

In this chapter, we used Monte Carlo simulation based on the Metropolis algorithm, in order to study the ferrimagnetic mixed spins- $(7/2, 3)$; the system is modelled by Eq(1), alternated on a square lattice with periodic boundary conditions. In particular, after investigating the phase diagram of the ground state for the $J-\Delta_{7/2}-\Delta_3$ model, we examined the crystal field effects on the magnetic properties. The total and sublattice magnetizations are also explored as a function of temperature in order to investigate the compensation temperatures. We demonstrated the existence of the compensation temperature, even if we consider only the first nearest neighbours. Also, we should mention that the compensation temperature values T_c depend on the sign of the anisotropy and T_{comp} seems sensitive to negative values, but insensitive to positive ones of both $\Delta_{7/2}$ and Δ_3 . We discussed different cases ($\Delta_{7/2}=\Delta_3=\Delta\neq 0$), ($\Delta_{7/2}=0, \Delta_3\neq 0$), ($\Delta_{7/2}\neq 0, \Delta_3=0$) and ($\Delta_{7/2}\neq 0, \Delta_3\neq 0$). Furthermore, we have obtained different kinds of curves of the compensation temperatures, and the system exhibits the Q-, P- L-, and S-type behaviours as classified by the Néel theory.

Chapter 5

**Hysteresis Cycle and
Magnetization Behaviours of
a Mixed–spin ($7/2, 3/2$)
Ferrimagnetic Ising Model:
Monte Carlo Investigation**

1. Introduction:

The ferrimagnetic systems have attracted a lot of attention because they are stable with spontaneous moments above room temperature and have many useful technological applications in several domains such as information storage devices, thermomagnetic recording, photo-induced magnetization and field-induced magnetic relaxation.

In this work the effects of single-ion anisotropies and an external magnetic field on the magnetization of the mixed spin (7/2, 3/2) ferrimagnetic Ising system are investigated within Monte Carlo simulation. Under certain values of the physical parameters, multiple hysteresis loop behaviours such as double, triple and quintuple hysteresis cycles have been observed. Particularly, the superparamagnetic phase has been shown. The ground-state phase diagrams are presented. This work is presented as follows: in Section 2, we described the model and we used the details of our method. In Section 3, we presented and discussed the obtained results. Finally, we concluded this study in Section 4.

2. Model and Monte Carlo Details

We consider two dimensional Ising model with spins, $S = \pm 7/2, \pm 5/2, \pm 3/2$ and $\sigma = \pm 3/2$ and $\pm 1/2$, located in alternating sites of a square lattice, with periodic boundary conditions, containing $N = 100 \times 100$ spins. In the presence of an external longitudinal magnetic field h and two crystal-fields $\Delta_{7/2}$ and $\Delta_{3/2}$, the system is described by the Hamiltonian:

$$H = -J \sum_{\langle i,j \rangle} S_i \sigma_j - \Delta_{7/2} \sum_i S_i^2 - \Delta_{3/2} \sum_i \sigma_i^2 - h \left(\sum_i S_i + \sum_i \sigma_i \right) \quad (5.1)$$

Where the first summation is over all nearest-neighbour pair of spins, the other ones are over all spin sites. $J(= -1)$ is the antiferromagnetic nearest exchange interaction.

Monte Carlo method is used to simulate our system modelled by the Hamiltonian (1), we employed a single-spin-flip algorithm, under periodic boundary conditions. In each spin-flip attempt, a spin was randomly chosen from the possible projections with a uniform probability. According to the Metropolis approximation [129], the flips are rejected or accepted. Data were obtained with 2×10^5 Monte Carlo steps per spin after discarding the first 10^4 steps per site for equilibrium. We calculate the following quantities:

$$\text{-- The } S\text{-sublattice magnetization: } M_{7/2} = \frac{1}{N_S} \langle \sum_i S_i \rangle \quad (5.2)$$

$$\text{-- The } \sigma\text{-sublattice magnetization: } M_{3/2} = \frac{1}{N_\sigma} \langle \sum_i \sigma_i \rangle \quad (5.3)$$

– The total magnetization $M = \frac{M_{7/2} + M_{3/2}}{2}$ (5.4)

Where N_S and N_σ are the numbers of S– and σ –spins, respectively. We consider, $N_S = N_\sigma = N/2$.

3. Results and discussion

In this section, we present some results showing the effects of the external magnetic field, the single–ion anisotropy and the temperature on the magnetization. In what follow, we use the notation $\Delta = \Delta_{7/2} = \Delta_{3/2}$.

3.1. Ground–state phase diagrams

We begin our study with investigating the ground–state phase diagrams by comparing the ground–state energies of the possible phases from the Hamiltonian given in equation (1) in the planes $(\Delta/|J|, \mathbf{h}/|J|)$, $(\Delta_{7/2}/|J|, \mathbf{h}/|J|)$ and $(\Delta_{3/2}/|J|, \mathbf{h}/|J|)$ to determine the spin states at $T = 0K$ in the mixed Ising system.

In Figure 1, we show the ground–state phase diagram of the alternated mixed spin–(7/2,3/2) system in the plane $(\Delta/|J|, \mathbf{h}/|J|)$ in the ranges $-3 \leq \Delta \leq 1$ and $-10 \leq \mathbf{h} \leq 10$. The diagram consists of twelve spin configurations, noted by letters "R", with ten different regions. The two phases R₇ and R₁₀ have the same energy. A similar thing is observed for R₈ and R₉. The phases and their energies are presented in Table 1. In the absence of the magnetic field, the system can exhibit only six phases R₁, R₂, R₃, R₄, R₁₁ and R₁₂ with the saturation values 7/2, 5/2, 3/2 and 1/2 for the sublattice of 7/2–spins magnetization and the saturation values of the other sublattice are –3/2 and –1/2 when $-3 \leq \Delta \leq 1$.

In Figure 2, the ferrimagnetic (7/2,3/2) Ising system ground–state phase diagram is depicted in the plane $(\Delta_{7/2}/|J|, \mathbf{h}/|J|)$ with $-5 \leq \Delta_{7/2} \leq 1$ and $-10 \leq \mathbf{h} \leq 10$ for the fixed value of $\Delta_{3/2} = 1$. The system exhibits seven regions. The available configurations are presented by "A" letters. The phases and their energies are presented in Table2. When $\mathbf{h} = 0$ in the case $-5 \leq \Delta_{7/2} \leq 1$, all the phases A₁, A₂, A₃, A₄, A₅, A₆ and A₇ are possible.

In Figure 3, we present the ground–state phase diagram of the studied Ising ferrimagnet (7/2,3/2) in the plane $(\Delta_{3/2}/|J|, \mathbf{h}/|J|)$ with $-5 \leq \Delta_{3/2} \leq 1$ and $-10 \leq \mathbf{h} \leq 10$ for the fixed value of $\Delta_{7/2} = -1.5$. The system has eleven phases. The phases and their energies are shown in Table3. The letters "B" on the figure symbolize the obtained configurations. For $\mathbf{h} = 0$, only the three phases B₃, B₄ and B₁₁ can be displayed with the saturation values 5/2 and 1/2 of $M_{7/2}$ while 3/2 and 1/2 for $M_{3/2}$ if $-5 \leq \Delta_{3/2} \leq 1$.

It is noteworthy that the ground–state phase diagrams are all symmetric around the line $\mathbf{h} = 0$ as in the Refs. [130-131]. Moreover, all these diagrams show the existence of

multicritical points where more than two phases can coexist. The diagrams are topologically different.

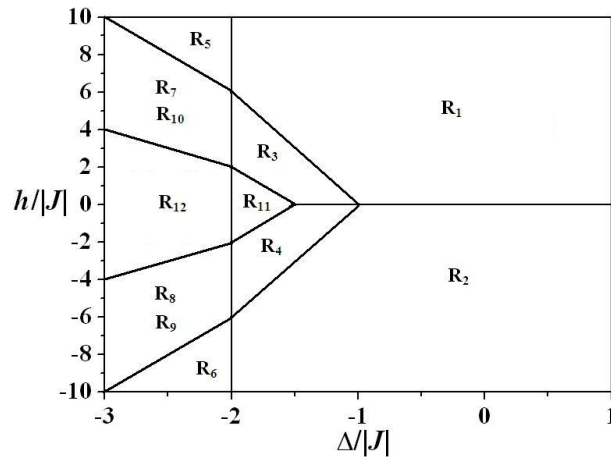


Fig. 1. Ground state-phase diagram of the mixed $(7/2, 3/2)$ Ising ferrimagnetic system for the model $J-\Delta-h$ for $J = -1$.

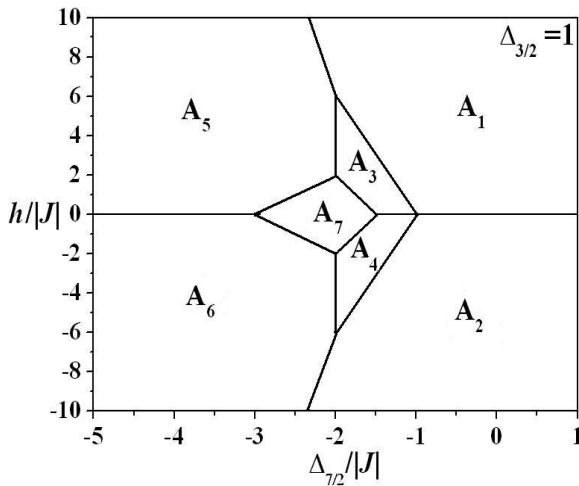


Fig. 2. Ground state-phase diagram of the mixed $(7/2, 3/2)$ Ising ferrimagnetic system for the model $J-\frac{\Delta_7}{2}-h$ when $\Delta_{3/2} = 1$ for $J = -1$.

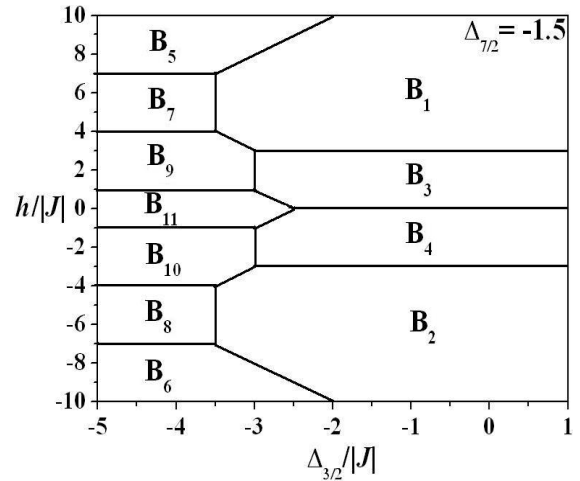


Fig. 3. Ground state-phase diagram of the mixed $(7/2, 3/2)$ Ising ferrimagnetic system for the model $J-\Delta_{3/2}-h$ when $\Delta_{7/2} = -1.5$ for $J = -1$.

Table 1

Ground-state energies of the model $J-\Delta-h$ with $J = -1$.

Region	Ground-state	Energy	Region	Ground-state	Energy
--------	--------------	--------	--------	--------------	--------

\mathbf{R}_1	$\begin{pmatrix} \frac{7}{2} & -\frac{3}{2} \\ 3 & 7 \\ -\frac{7}{2} & +\frac{3}{2} \end{pmatrix}$	$-42 J -29\Delta-4h$	\mathbf{R}_2	$\begin{pmatrix} -\frac{7}{2} & +\frac{3}{2} \\ 3 & 7 \\ +\frac{7}{2} & -\frac{3}{2} \end{pmatrix}$	$-42 J -29\Delta+4h$
\mathbf{R}_3	$\begin{pmatrix} \frac{5}{2} & -\frac{3}{2} \\ 3 & 5 \\ -\frac{5}{2} & +\frac{3}{2} \end{pmatrix}$	$-30 J -17\Delta-2h$	\mathbf{R}_4	$\begin{pmatrix} -\frac{5}{2} & +\frac{3}{2} \\ 3 & 5 \\ +\frac{5}{2} & -\frac{3}{2} \end{pmatrix}$	$-30 J -17\Delta+2h$
\mathbf{R}_5	$\begin{pmatrix} \frac{5}{2} & -\frac{1}{2} \\ 1 & 5 \\ -\frac{1}{2} & +\frac{5}{2} \end{pmatrix}$	$-10 J -13\Delta-4h$	\mathbf{R}_6	$\begin{pmatrix} -\frac{5}{2} & +\frac{1}{2} \\ 1 & 5 \\ +\frac{1}{2} & -\frac{5}{2} \end{pmatrix}$	$-10 J -13\Delta+4h$
\mathbf{R}_7	$\begin{pmatrix} \frac{3}{2} & -\frac{1}{2} \\ 1 & 3 \\ -\frac{3}{2} & +\frac{1}{2} \end{pmatrix}$	$-6 J -5\Delta-2h$	\mathbf{R}_8	$\begin{pmatrix} -\frac{3}{2} & +\frac{1}{2} \\ 1 & 3 \\ +\frac{3}{2} & -\frac{1}{2} \end{pmatrix}$	$-6 J -5\Delta+2h$
\mathbf{R}_9	$\begin{pmatrix} \frac{1}{2} & -\frac{3}{2} \\ 3 & 1 \\ -\frac{1}{2} & +\frac{3}{2} \end{pmatrix}$	$-6 J -5\Delta+2h$	\mathbf{R}_{10}	$\begin{pmatrix} -\frac{1}{2} & +\frac{3}{2} \\ 3 & 1 \\ +\frac{1}{2} & -\frac{3}{2} \end{pmatrix}$	$-6 J -5\Delta-2h$
\mathbf{R}_{11}	$\begin{pmatrix} \frac{3}{2} & \mp\frac{3}{2} \\ 3 & 3 \\ \mp\frac{3}{2} & \pm\frac{3}{2} \end{pmatrix}$	$-18 J -9\Delta$	\mathbf{R}_{12}	$\begin{pmatrix} \frac{1}{2} & \mp\frac{1}{2} \\ 1 & 1 \\ \mp\frac{1}{2} & \pm\frac{1}{2} \end{pmatrix}$	$-2 J -\Delta$

Table 2

Ground-state energies of the model $J-\Delta_{7/2}-h$ when $\Delta_{3/2} = 1$ with $J = -1$.

Region	Ground-state	Energy	Region	Ground-state	Energy
\mathbf{A}_1	$\begin{pmatrix} \frac{7}{2} & -\frac{3}{2} \\ 3 & 7 \\ -\frac{7}{2} & +\frac{3}{2} \end{pmatrix}$	$-42 J -24.5\Delta_{7/2}-4.5\Delta_{3/2}$ $-4h$	\mathbf{A}_2	$\begin{pmatrix} -\frac{7}{2} & +\frac{3}{2} \\ 3 & 7 \\ +\frac{7}{2} & -\frac{3}{2} \end{pmatrix}$	$-42 J -24.5\Delta_{7/2}-4.5\Delta_{3/2}+4h$
\mathbf{A}_3	$\begin{pmatrix} \frac{5}{2} & -\frac{3}{2} \\ 3 & 5 \\ -\frac{5}{2} & +\frac{3}{2} \end{pmatrix}$	$-30 J -12.5\Delta_{7/2}-4.5\Delta_{3/2}$ $-2h$	\mathbf{A}_4	$\begin{pmatrix} -\frac{5}{2} & +\frac{3}{2} \\ 3 & 5 \\ +\frac{5}{2} & -\frac{3}{2} \end{pmatrix}$	$-30 J -12.5\Delta_{7/2}-4.5\Delta_{3/2}+2h$
\mathbf{A}_5	$\begin{pmatrix} \frac{1}{2} & -\frac{3}{2} \\ 3 & 1 \\ -\frac{1}{2} & +\frac{3}{2} \end{pmatrix}$	$-6 J -0.5\Delta_{7/2}-4.5\Delta_{3/2}+2h$	\mathbf{A}_6	$\begin{pmatrix} -\frac{1}{2} & +\frac{3}{2} \\ 3 & 1 \\ +\frac{1}{2} & -\frac{3}{2} \end{pmatrix}$	$-6 J -0.5\Delta_{7/2}-4.5\Delta_{3/2}-2h$
\mathbf{A}_7	$\begin{pmatrix} \frac{3}{2} & \mp\frac{3}{2} \\ 3 & 3 \\ \mp\frac{3}{2} & \pm\frac{3}{2} \end{pmatrix}$	$-18 J -4.5\Delta_{7/2}-4.5\Delta_{3/2}$			

Table 3

Ground-state energies of the model $J-\Delta_{3/2}-h$ when $\Delta_{7/2} = -1.5$ with $J = -1$.

Region	Ground-state	Energy	Region	Ground-state	Energy
B₁	$\begin{pmatrix} \frac{7}{2} & -\frac{3}{2} \\ -\frac{3}{2} & +\frac{7}{2} \end{pmatrix}$	$-42 J -24.5\Delta_{7/2}-4.5\Delta_{3/2}$ $-4h$	B₂	$\begin{pmatrix} -\frac{7}{2} & +\frac{3}{2} \\ +\frac{3}{2} & -\frac{7}{2} \end{pmatrix}$	$-42 J -24.5\Delta_{7/2}-4.5\Delta_{3/2}+4h$
B₃	$\begin{pmatrix} \frac{5}{2} & -\frac{3}{2} \\ -\frac{3}{2} & +\frac{5}{2} \end{pmatrix}$	$-30 J -12.5\Delta_{7/2}-4.5\Delta_{3/2}$ $-2h$	B₄	$\begin{pmatrix} -\frac{5}{2} & +\frac{3}{2} \\ +\frac{3}{2} & -\frac{5}{2} \end{pmatrix}$	$-30 J -12.5\Delta_{7/2}-4.5\Delta_{3/2}+2h$
B₅	$\begin{pmatrix} \frac{7}{2} & -\frac{1}{2} \\ -\frac{1}{2} & +\frac{7}{2} \end{pmatrix}$	$-14 J -24.5\Delta_{7/2}-0.5\Delta_{3/2}$ $-6h$	B₆	$\begin{pmatrix} -\frac{7}{2} & +\frac{1}{2} \\ +\frac{1}{2} & -\frac{7}{2} \end{pmatrix}$	$-14 J -24.5\Delta_{7/2}-0.5\Delta_{3/2}+6h$
B₇	$\begin{pmatrix} \frac{5}{2} & -\frac{1}{2} \\ -\frac{1}{2} & +\frac{5}{2} \end{pmatrix}$	$-10 J -12.5\Delta_{7/2}-0.5\Delta_{3/2}$ $-4h$	B₈	$\begin{pmatrix} -\frac{5}{2} & +\frac{1}{2} \\ +\frac{1}{2} & -\frac{5}{2} \end{pmatrix}$	$-10 J -12.5\Delta_{7/2}-0.5\Delta_{3/2}+4h$
B₉	$\begin{pmatrix} \frac{3}{2} & -\frac{1}{2} \\ -\frac{1}{2} & +\frac{3}{2} \end{pmatrix}$	$-6 J -4.5\Delta_{7/2}-0.5\Delta_{3/2}-2h$	B₁₀	$\begin{pmatrix} -\frac{3}{2} & +\frac{1}{2} \\ +\frac{1}{2} & -\frac{3}{2} \end{pmatrix}$	$-6 J -4.5\Delta_{7/2}-0.5\Delta_{3/2}+2h$
B₁₁	$\begin{pmatrix} \pm\frac{1}{2} & \mp\frac{1}{2} \\ \mp\frac{1}{2} & \pm\frac{1}{2} \end{pmatrix}$	$-2 J -0.5\Delta_{7/2}-0.5\Delta_{3/2}$			

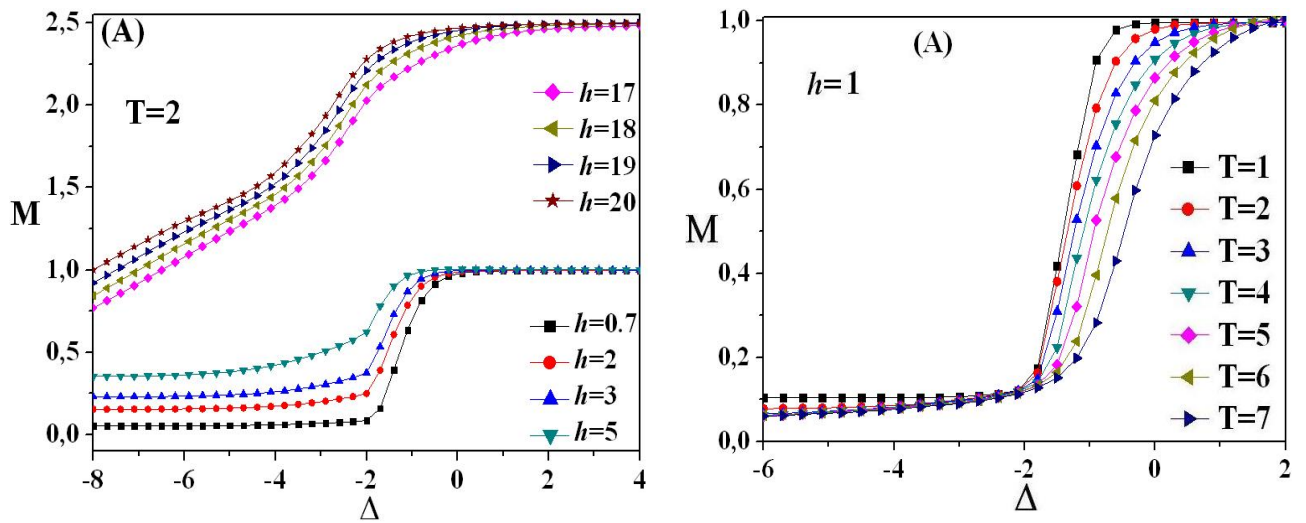
3.2. Variation of the magnetization as a function of the crystal field

In this subsection, we consider $\Delta = \Delta_{7/2} = \Delta_{3/2}$ to study the effects of the temperature and the external magnetic field.

In Figure 4, we plot the behaviours of the total magnetization of the system as a function of the crystal field Δ for various values of the external magnetic field h when $T = 2$. From Fig. 4(A), one can see that M increases from diverse values at $\Delta = -8$ with the increase of Δ . For $h = 0.7, 2, 3$ and 5 , the saturation value of M is 1 at $\Delta = 4$. By contrast, M saturates to 2.5 for $h = 17, 18, 19$ and 20 when $\Delta = 4$. However, Fig. 4(B) shows that M decreases from various values with the increase of Δ and the curves tend to a fixed point ($M = -1$) for $h = -0.7, -2, -3$ and -4 but to a fixed point ($M = -2.5$) for $h = -17, -18, -19$ and -20 . As a result, Fig. 4 demonstrates that the two behaviours are opposite when changing the sign of h . In fact, the magnetization M increases and decreases with increasing Δ for the positive and for

the negative values of h , respectively. These results can be compared with those of Refs. [132]. We note that the values $M = \pm 1$ come from the fact that the two spins are oppositely aligned but the values $M = \pm 2.5$ originate from that the two spins have the same direction under the large value of $|h|$.

In Figure 5, we present the crystal field Δ dependence of the total magnetization M for different values of the temperature when $h = 1$ and -1 . From Fig. 5(A), it is clear that M increases to its saturation value $M = 1$ with increasing Δ when $h = 1$. The same behaviours of variation of magnetization with the crystal field is found in the mixed-spin (5/2,3/2) Ising model in the two-dimensional decorated square and triangular lattices for the selected value $h = 1$ [133-134] and in a Blume-Capel model with the mixed 2- and 7/2-spins [135] using Monte Carlo simulations. By contrast, it is seen from Fig. 5 (B) that the magnetization decreases from different values at $\Delta = -6$ as Δ increases and saturates to $M = -1$. From Fig. 5, we conclude that the magnetization is an increasing function for $h = 1$ while it is a decreasing function for $h = -1$ for the selected values of T. This behaviours is in line with by the results given in Fig. 4. Also, it is worth noting that all magnetization curves cross at the crystal field point $\Delta = -2$ for all values of the temperature when $h = \pm 1$.



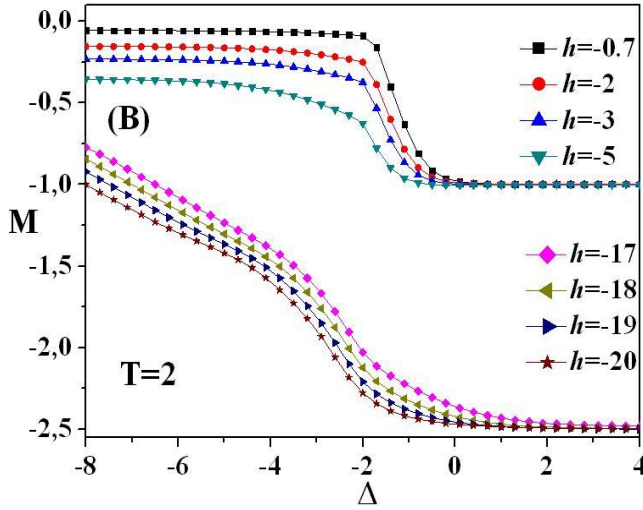


Fig. 4. The total magnetization versus $\Delta = \Delta 7/2 = \Delta 3/2$ for various h when $T = 2$.

(A) for h positive and (B) for h negative.

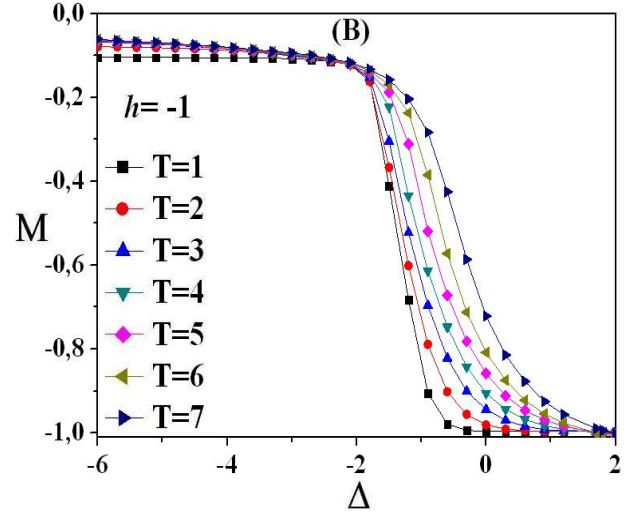


Fig. 5. The total magnetization versus $\Delta = \Delta 7/2 = \Delta 3/2$ for various T.

(A) for $h = 1$ and (B) for $h = -1$.

3.3. hysteresis loops under the effects of the temperature and the crystal fields

Now, we investigate the response of the magnetic properties of our system in an applied external magnetic field. Figs. 6–9 show the effects of the temperature T and the single-ion anisotropies ($\Delta 7/2, \Delta 3/2$) on the magnetic hysteresis loops of the total system (M) and the two sublattices ($M_{7/2}$ and $M_{3/2}$).

Fig. 6 presents the hysteresis loops in the absence of crystal fields ($\Delta 7/2 = \Delta 3/2 = 0$) in the range $-20 \leq h \leq 20$ for the values 0.5, 3, 6, 7 and 10 of the temperature T that has strong influence on the hysteresis cycles. In fact, the remanence and the coercivity decrease with increasing T until they become zero at relatively higher temperature. As a result, the total area of the hysteresis loop reduces as T increases. Also, It can be noticed that on increasing the temperature T from 0.5 and 7, the system shows one single loop whereas there is no loop when $T = 10$ for the total and the sublattices as presented in Fig. 6 (a–e) and (f–j), respectively. The same behaviours are observed in other Refs. [136–140]. Fig. 7 displays the total and the sublattice magnetizations versus the applied magnetic field h for several values of the anisotropy Δ at $T = 3$ within the interval $-20 \leq h \leq 20$. The decreasing of the crystal field results in lowering of the surface of the hysteresis cycle. Moreover, the remaining magnetization and the coercive field decrease as Δ decreases. These results are consistent with the ones in Refs. [137,141]. It appears that the shape of the cycle is single when $\Delta = 1, 0, -1$ and -1.5 . However, the system does not have a hysteresis loop when $\Delta = -1.77$ at $T = 3$ for M

and $(M_{7/2}, M_{3/2})$ sublattices as is seen in Fig. 7 (a–e) and (f–j), respectively. These behaviours are found in other papers [137, 142].

We note that the hysteresis loops presented in Figs. 6–7 are similar to those found in Refs.[136,141] under the effects of temperature and single-ion anisotropy. The effect of increasing T on hysteresis cycle (Figs. 6) is the same as that of decreasing Δ (Figs. 7) and the hysteresis cycles loss their squareness. It is important to note that some curves are reversible with no remanence and no coercive field as we can see in Figs. 6–7(e).

Fig. 8 demonstrates the magnetic hysteresis loops when $T = 0.5$ and $\Delta_{3/2} = 1$ for the total magnetization M and for the sublattice magnetizations $M_{7/2}$ and $M_{3/2}$ within the field range $-16 \leq h \leq 16$ for different values of $\Delta_{7/2}$. We mention that the single hysteresis loop is observed for $\Delta_{7/2} = 1, 0$ and -2.6 as in Fig. 8 (a), (b) and (f), respectively. It is important to note that the sublattices are also single as can be seen in Fig. 8 (g), (h) and (l). The single cycle (Fig. 8 (f)) does not have the same shape as the two ones in Fig. 8 (a) and (b). It can be also observed from this figure that the system can display hysteresis multi-loops. Really, the double and the triple loops are obtained for the values -2 and -1.65 of $\Delta_{7/2}$, as depicted in Fig. 8 (e) and (d), respectively. By contrast, the corresponding sublattices show single loops as shown in Fig. 8 (j) and (k). On the other hand, for $\Delta_{7/2} = -1.45$, see Fig. 8 (c), the loop is quintuple even if the sublattices are triple (Fig. 8 (i)). In addition, the double hysteresis loops obtained in Fig. 8 (e) are two separated cycles without a central loop. This type of hysteresis loops is different from the ones in the works [141, 143] but it is similar to the ones obtained in Refs. [137, 142].

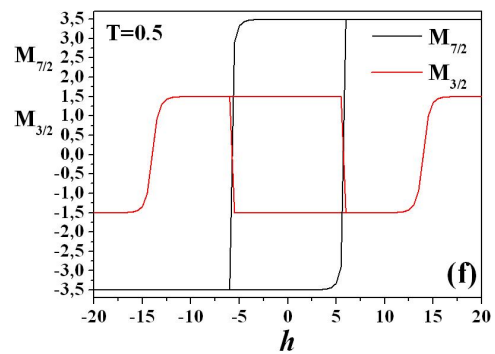
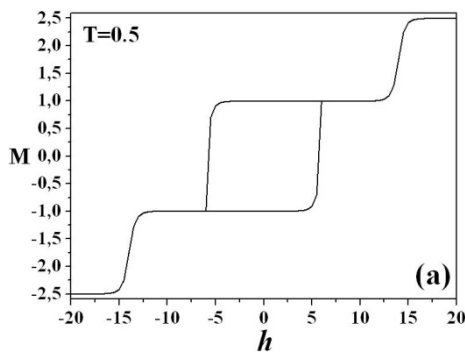
Fig. 9 illustrates the variations of the total and sublattice magnetizations as functions of the external magnetic field h with $T = 0.5$ and $\Delta_{7/2} = -1.5$ for diverse values of $\Delta_{3/2}$. One can remark that different shapes of the hysteresis loops are displayed. The single is observed for $\Delta_{3/2} = -1.5$ and -3.5 (Fig. 9 (d,f)), the triple is for $\Delta_{3/2} = 1, -0.8$ and -3.2 (Fig. 9 (a,c,e)) and the quintuple is obtained for the value $\Delta_{3/2} = 0$ (Fig. 9 (b)). We note that the sublattices cycles are single for $\Delta_{3/2} = 1, -0.8$ and -1.5 (Fig. 9 (g,i,j)) but they are triple for $\Delta_{3/2} = 0, -3.2$ and -3.5 (Fig. 9 (h,k,l)). It is noteworthy that the triple cycles in Fig. 9 (a) originates from single loops of $M_{7/2}$ and $M_{3/2}$ (Fig. 9 (g)) whereas the single loop in Fig. 9 (f) comes from triple cycles of $M_{7/2}$ and $M_{3/2}$ (Fig. 9 (l)). The loop in Fig. 9 (f) is different from the one found in Ref. [144].

From Figs. 8–9, we note that changing the value of $\Delta_{7/2}$ for fixed $\Delta_{3/2}$ or changing the value of $\Delta_{3/2}$ for fixed $\Delta_{7/2}$ may result in multiple hysteresis loops such as double, triple and quintuple hysteresis loops. However, in the case of equal anisotropy ($\Delta = \Delta_{7/2} = \Delta_{3/2}$) the

system cannot exhibit hysteresis multi-cycle behaviours as presented in Figs. 6–7. It is interesting to outline that the system displays double cycles when $T = 0.5$, $\Delta_{3/2} = 1$ and $\Delta_{7/2} = -2$ (Fig. 8(e)) and cannot show the double hysteresis loops for the values $T = 0.5$ and $\Delta_{7/2} = -1.5$ when $\Delta_{3/2}$ changes its value (Fig. 9). The absence of double hysteresis loops is also observed in the Refs. [136,137] for other values of the temperature and the crystal field. The single hysteresis loops obtained for $T = 0.5$ and $\Delta_{3/2} = 1$, see Fig. 8(a,b,f), are totally different from the single ones for $T = 0.5$ and $\Delta_{7/2} = -1.5$ in Fig. 9(d,f). The triple cycles shown in the cases $\Delta_{3/2} = 1, -0.8$ and -3.2 for the fixed values $T = 0.5$ and $\Delta_{7/2} = -1.5$ do not have the same shape as is seen in Fig. 8. The shapes of the double, the triple and the quintuple hysteresis loops we obtained are different from those found in Refs. [143,145].

Additionally, we mention that the multiple hysteresis loop behaviours have also been seen in other systems: the triple and the quintuple are found in the nano-graphene [145], the triple loop patterns in molecular-based magnetic materials [146], the double and triple cycles in nanoparticles. Experimentally hysteresis multi-loop phenomenon has also been shown in Co/Al₂O₃/Py. It is worthy to note that the hysteresis loops are all symmetric for the external magnetic field under the effects of both temperature and crystal fields as in [136,141].

From our computational calculations, it is found that the magnetic loops cannot appear for $T \geq 10$ in absence of anisotropy ($\Delta_{7/2} = \Delta_{3/2} = 0$) and for $\Delta \geq -1.77$ when $T = 3$ as one can see in Figs. 6(e)–7(e), respectively. Then, zero remanence and zero coercivity can be observed on the hysteresis curves. This indicates that the magnetic system enters in the superparamagnetic phase. Moreover, for $T = 0.5$, $\Delta_{3/2} = 1$ and $\Delta_{7/2} = -2$, the system show this phase when the applied magnetic field varies in the range $-8 \leq h \leq 8$ as shown in Fig. 8(e). This behaviours is also observed in previous theoretical studies [147].



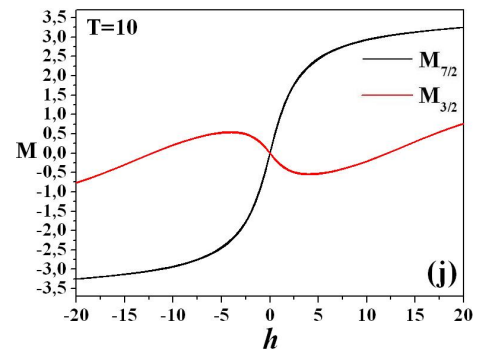
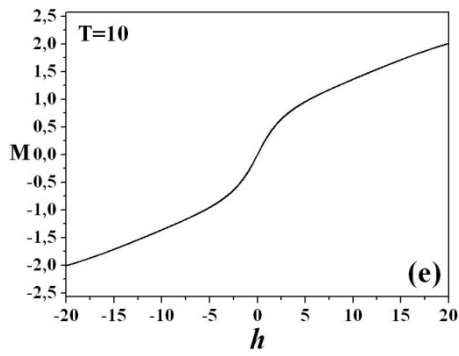
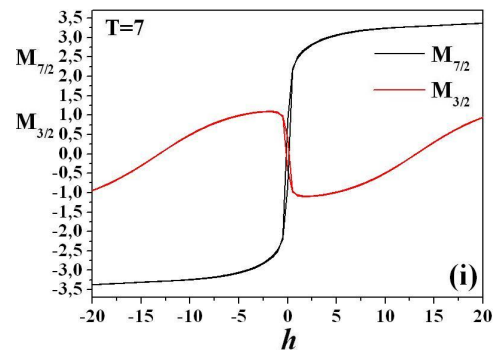
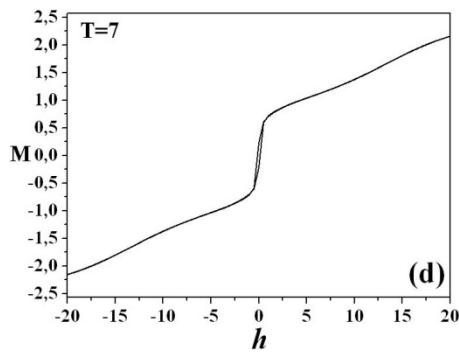
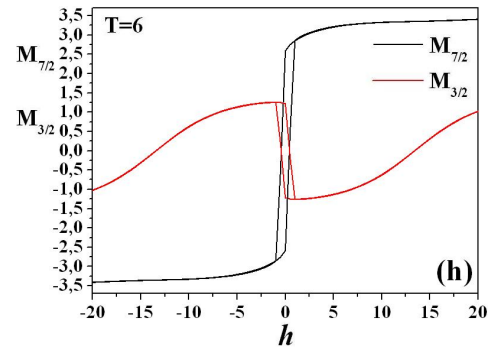
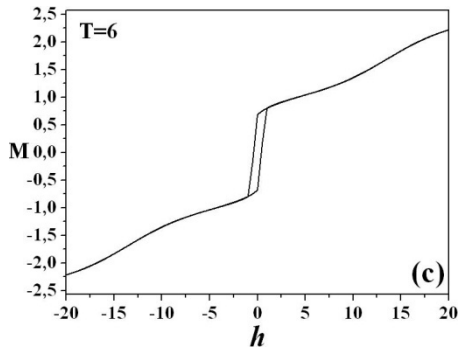
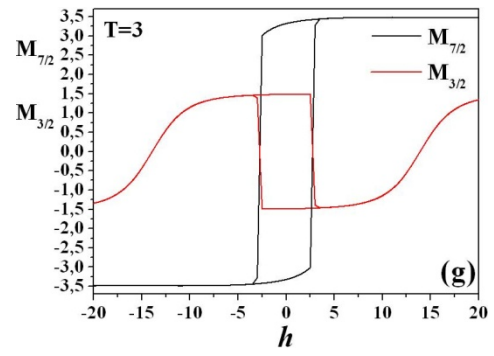
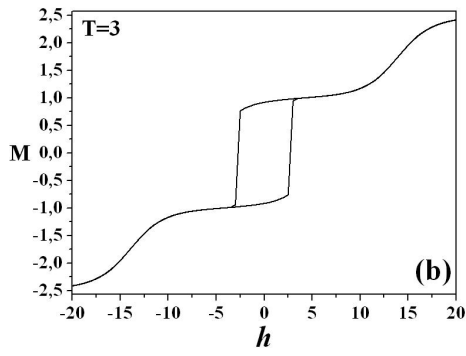
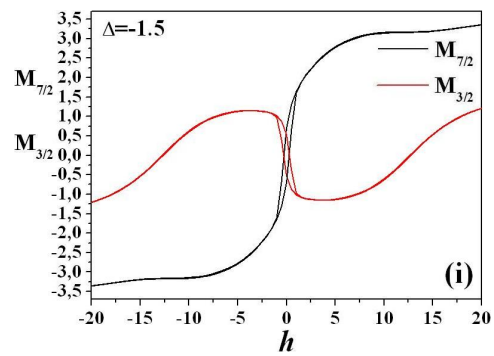
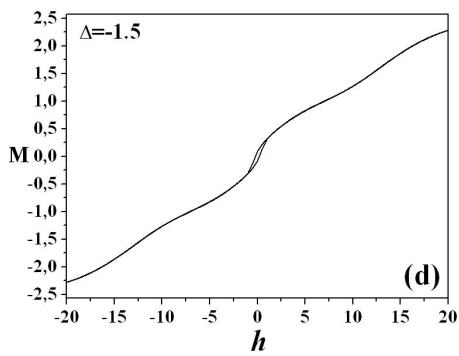
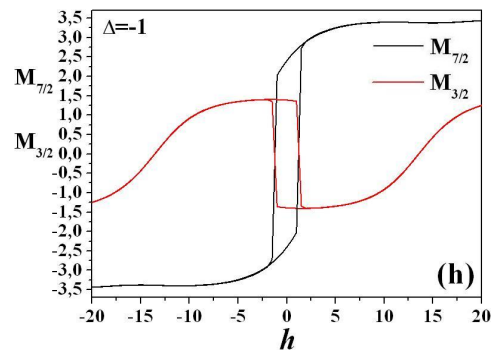
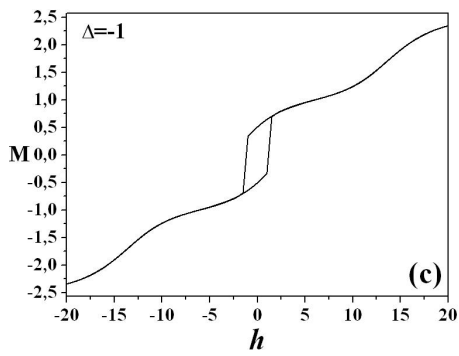
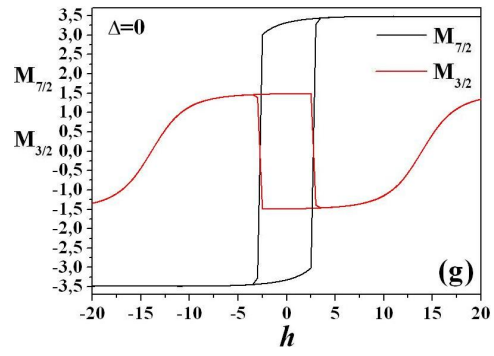
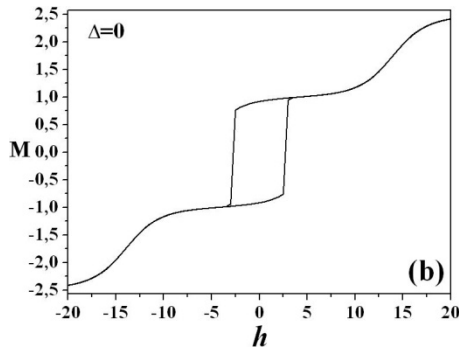
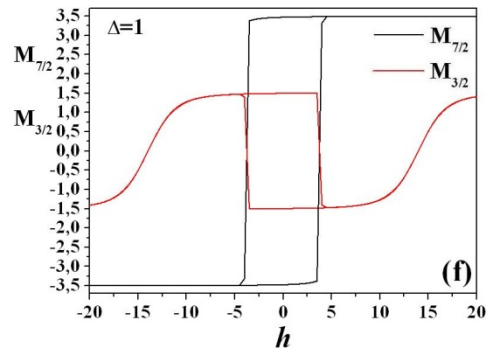
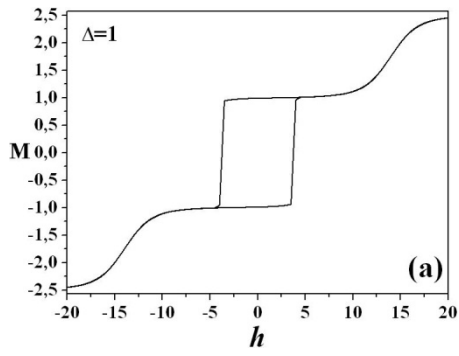


Fig. 6. Effect of the temperature on the hysteresis loops when $\Delta_{7/2} = \Delta_{3/2} = 0$ for M , $M_{7/2}$ and $M_{3/2}$.



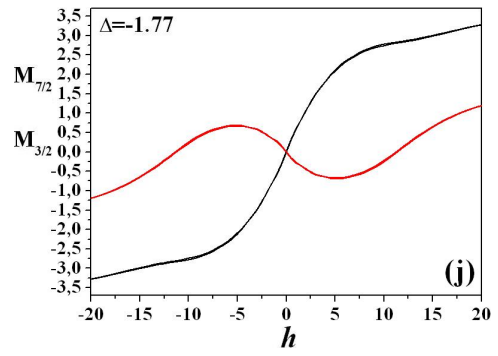
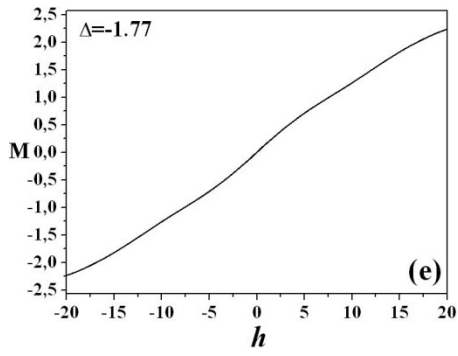
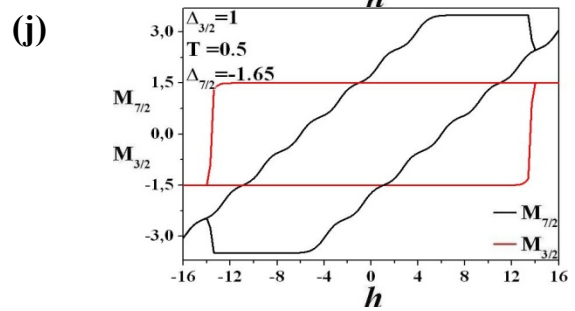
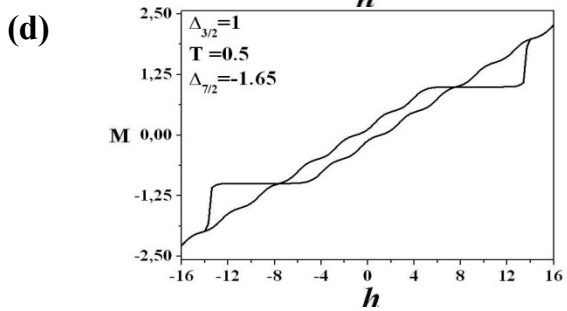
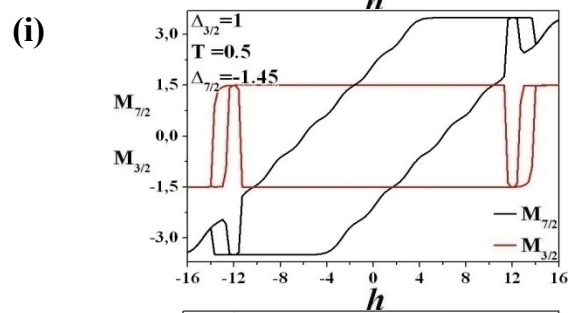
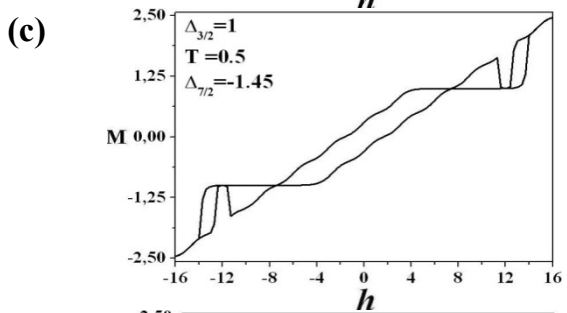
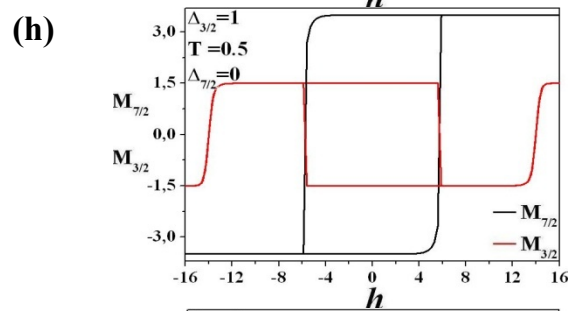
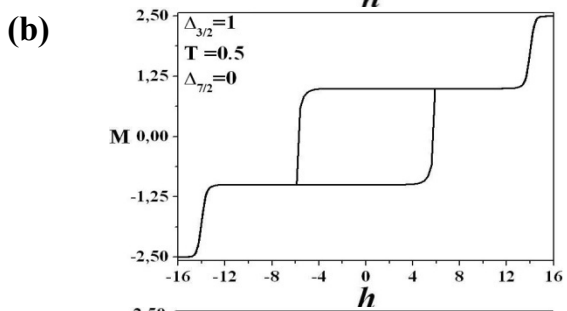
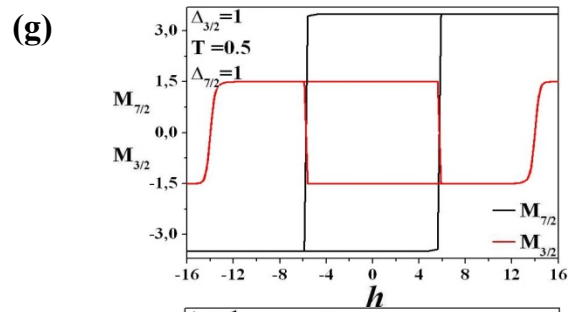
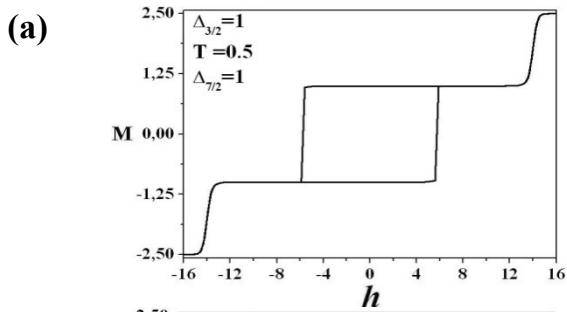


Fig. 7. Hysteresis loops with various $\Delta = \Delta_{7/2} = \Delta_{3/2}$ when $T = 3$ for M , $M_{7/2}$ and $M_{3/2}$.



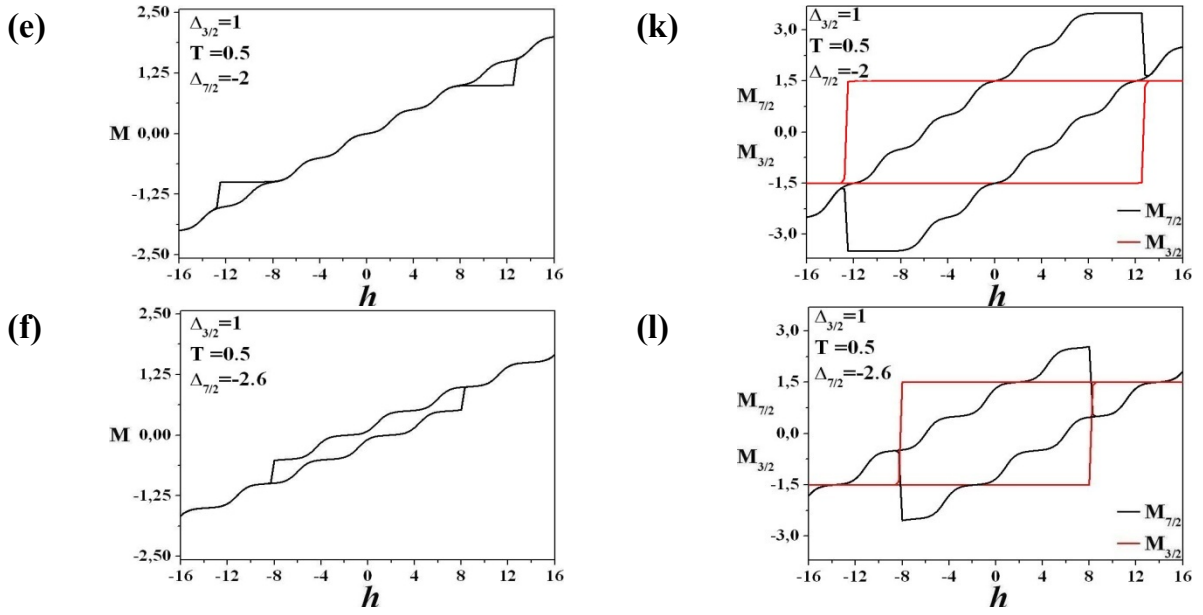
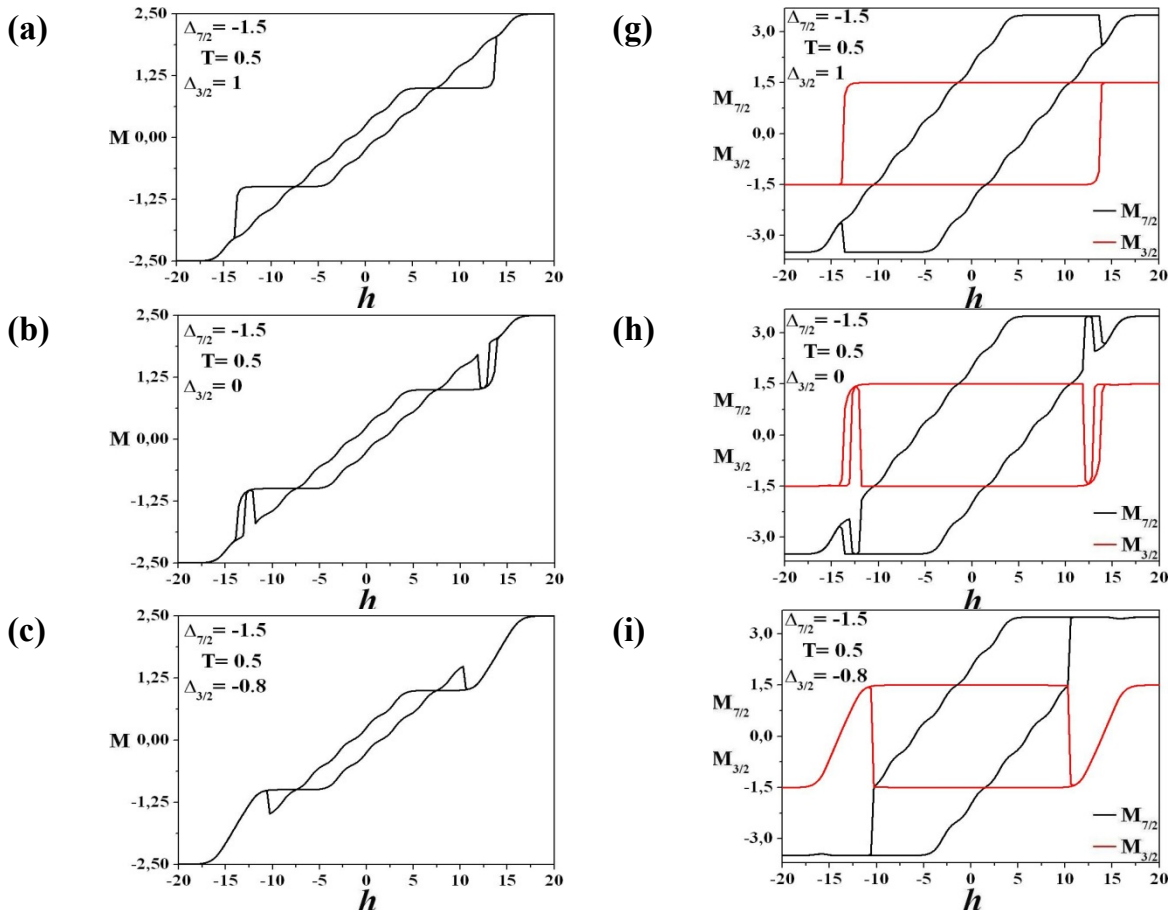


Fig. 8. Hysteresis loops for various $\Delta_{7/2}$ when $T = 0.5$ and $\Delta_{3/2} = 1$ for M , $M_{7/2}$ and $M_{3/2}$.



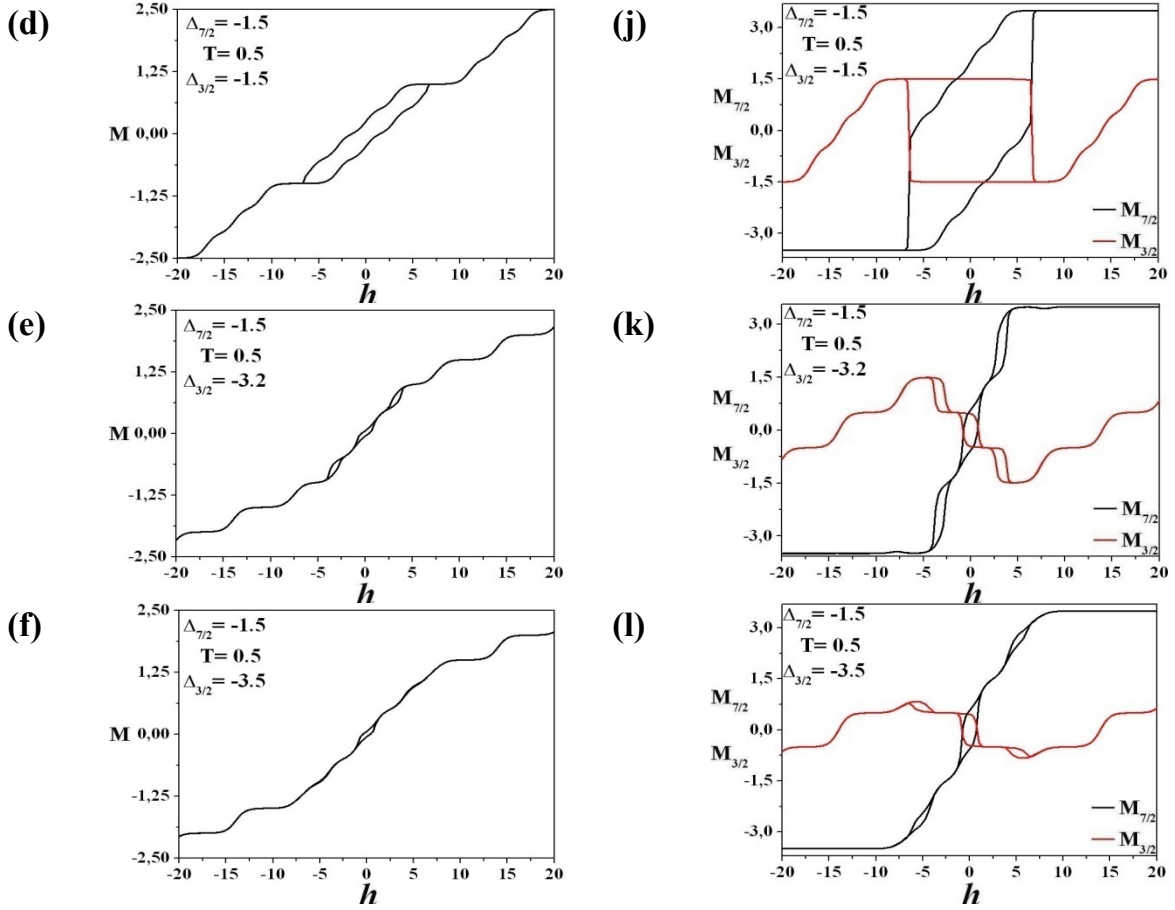


Fig. 9. Hysteresis loops for various $\Delta_{3/2}$ when $T = 0.5$ and $\Delta_{7/2} = -1.5$ for M , $M_{7/2}$ and $M_{3/2}$.

4. Conclusion

In this chapter, we have used a standard Monte Carlo simulation to examine the mixed spins $S = 7/2$ and $\sigma = 3/2$ Ising ferrimagnet on a square lattice. We have studied the variations of the magnetization as functions of the crystal field under the effects of the temperature and the external magnetic field. Consequently, on increasing the ion–single anisotropy, the total magnetization increases when the applied magnetic field takes positive values while decreases when the magnetic field is negative. In addition, we have found that the system can show multiple hysteresis cycles such as single, double, triple and quintuple loops. Also, the superparamagnetic phase has been detected.

Chapter 6

Unexpected Magnetic Behaviours of Ga Doped $\text{CuFe}_{1-x}\text{Ga}_x\text{O}_2$ Delafossite, $x =$ 0.04: First principle Calculation and Monte Carlo Simulation

1. Introduction

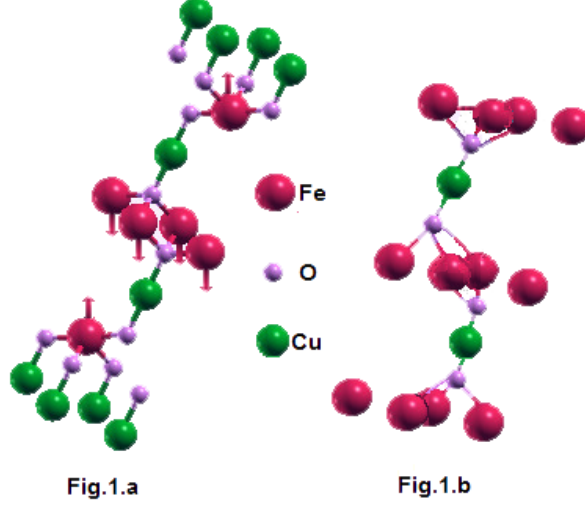
The structural electronic and magnetic properties of Ga doped delafossite $\text{CuFe}_{0.96}\text{Ga}_{0.04}\text{O}_2$ are investigated using first principle calculations and Monte Carlo simulation. The calculations are based on the density functional theory using the Wien2k package within Full Potential Linearized Augmented Plane Wave method and spin-polarized generalized gradient approximation of the exchange-correlation functional. The simulated results show that an ideal Ga doped Delafossite is an antiferromagnetic. Furthermore, we have explored the spin coupling interactions up to third nearest neighbours as well the coupling between adjacent layers, to examine the magnetism and thermo-dynamical properties. In addition, we have reported the magnetic properties of this element using Monte Carlo simulation. The obtained values of the Néel temperature decrease as the absolute value of the single ion anisotropy $|\Delta|$ increases. This result is in fair agreement with experiment.

2. Computational methods

2.1. Ab initio calculations

Delafossite crystallizes in two types of structures both are triangular, as represented in **Figure.1** [148-150], the crystal structures reported with the space group R3m with $a_h = 3.03 \text{ \AA}$ and $c_h = 17.09 \text{ \AA}$ in the hexagonal description (**Fig.1a**) [151-153] and P63/mmc, Hexagonal (Fig.1.b) [154-156]. The first structure is more stable and more abundant in the nature, because of these characteristics all results through this manuscript are related to this case. Ab initio calculations for Ga doped $\text{CuFe}_{1-x}\text{Ga}_x\text{O}_2$ with $x=0.04$ were performed using the Full Potential Linearized Augmented Plane Wave (FP-LAPW) method based on spin-polarized density functional theory, as implemented in the Wien2k code [105]. The exchange and correlation potential were treated with the generalized gradient approximation parametrized by Perdew, Burke and Ernzerhof (GGA-PBE) [158] and GGA+U (Hubbard coefficient) [162-163] with $U_{Fe} = 6 \text{ eV}$, increasing U conducts to slightly increasing the value of the magnetic moment [162]. After structure optimization, we performed calculations using $R_{MT} \times K_{max} = 8$, to determine the matrix size, where K_{max} is the plane wave cut-off and R_{MT} is the smallest of all atomic sphere radii, the convergence criterion for energy was considered when total

energy and density of charge were stable with 10^{-5} Ry, to show the doping effect we generate a 72 atoms supercell $3 \times 2 \times 1$. The fixed spin moment trick comes back to Schwarz and Mohn [164], by fixing spin up and spin down separately, the computed energy difference between $E_{AFM} - E_{FM} = \Delta E$ allows us to indicate the magnetic type in CuFeO_2 systems.



Figur-1. Delafossite structure with hexagonal structure
(The structures in the figure 1. Have been constructed using xcrystden [158]).

2.2. Ising model and Monte Carlo simulations

The system we study is described by the Hamiltonian given by the following formula:

$$H = -J_1 \sum_{[i,j]1} c_i c_j S_i S_j - J_2 \sum_{[i,j]2} c_i c_j S_i S_j - J_3 \sum_{[i,j]3} c_i c_j S_i S_j - J_{int} \sum_{[i,j]int} c_i c_j S_i S_j - \Delta \sum_i S_i^2 \quad (6.1)$$

Where i and j are the site indices on a triangular lattice. The sum $\sum_{[i,j]1}$ runs over all pair neighbours on the lattice. The sum $\sum_{[i,j]2}$ and $\sum_{[i,j]3}$ are taken over all second and third neighbours of the lattice, respectively. The sum $\sum_{[i,j]int}$ is over all inter-planar lattice sites. Δ is the single ion anisotropy acting on S -spins. J_1 , J_2 and J_3 correspond to the bilinear spin-exchange interaction strengths between the central spin and its first, second and third next nearest neighbours respectively and J_{int} is the inter-planer coupling between layers. The c_i variables can take the values 0 or 1 depending on whether the non-magnetic atom Ga exists or not on the site i or the site j . The magnetic sites are occupied by the ions of iron ($Z=26$) Fe^{3+} with the electronic configuration $[\text{Ar}] 4s^0 3d^5$, which can take the values: $S = \pm \frac{5}{2}; \pm \frac{3}{2}; \pm \frac{1}{2}$.

It is worth nothing that this system contains a high anisotropy due to the difference along different axes [165]. Such magnetic materials usually can be described by Ising model.

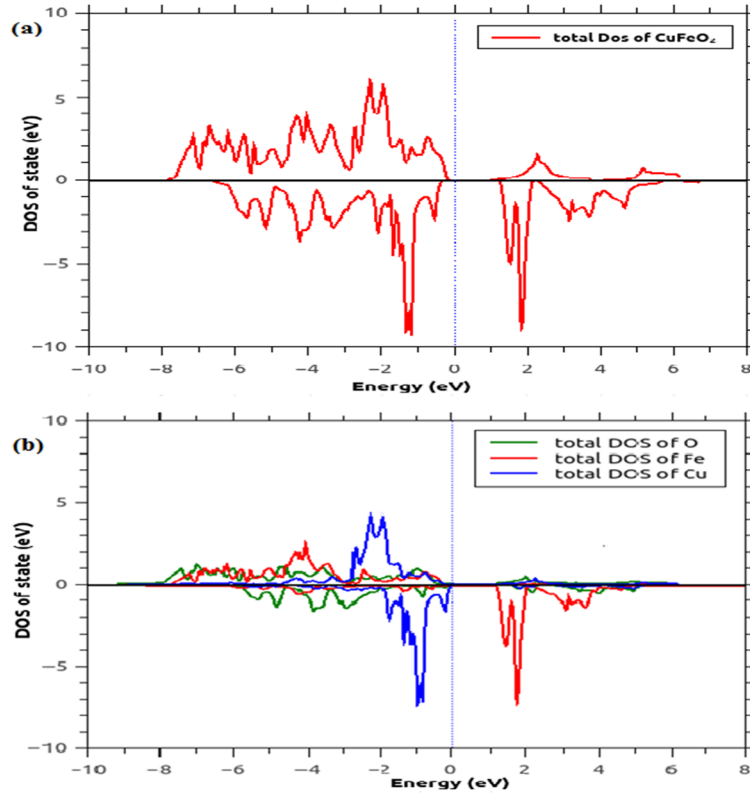
Standard sampling method has been adopted to simulate the Hamiltonian given by eq. (1). Periodic boundary conditions have been imposed on the whole lattice and initial configurations

have been randomly generated by sequentially traversing the lattice and making single-spin flip attempts. The flips are accepted or rejected according to a heat-bath algorithm under the Metropolis approximation [110]. Our data were generated with 10^4 Monte Carlo steps per spin, after discarding the first 10^3 Monte Carlo steps per site for equilibrium. Starting from different initial conditions, we performed the average of each parameter and estimated the Monte Carlo simulations, averaging over many initial conditions.

3. Results and discussion

We consider the structure with space group R3m with $a_h = 3.03 \text{ \AA}$ and $c_h = 17.09 \text{ \AA}$ in the hexagonal description Fig.1.a; after optimizing the structural parameters and interatomic positions for CuFeO_2 , the relaxed atomic lattice parameters that we have obtained are $a_{h\text{-opt}} = 3.029 \text{ \AA}$ and $c_{h\text{-opt}} = 17.088 \text{ \AA}$. We find that the energy difference in ground state of ferromagnetic and antiferromagnetic state along the c axis $E_{AFM} - E_{FM} = -0.000852 \text{ (Ry)} < 0$ which means that the antiferromagnetic state is more stable in Ga doped CuFeO_2 .

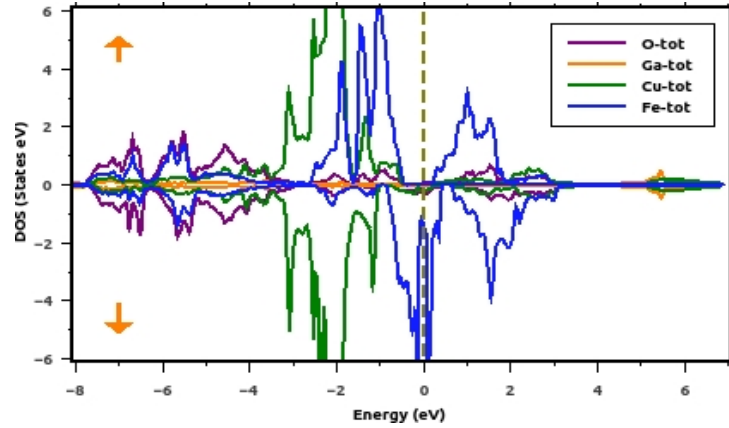
The calculation of the electronic structure plays an important role in determining the magnetic properties of Delafossite compound. There is no band gap both in the LDA as well as in the GGA calculations, However, the experimental value of bulk CuFeO_2 is 1.15eV [163]. We have therefore made a correction to the band gap by using a GGA+U with the potential $U_{Fe} = 6 \text{ eV}$ for Iron atoms. With this approach the band gap of bulk CuFeO_2 is about $E_g = 1.02 \text{ eV}$ as shown in **Figure.2**, this value comes around the experimental value [163] and by the ab initio calculations [164].



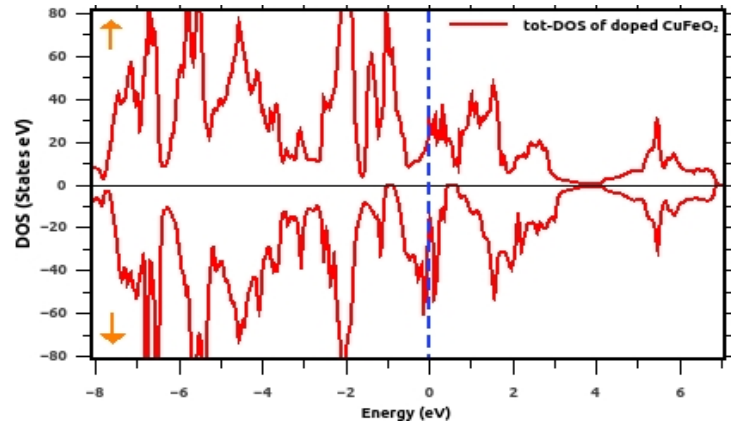
Figur-2. Total DOS (a) and partial DOS (b) of CuFeO₂.

The origin of magnetism in several materials has been explained by various physical mechanisms depending on the concentration of magnetic ions and free carriers. The calculated magnetic moment in the bulk CuFeO₂ is $m = 2.89 \mu_B$ and when we doped the system with 4.17% of Ga the magnetic moment increase to $m = 3.91 \mu_B$ which is in accordance with $m_{eff} = 4.65 \mu_B$ determined by the experiment [166]. In Ga doped Delafossite CuFeO₂ compound, the elements have the following atomic structures configurations: [Ar]3d64s2 for Fe, [Ar]3d94s2 for Cu, [Ar]3d104s2p1 for Ga and 2s22p6 for O. Figure.3 illustrates the density of iron is shifted around the Fermi energy ($E_F = 0$); this suggests that Ga³⁺ preferably chooses to occupy Fe ³⁺ sites, where the 4s-electrons bind in much the same way as the two Ga 4s electrons. It is also possible and common that Ga occupies an interstitial site and this is the origin of undesirable effects like clustering and quenching of magnetism which is the result of the symmetry lowering of the ionic one-electron effective potential due to the charge distribution around the magnetic ion. Figure .4 represents the total DOS of Ga doped CuFeO₂, so the dopant pushes the electronic states of the iron to localize around the Fermi level, the 3d orbital of iron is split up into t_{2g} and e_g orbitals as shown in Figure.3. Thus, the magnetic behaviours can be reverting to the antiferromagnetic super-exchange between the iron and oxygen; this impact can be also seen in experimental results [167]. Regularly, doping a system with non-magnetic impurities led to non-magnetic system, however, in this work the results

demonstrate that doping the system with a non-magnetic Ga³⁺ ion may have an important effect on the magnetic stabilities behaviours of the system, similar result has been observed experimentally [167].



Figur-3. Partial DOS of components for spin up (a) and spin down (b).



Figur-4. Total DOS of $\text{CuFe}_{0.96}\text{Ga}_{0.04}\text{O}_2$ delafossite.

On the other hand, to calculate the interaction coupling, we consider four next nearest neighbours coupling interactions, J_1 , J_2 , J_3 , and J_{int} is the inter-planer coupling between layers, as depicted in **Figure.5**, we calculated five possible configurations of ordered spin states using the Hamiltonian given by the formula in (1): C_1, C_2, C_3, C_4 and C_5 (see **Fig.6**). To compute energy for different configurations we generate supercell $3 \times 2 \times 1$ with 72 atoms.

$$E_{c1} = E_0 - 25(54J_1 + 54J_2 + 54J_3 + 54J_{int})/4 \quad (6.2)$$

$$E_{c2} = E_0 - 25(54J_1 + 54J_2 + 54J_3 - 18J_{int})/4 \quad (6.3)$$

$$E_{c3} = E_0 - 25(6J_1 - 18J_2 + 6J_3 + 22J_{int})/4 \quad (6.4)$$

$$E_{c4} = E_0 - 25(-18J_1 - 18J_2 + 54J_3 + 6J_{int})/4 \quad (6.5)$$

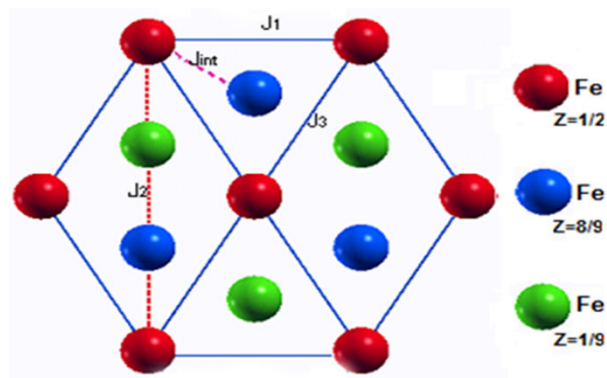
$$E_{c5} = E_0 - 25(-18J_1 + 6J_2 + 6J_3 + 6J_{int})/4 \quad (6.6)$$

The calculation shows that the interaction coupling between J_1 , J_2 , J_3 and J_{int} of CuFeO₂ are antiferromagnetic. These values are comparable to the corresponding spin exchange deduced from the inelastic neutron scattering and other theoretical studies as presented in **Table 1**.

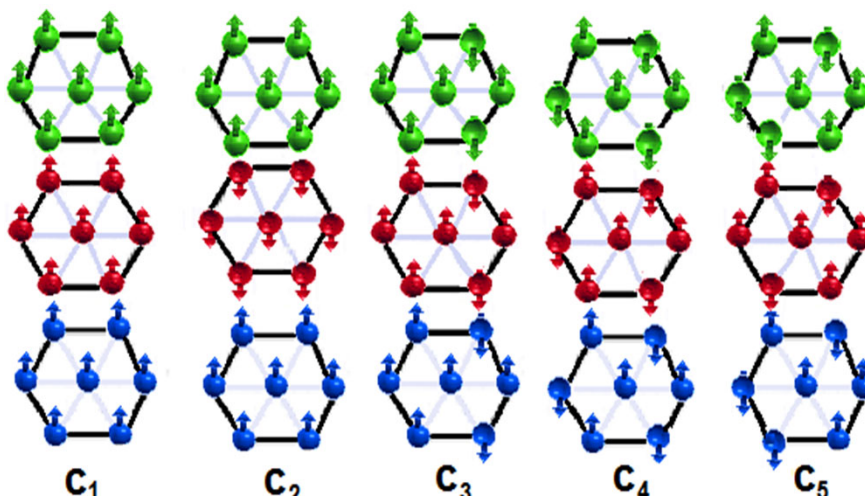
References	Method	$J_1(meV)$	$J_2(meV)$	$J_3(meV)$	$J_{int}(meV)$
This work	LDA	-1.15	-0.21	-0.13	-0.17
This work	GGA+U (Wien2K)	-0.81	-0.11	-0.22	-0.16
[168]	GGA+U (Vasp) ^a	-0.77	-0.15	-0.28	-0.24
[169]	Experimental	-0.45	-0.20	-0.26	-0.13

^a Ref [170].

Table1. The calculated coupling interactions on doped Delafossite CuFeO₂.



Figur-5. Coupling interaction between next nearest neighbours.



Figur-6. Configurations of ordered spin states.

On the other hand, we use the Monte Carlo simulation to investigate thermo-dynamical properties of Ga doped CuFeO₂. Our program calculates the following parameters, namely:

The magnetization of the system per spin can be written as:

$$M = \frac{1}{N} \langle \sum_{i=1}^N S_i \rangle \quad (6.7)$$

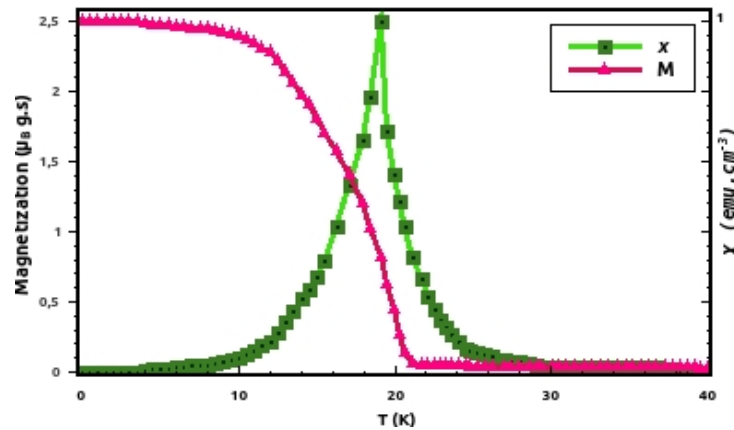
With $N = N_x \times N_y \times N_z = 27 \times 27 \times 81$ are the numbers of spins S on each direction x , y and z , respectively.

To locate the transition temperature, we exploit the magnetic susceptibility per site defined as follow:

$$\chi = \beta \left(\left\langle \left(\frac{1}{N} \sum_{i=1}^N S_i \right)^2 \right\rangle - \left\langle \frac{1}{N} \sum_{i=1}^N S_i \right\rangle^2 \right) \quad (6.8)$$

where $\beta = 1/k_{BT}$, T denotes the absolute temperature and k_B is the Boltzmann's constant.

Figure.7 shows the variation of magnetization and the magnetic susceptibility as functions of the temperature in the absence of the magnetic anisotropy. From this figure, one can see that the Magnetization decreases from its saturation values at $T = 0$ which is 2.5 with increasing T . Also, the maximum value of the susceptibility is reached at the Néel temperature $T_C = 20 K$.



Figur-7. Thermal dependence of the magnetization M and Magnetic susceptibility χ in the absence of the single-ion anisotropy $\Delta = 0$.

Figure.8a, illustrates thermal variations of the magnetization as a function of the temperature for various values of the magnetic anisotropy $\Delta = -1, -2, -3$ and -3.5 for further reading about the impact of the next-nearest neighbour interactions and the single ion anisotropy on the magnetization behaviours [171]. We shall mention that the critical temperature decreases as the absolute value $|\Delta|$ increases. This result agrees well with the one obtained in **Figure.8b** where the magnetic susceptibility is depicted for diverse values of the single ion anisotropy $\Delta = -1, -2, -3$ and -3.5 . This value is consistent with the obtained one found experimentally [53].

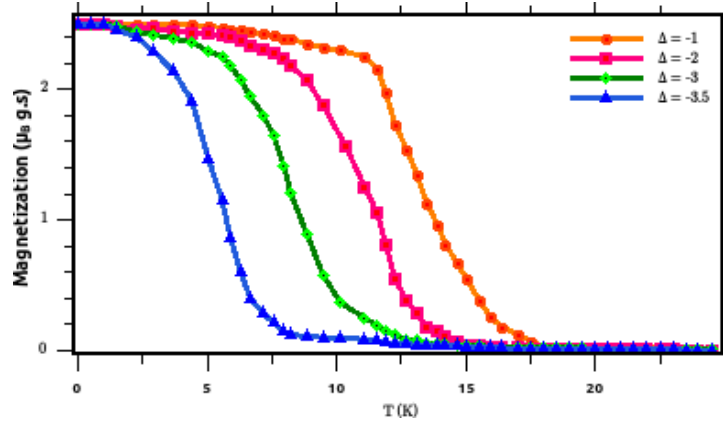


Figure 8a. Thermal dependence of the magnetization for three different values of the single-ion anisotropy $\Delta = -1, -2$ and -3 .

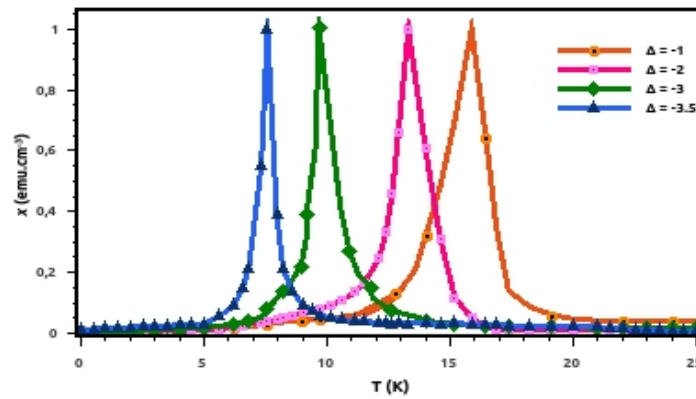


Figure 8b. Magnetic susceptibility vs. the temperature for three different values of the single-ion anisotropy $\Delta = -1, -2$ and -3 .

4. Conclusions

In this work we have seen the impact of doping $\text{CuFe}_{0.96}\text{Ga}_{0.04}\text{O}_2$ Delafossite with a non-magnetic element by first principle calculation using Wien2k package the computation method were performed with generalized gradient approximation GGA+U approach which give more accuracy for the band gap value $E_g = 1.02\text{eV}$, we have reached that the doping the system by a non-magnetic Ga^{3+} ion may have an important effect on the magnetic behaviours. Additionally, we have investigated the coupling magnetic moments which are compared to experimental data. On the other hand, we have examined certain properties using Monte Carlo simulation; we found that the determined Néel temperature decreases as the absolute value of the single ion anisotropy $|\Delta|$ increases. In order to make meaningful conclusion it is important to note that reunion between theoretical and experimental studies of systems doped with non magnetic materials, will lead to more understanding the magnetic behaviours in many materials elements and open a pathway to predict new magnetic materials.

General Conclusion

In this thesis We have applied Monte Carlo simulation to study certain mixed Ising ferrimagnetic systems on a square lattice, with high spin $7/2$. With the purpose of doing that, we implemented Metropolis algorithm with periodic boundary conditions. We can highlight the main obtained results as follows:

mixed-Spin ($7/2$, $5/2$)

- ✓ the impact of the nearest-neighbour interactions with crystal field.
- ✓ We demonstrated the existence of the compensation temperature, even if we consider only the first nearest neighbours.
- ✓ multiple ground state phase diagrams of partial and total magnetization have been depicted, for several combinations of the parameters exchange interactions and crystal field values.
- ✓ Several compensation temperatures (T_{comp}) for appropriate values of coupling interaction have been detected.
- ✓ we have also examined the effect of coupling interactions on the compensation temperature.
- ✓ The influences of the exchange interactions and crystal fields on the magnetization, compensation and critical temperatures have been studied.
- ✓ We found that the system has compensation temperatures for appropriate values of J_S , J_σ in absence of any crystal field.
- ✓ We found that for each value of the next-nearest neighbours' interaction, there are several values of the next-nearest neighbours for which compensation temperatures exist and vice versa.
- ✓ The system cannot show compensation points for some selected values of the crystal fields only if the interactions between pairs of next-nearest neighbours are included in the system.
- ✓ We obtained different types of magnetization curves.
- ✓ We have studied the variations of the magnetization as functions of the crystal field under the effects of the temperature and the external magnetic field.
- ✓ on increasing the ion-single anisotropy, the total magnetization increases when the applied magnetic field takes positive values, while decreases when the magnetic field is negative.

mixed-Spin ($7/2$, $3/2$) case

- ✓ we have found that the system can show multiple hysteresis cycles such as single, double, triple, and quintuple loops. Also, the superparamagnetic phase has been detected.

On the other hand we have seen the impact of doping $\text{CuFe}_{0.96}\text{Ga}_{0.04}\text{O}_2$ Delafossite with a non-magnetic element by first principle calculation using Wien2k package the computation method were performed with generalized gradient approximation GGA+U approach which give more accuracy for the band gap value $E_g = 1.02\text{eV}$, we have also, investigated the coupling magnetic moments which are compared to other literature works. Hence, using Monte Carlo simulation; we found that the determined Néel temperature decreases as the absolute value of the single ion anisotropy $|\Delta|$ increases. In order to make meaningful conclusion it is important to note that reunion between theoretical and experimental studies of systems doped with non-magnetic materials, will lead to more understanding the magnetic behaviours in many materials elements and open a pathway to predict new magnetic materials.

References

- [1]. T. Mallah, S. Thiébaud, M. Verdaguer, P. Veillet, "High-Tc molecular-based magnets: Ferrimagnetic mixed-valence chromium (III)-chromium (II) cyanides", *Science* 262 (1993) 1554.
- [2]. K. Inoue, T. Hayamizu, H. Iwamura, D. Hashizume, Y. Ohashi, "Assemblage and alignment of the spins of the organic trinitroxide radical with a quartet ground state by means of complexation with magnetic metal ions. A molecule-based magnet with three-dimensional structure and high Tc of 46 K." *J. Am. Chem. Soc.* 118 (1996) 1803.
- [74]. M. Louis Néel (1948). "Propriétés magnétiques des ferrites; Férrimagnétisme et antiferromagnétisme". *Annales de Physique*. 12 (3): 137–198.
Bibcode:1948AnPh.12.137N. doi:10.1051/anphys/194812030137.
- [3]. H.D. Shieh, M.H. Kryder. "Magneto-optic recording materials with direct overwrite capability.", *Appl. Phys. Lett.* 49 (1986) 473.
- [4]. V.S. Leite, M. Godoy, W. Figueiredo. "Finite-size effects and compensation temperature of a ferrimagnetic small particle.", *Phys. Rev. B* 71 (2005) 094427.
- [5]. G.A.N. Connell, R. Allen, M. Mansuripur. "Magneto-optical properties of amorphous terbium–iron alloys.", *J. Appl. Phys.* 53 (1982) 7759.
- [6]. J. Ostoréro, M. Escorne, A. Guegan, F. Soulette, H. L. Gall. "Dy₃Fe₅O₁₂ garnet thin films grown from sputtering of metallic targets.", *J. Appl. Phys.* 75 (1994) 6103.
- [7]. J. P. Perdew, K. Burke, M. Ernzerhof. *Phys. Rev. Lett.* 77 (1996) 3865.
- [8]. P. Mukherjee, B. C. Gupta, P. Jena. "Magnetic properties of bimetallic clusters composed of Gd and transition metals." *J. Appl. Phys.* 119 (2016) 074301.
- [9]. N. Iwata, K. Hattori, T. Shigeoka, "Exchange interaction and magnetocrystalline anisotropy in GdMn₂Ge₂.", *J. Magn. Magn. Mater.* 53 (1986) 318.
- [10]. B. Wu. *Dalton Trans.* "Synthesis, structure and magnetic properties of the first Mn (II)-Gd (III) heteronuclear complex.", 43 (2006) 5113.
- [11]. Huan, J., Hu, L., Fang, X.: "Dense Assembly of Gd₂O₃: 0.05 X³⁺ (X= Eu, Tb) Nanorods into Nanoscaled Thin-Films and Their Photoluminescence Properties.", *ACS Appl. Mater. Interfaces* 6(3), 1462–1469 (2014)
- [12]. Petoral, R.M. Jr., Söderlind, F., Klasson, A., Suska, A., Fortin, M.A., Abrikosova, N., Selegard, L., Käll, P.O., Engström, M., Uvdal, K.: "Synthesis and characterization of Tb³⁺-doped Gd₂O₃ nanocrystals: a bifunctional material with combined fluorescent labeling and MRI contrast agent properties.", *J. Phys. Chem. C* 113(17), 6913–6920 (2009)

- [13]. Song, Y., You, H., Huang, Y., Yang, M., Zheng, Y., Zhang, L., Guo, N.: "Highly uniform and monodisperse Gd₂O₂S: Ln³⁺ (Ln= Eu, Tb) submicrospheres: solvothermal synthesis and luminescence properties.", *Inorg. Chem.* 49(24), 11499–11504 (2010)
- [14]. Yin, J., Li, C., Chen, D., Yang, J., Liu, H., Hu, W., Shao, Y.: "Structure and dysprosium dopant engineering of gadolinium oxide nanoparticles for enhanced dual-modal magnetic resonance and fluorescence imaging.", *Phys. Chem. Chem. Phys.* 19, 5366–5376 (2017)
- [15]. Li, Z., Kim, J., Kioussis, N., Ning, S.Y., Su, H., Iitaka, T., Tohyama, T., Yang, X., Zhang, J.X.: GdN thin film: chern insulating state on square lattice. *Phys. Rev. B* 92, 201303(R) (2015)
- [16]. Figuerola, A., Diaz, C., El Fallah, M.S., Ribas, J., Maestro, M., and Mahía, J.: Structure and magnetism of the first cyano-bridged hetero one-dimensional Gd^{III}–Cr^{III} complexes *Chem. Commun.* 13, 1204 (2001)
- [17]. Verdaguer, M.: Molecular electronics emerges from molecular magnetism. *Science*. 272(5262), 698–699 (1996)
- [18]. Coronado, E., Delhaès, P., Gatteschi, D., Miller, J.S. (eds.): *Molecular magnetism: from molecular assemblies to the devices*, vol. 321. Springer Science & Business Media, Berlin (2013)
- [19]. Linert, W., Verdaguer, M. (eds.): *Molecular magnets: recent highlights*. Springer, Berlin
- [20]. Yoshii, K.: Magnetic properties of perovskite GdCrO₃. *J. Solid State Chem.* 159, 204–208 (2001)
- [21]. Jabar, A., Masrour, R., Benyoussef, A., Hamedoun, M.: Monte Carlo study of alternate mixed spin-5/2 and spin-2 Ising ferrimagnetic system on the Bethe lattice. *J. Magn. Mater.* 397, 287–294 (2016)
- [22]. Wang, W., Chen, D., Lv, D., Liu, J., Li, Q., Peng, Z.: "Monte Carlo study of magnetic and thermodynamic properties of a ferrimagnetic Ising nanoparticle with hexagonal core-shell structure.", *J. Phys. Chem. Solids.* 108(39), (2017)
- [23]. Prijic, S., Scancar, J., Romih, R., Cemazar, M., Bregar, V.B, Znidarsic, A., Sersa, G.: Increased cellular uptake of biocompatible superparamagnetic iron oxide nanoparticles into malignant cells by an external magnetic field. *J. Membr. Biol.* 236, 167–179 (2010)
- [24]. Alborzi, Z., Hassanzadeh, A., Golzan, M.: "Superparamagnetic behavior of the magnetic hysteresis loop in the Fe₂O₃@ Pt core-shell nanoparticles.", *Int. J. Nanosci. Nanotechnol.* 8, 93 (2012)

- [25]. Sun, C., Du, K., Fang, C., et al.: PEG-mediated synthesis of highly dispersive multifunctional superparamagnetic nanoparticles: their physicochemical properties and function in vivo. *J. Am. Chem. Soc. nano* 4(4), 2402 (2010)
- [26]. Bulte, J.W.M., Brooks, R.A., Moskowitz, B.M, Bryant Jr, L. H., Frank, J. A.: Relaxometry and magnetometry of the MR contrast agent MION-46L. *Magn. Reson Med.* 42, 379 (1999)
- [27]. Bouhou, S., Essaoudi, I., Ainane, A., Saber, M., Dujardin, F., de Miguel, J.J.: Hysteresis loops and susceptibility of a transverse Ising nanowire. *J. Magn. Magn. Mater.* 324, 2434–2441 (2012)
- [28]. P. Lunca-Popa, J. Afonso, P. Grysan, J. Crepellere, R. Leturcq, D. Lenoble, "Tuning the electrical properties of the p-type transparent conducting oxide $\text{Cu}_{1-x}\text{Cr}_x\text{O}_2$ by controlled annealing.", *Sci. Rep.* 8, 7216 (2018).
- [29]. S.W. Cheong, M. Mostovoy, "Multiferroics: a magnetic twist for ferroelectricity.", *Nat. Mater.* 6, 13 (2007).
- [30]. T. Elkhouni, M. Amami, C.V. Colin, P. Strobel, A. Ben Salah, "Synthesis, structural and magnetic studies of the $\text{CuCr}_{1-x}\text{Co}_x\text{O}_2$ delafossite oxide.", *J. Magn. & Magn. Mater.* 330, 101 (2013).
- [31]. Maocai Zhang, Lingyan Dang, Chen Tian, Shifeng Zhao, Qingshan Lu, Superlattices *Microstruct.* 111, 423 (2017).
- [32]. G. Xiao, Z. Xia, M. Wei, S. Huang, L. Shi, X. Zhang, H. Wu, F. Yang, Y. Song, Z. Ouyang, *J. Magn. & Magn. Mater.* 449, 214 (2018).
- [33]. David O. Scanlon, Aron Walsh, Graeme W. Watson, "Understanding the p-type conduction properties of the transparent conducting oxide CuBO_2 : a density functional theory analysis.", *Chem. Mater.* 21, 4568 (2009).
- [34]. David O. Scanlon, Graeme W. Watson, "Understanding the p-type defect chemistry of CuCrO_2 .", *J. Mater. Chem.* 21, 3655 (2011).
- [35]. David O. Scanlon, Graeme W. Watson, "Conductivity limits in CuAlO_2 from screened-hybrid density functional theory.", *J. Phys. Chem. Lett.* 1, 3195 (2010).
- [36]. J. Vidal, F. Trani, F. Bruneval, M.A. Marques, S. Botti, "Effects of electronic and lattice polarization on the band structure of delafossite transparent conductive oxides.", *Phys. Rev. Lett.* 104, 136401 (2010).
- [37]. F. Trani, J. Vidal, S. Botti, M.A. Marques, "Erratum: Band structures of delafossite transparent conductive oxides from a self-consistent GW approach [*Phys. Rev. B* 82, 085115 (2010)].", *Phys. Rev. B* 82, 085115 (2010) 83, 039901(E) (2011).

- [38]. T.F. Cerqueira, S. Lin, M. Amsler, S. Goedecker, S. Botti, M.A. Marques, "Identification of novel Cu, Ag, and Au ternary oxides from global structural prediction.", *Chem. Mater.* 27, 4562 (2015).
- [39]. F. Trani, J. Vidal, S. Botti, M.A. Marques, "Band structures of delafossite transparent conductive oxides from a self-consistent G W approach.", *Phys. Rev. B* 82, 085115 (2010).
- [40]. T. Kimura, T. Goto, H. shintani, H. Ishzaka, T. Amira, Y. Tokura, *Nature (London)* 426, 55 (2003).
- [41]. N.A. Spaldin, M. Fiebig, "The renaissance of magnetoelectric multiferroics.", *Science* 309, 391 (2005).
- [42]. H.N. Abdelhamid, *Mater.* "Delafossite nanoparticle as new functional materials: advances in energy, nanomedicine and environmental applications.", *Sci. Forum* 832, 28 (2015).
- [43]. H.N. Abdelhamid, S. Kumaran, H.F. Wu, "One-pot synthesis of CuFeO₂ nanoparticles capped with glycerol and proteomic analysis of their nanocytotoxicity against fungi.", *RSC Adv.* 6, 97629 (2016).
- [44]. H. Jiang, X. Wang, X. Zang, W.f. Wu, S. Sun, C. Xiong, W. Yin, C. Gui, X. Zhu, "Electronic properties of bivalent cations (Be, Mg and Ca) substitution for Al in delafossite CuAlO₂ semiconductor by first-principles calculations.", *J. Alloys Compd.* 553, 245 (2013).
- [45]. H. Hiraga, T. Makino, T. Fukuura, H.M. Weng, M. Kawasaki, "Electronic structure of the delafossite-type Cu M O₂ (M= Sc, Cr, Mn, Fe, and Co): Optical absorption measurements and first-principles calculations.", *Phys. Rev. B* 84, 041411 (2011).
- [46]. J.L. Ribeiro, J.M. Perez-Mato, L.G. Vieira, "Landau model for the multiferroic delafossite antiferromagnets.", *J. Magn. & Magn. Mater.* 416, 15 (2016).
- [47]. M.N. Huda, Y. Yan, A. Walsh, S.-H. Wei, M.M. Al-Jassim, "Group-IIIA versus IIIB delafossites: Electronic structure study.", *Phys. Rev. B* 80, 035205 (2009).
- [48]. R.D. Shannon, D.B. Rogers, C.T. Prewitt, "Chemistry of noble metal oxides. I. Syntheses and properties of ABO₂ delafossite compounds.", *Inorg. Chem.* 10, 713 (1971).
- [49]. R.A. Wheatley, S. Rojas, C. Oppolzer, T. Joshi, P. Borisov, D. Lederman, A.L. Cabrera, *Thin Solid Films* 626, 110 (2017).
- [50]. W. Soller, A.J. Thompson, "The crystal structure of cuprous ferrite.", *Phys. Rev.* 47, 644 (1935).

- [51]. M.A. Sarabia, S.D. Rojas, Z. L'opez-Cabaña, R. Villalba, G. Gonz'alez, A.L. Cabrera, "Carbon dioxide adsorption studies on delafossite CuFeO₂ hydrothermally synthesized.", *J. Phys. Chem. Solids* 98, 271 (2016).
- [52]. L. Shi, Z. Jin, B. Chen, N. Xia, H. Zuo, Y. Wang, Z. Ouyang, Z. Xia, "Unusual doping effect of non-magnetic ion on magnetic properties of CuFe_{1-x}Ga_xO₂.", *J. Magn. & Magn. Mater.* 372, 7 (2014).
- [53]. D. Song, X.M. Wang, Z.Y. Zhao, J.C. Wu, J.Y. Zhao, X.G. Liu, X. Zhao, X.F. Sun, *Phys. Rev. B* 95, 224419 (2017).
- [54]. J.W. Lekse, M.K. Underwood, J.P. Lewis, C. Matrangola, "Synthesis, Characterization, Electronic Structure, and Photocatalytic Behavior of CuGaO₂ and CuGa_{1-x}Fe_xO₂ (x= 0.05, 0.10, 0.15, 0.20) Delafossites.", *J. Phys. Chem. C* 116, 1865 (2012).
- [55]. J. Gu, A. Wuttig, J.W. Krizan, Y. Hu, Z.M. Detweiler, R.J. Cava, A.B. Bocarsly, *J. Phys. Chem. C* 117, 12415 (2013).
- [56]. O. Aktas, K.D. Truong, T. Otani, G. Balakrishnan, M.J. Clouter, T. Kimura, G. Quirion, *J. Phys.: Condens. Matter* 24, 036003 (2012).
- [57]. H.J. Xiang, E.J. Kan, Su-Huai Wei, M.-H. Whangbo, X.G. Gong, "Predicting the spin-lattice order of frustrated systems from first principles.", *Phys. Rev. B* 84, 224429 (2011).
- [58]. A.P. Ramirez, "Geometrical frustration.", *Handb. Magn. Mater.* 13, 423 (2001).
- [59]. T. Kimura, J.C. Lashley, A.P. Ramirez, "Inversion-symmetry breaking in the noncollinear magnetic phase of the triangular-lattice antiferromagnet Cu Fe O₂." *Phys. Rev. B* 73, 220401 (2006).
- [60]. M. Mekata, N. Yaguchi, T. Takagi, S. Mitsuda, H. Yoshizawa, "Magnetic ordering in delafossite CuFeO₂.", *J. Magn. & Magn. Mater.* 104–107, 823 (1992).
- [61]. S. Mitsuda, H. Yoshizawa, N. Yaguchi, M. Mekata, "Neutron diffraction study of CuFeO₂.", *J. Phys. Soc. Jpn.* 60, 1885 (1991).
- [62]. S. Mitsuda, M. Mase, K. Prokes, H. Kitazawa, H. Katori, "Field-induced magnetic phase transitions in a triangular lattice antiferromagnet CuFeO₂ up to 14.5 T.", *J. Phys. Soc. Jpn.* 69, 3513 (2000).
- [63]. R.D. Shannon, D.B. Rogers, D. Burl, C.T. Prewitt, J.L. Gillson, "Chemistry of noble metal oxides. III. Electrical transport properties and crystal chemistry of ABO₂ compounds with the delafossite structure.", *Inorg. Chem.* 10, 723 (1971).
- [64]. S.Seki, "Magnetoelectric response in triangular lattice antiferromagnets, in *Magnetoelectric Response in Low-Dimensional Frustrated Spin Systems* (Springer, Tokyo, 2012) pp. 25–83.

- [65]. T. Takagi, M. Mekata, "New partially disordered phases with commensurate spin density wave in frustrated triangular lattice.", *J. Phys. Soc. Jpn.* 64, 4609 (1995).
- [66]. Cristiana Di Valentin, Silvana Botti, Matteo Cococcioni (Editors), *First Principles Approaches to Spectroscopic Properties of Complex Materials*, Vol. 347 (Springer, 2014).
- [67]. R.M. Dreizler, E.K. Gross, *Density Functional Theory: An Approach to the Quantum Many-body Problem* (Springer Science & Business Media, 2012).
- [68]. R. Car, F. de Angelis, P. Giannozzi, N. Marzari, First-principles molecular dynamics, in *Handbook of Materials Modelling*, edited by S. Yip (Springer, Dordrecht, 2005).
- [69]. T.F. Cerqueira, R. Sarmiento-Pérez, F. Trani, M. Amsler, S. Goedecker, M.A. Marques, S. Botti, *MRS Commun.* 3, 157 (2013).
- [70]. J. Shi, T.F. Cerqueira, W. Cui, F. Nogueira, S. Botti, M.A. Marques, "High-throughput search of ternary chalcogenides for p-type transparent electrodes.", *Sci. Rep.* 7, 43179 (2017).
- [71]. A.P. Amrute, Z. Lodziana, C. Mondelli, F. Krumeich, J. Perez-Ramirez, *Chem. Mater.* 25, 4423 (2013). "Solid-state chemistry of cuprous delafossites: Synthesis and stability aspects."
- [72]. K. Lejaeghere, G. Bihlmayer, T. Bjorkman, P. Blaha et al., "Reproducibility in density functional theory calculations of solids.", *Science* 351, 1415 (2016).
- [75]. Stancil, Daniel D. "Propagation characteristics and excitation of magnetostatic waves." *Theory of Magnetostatic Waves*. Springer, New York, NY, 1993. 119-153. R.Thompson, *environmental Magnetism*, springer 2012.
- [76]. J.M.D. coey, *Magnetism and magnetic Materials*, Caambridge university press, 2010
- [77]. K. H. J. Buschow et F. R. de Boer, *Physics of Magnetism and Magnetic Materials*, New York : Kluwer Academic/Plenum Publishers, 2003.
- [78]. C. G. Shull and J. S. Smart, "Detection of antiferromagnetism by neutron diffraction.", *Phys. Rev.*, 76 (1949), 1256.
- [79]. J. B. Goodenough, "Theory of the role of covalence in the perovskite-type manganites [La, M (II)] Mn O 3.", *Phys.Rev.*, 100 (1955) 564.
- [80]. J. Kanamori, "Superexchange interaction and symmetry properties of electron orbitals.", *Journal of Physics and Chemistry of Solids*, 10 (1959) 87.
- [81]. Anderson, Philip W. "New approach to the theory of superexchange interactions." *Physical Review* 115.1 (1959): 2.C.Zener, *Phys.Rev.*, 81(1951)440.108
- [82]. C.Zener, "Interaction between the d-shells in the transition metals. II. Ferromagnetic compounds of manganese with perovskite structure.", *Phys.Rev.*, 82(1951)403.

- [83]. M. A. Ruderman and C. Kittel, "Indirect exchange coupling of nuclear magnetic moments by conduction electrons." *Physical Review* 96.1 (1954): 99. *Phys. Rev.*, 96 (1954) 99.
- [84]. T. Kasuya, , *Prog. Theo. Phys.*, 16 (1956) 45. Kasuya, Tadao. "A theory of metallic ferro-and antiferromagnetism on Zener's model." *Progress of theoretical physics* 16.1 (1956): 45-57.
- [85]. Yosida, Kei. "Magnetic properties of Cu-Mn alloys." *Physical Review* 106.5 (1957): 893.
- [86]. D. Born and J. Oppenheimer, *J.R. Ann.* "On the quantum theory of molecules.", *Phys. Rev.* 84, 457 (1927).
- [87]. Lascaux and R. Theodor. *Analyse numérique matricielle appliquée à l'art de l'ingénieur*. Masson, Tome 2, 2eme ed., Paris, (1987).
- [88]. Hartree, D. R. "the waves mechanics of an atom with non-coulombic central field: parts I, II, III." *Proc. Cambridge Phil. Soc.* Vol. 24. No. 89. 1928.
- [89]. Hohenberg, Pierre, and Walter Kohn. "Inhomogeneous electron gas." *Physical review* 136.3B (1964): B864. P. Hohenberg and W. Kohn, *Phys. Rev.* 136, B864 (1964).
- [90]. Hohenberg, P., and W. Kohn. "Phys Rev 136: B864." Kohn W, Sham LJ (1965) *Phys Rev* 140 (1964): A1133.
- [91]. E. Fermi, *Rend.* "The exchange-correlation energy of a metallic surface.", *Accad. Naz. Lincei* 6: 602, (1927).
- [92]. Ceperley, David M., and Berni J. Alder. "Ground state of the electron gas by a stochastic method." *Physical Review Letters* 45.7 (1980): 566. J.C. Slater, *Phys.rev.* 81 (1951) 385
- [93]. Perdew, John P., and Yue Wang. "Accurate and simple analytic representation of the electron-gas correlation energy." *Physical review B* 45.23 (1992): 13244.
- [94]. Brush, Stephen G. "History of the Lenz-Ising model." *Reviews of modern physics* 39.4 (1967): 883. Onsager, L., 1944. Crystal statistics. I. A two-dimensional model with an order-disorder transition. *Physical Review*, 65(3-4), p.117.
- [95]. Kragh, Helge. "Equation with the many fathers. The Klein–Gordon equation in 1926." *American Journal of Physics* 52.11 (1984): 1024-1033.
- [96]. Wu, Fa-Yueh. "The potts model." *Reviews of modern physics* 54.1 (1982): 235.
- [97]. M. Blume, V. J. Emery, and Robert B. Griffiths. Ising model for the λ transition and phase separation in He3-He4 mixtures. *Phys. Rev. A*, 4:1071–1077, Sep 1971.
- [98]. Harrison, Walter A. *Solid state theory*. Courier Corporation, 1970

- [99]. Djaidja, Fawzia. Calcul de premier principe des propriétés électroniques de CdSe et CdTe sous pression. Diss. Université Mohamed BOUDIAF de M'Sila, 2014.
- [100]. P. Blaha, K. Schwarz, G.K.H. Madsen, D. Kvasnicka, J. Luitz, R. Laskowski, F. Tran, L.D. Marks, Wien2k, An Augmented-Plane-Wave+Local Orbitals Program for Calculating Crystal Properties (TechnWien, Universitat, Wien, Austria, 2001).
- [101]. P. Blaha, K. Schwarz, G.K.H. Madsen, D. Kvasnicka J. Luitz, « WIEN2k-userguide », Vienna University of Technology (2001).
- [102]. Korringa, J. "On the calculation of the energy of a Bloch wave in a metal." *Physica* 13.6-7 (1947): 392-400.
- [103]. W. Kohn and N. Rostoker, *Phys. Rev.* 94, 1111 (1954) A. Lodder and P.J. Braspenning, *Phys. Rev. B* 49, 10215 (1994).
- [104]. O.K. Andersen, "Linear methods in band theory.", *Phys. Rev. B* 12, 3060 (1975).
- [105]. N. Metropolis, A.W. Rosenbluth, M.N. Rosenbluth, A.H. Teller, E. Teller, "Equation of state calculations by fast computing machines.", *J. Chem. Phys.* 21 (1953) 1087.
- [106]. C.A. Mercado, N. De La Espriella, L.C. Sánchez. Ground state phase diagrams for the mixed Ising 2 and 5/2 spin model.", *J. Magn. Magn. Mater.* 382 (2015) 288.
- [107]. N. De La Espriella, G.M. Buendía, J "Ground state phase diagrams for the mixed Ising 3/2 and 5/2 spin model.", *Phys. A* 389 (2010) 2725.
- [108]. J.D. Alzate-Cardona, D. Sabogal-Suárez, E. Restrepo-Parra. *J. Magn. Magn. Mater.* 429 (2017) 34.
- [109]. Y. Nakamura. "Existence of a compensation temperature of a mixed spin-2 and spin-5 2 Ising ferrimagnetic system on a layered honeycomb lattice.", *Phys. Rev. B* 62 (2000) 11742.
- [110]. A. Hu, A. Zhang. "The magnetic properties of a mixed spin-1/2 and spin-1 Heisenberg ferrimagnetic system on a two-dimensional square lattice.", *J. Magn. Magn.Mater.*399 (2016) 22.
- [111]. A. Dakhama and N. Benayad, "On the existence of compensation temperature in 2d mixed-spin Ising ferrimagnets: an exactly solvable model.", *J. Magn. Magn.Mater.*213 (2000) 117.
- [112]. G. M. Buendía, M. A. Novotny, "Numerical study of a mixed Ising ferrimagnetic system.", *J. Phys.: Condens. Matter* 9 (1997) 5951.
- [113]. W.Selke, J. Oitmaa, "Monte Carlo study of mixed-spin $S=(1/2, 1)$ Ising ferrimagnets.", *J Phys.: Condens. Matter.*22 (2010) 076004.

- [114]. Bahlagui, T., Bouda, H., El Kenz, A., Bahmad, L., Benyoussef, A.: Superl. Microstruct. 110, 90 (2017),
- [115]. Karimou, M., Yessoufou, R.A., Guedje, F.K., Ainamon, C., Hontinfinde, F.: Phase Transit. 90(3), 268–288 (2017)
- [116]. Karimou, M., Yessoufou, R.A., Oke, T.D., Kpadonou, A., Hontinfinde, F.: arXiv preprint arXiv:1609.04687 (2016)
- [117]. Wang, W., Lv, D., Zhang, F., Bi, J., Chen, J. "Monte Carlo simulation of magnetic properties of a mixed spin-2 and spin-5/2 ferrimagnetic Ising system in a longitudinal magnetic field.", J. Magn. Magn. Mater. 385, 16–26 (2015)
- [118]. Bahlagui, T., Bouda, H., El Kenz, A., Bahmad, L., Benyoussef, A.: Superl. Microstruct. 110, 90 (2017),
- [119]. Yin, J., Li, C., Chen, D., Yang, J., Liu, H., Hu, W., Shao, Y.: Phys.Chem. Chem. Phys. 19, 5366–5376 (2017)
- [120]. Kaneyoshi, T., Jascur, M.: "Compensation temperatures of ferrimagnetic bilayer systems.", J. Magn. Magn. Mater. 118, 17 (1993)
- [121]. Kaneyoshi, T "Tricritical behavior of a mixed spin-1/2 and spin-2 Ising system.", Physica A 205, 67 (1994)
- [122]. Buenedia, G.M., Liendo, J.A.: "Monte Carlo simulation of a mixed spin 2 and spin Ising ferrimagnetic system.", Condens. Matter 9, 5439 (1997)
- [123]. DAKHAMA, A. Exact solution of a decorated ferrimagnetic Ising model. Physica A: Statistical Mechanics and its Applications, 1998, vol. 252, no 1-2, p. 225-237.
- [124]. Deviren, B., Batı, M., Keskin, M.: The effective-field study of a mixed spin-1 and spin-5/2 Ising ferrimagnetic system. Phys. Scr. 79, 065006 (2009)
- [125]. Jabar, A., Masrou, R., Benyoussef, A., Hamedoun, M.: Monte Carlo study of alternate mixed spin-5/2 and spin-2 Ising ferrimagnetic system on the Bethe lattice. J. Magn. Magn. Mater. 397, 287–294 (2016),
- [126]. Masrou, R., Jabar, A., Benyoussef, A., Hamedoun, M., Bahmad, L.: Hysteresis and compensation behaviours of mixed spin-2 and spin-1 hexagonal Ising nanowire core-shell structure. Phys. B. 472, 19–24 (2015)
- [127]. Mohamad, H.K.: "Magnetic and thermodynamic properties of a mixed spin-1 and spin-7/2 Blume-Capel Ising ferrimagnetic system.", Int. J. Adv. Res. 2, 442 (2014),
- [128]. Lv, D., Wang, F., Liu, R., Xue, Q., Li, S.: Monte Carlo study of magnetic and thermodynamic properties of a ferrimagnetic mixed spin (1, 3/2) Ising nanowire with hexagonal core-shell structure. J. Alloys Compd. 701, 935–949 (2017)

- [129]. Wang, W., Liu, R., Lv, D., Luo, X.: Monte Carlo simulation of magnetic properties of a nano-graphene bilayer in a longitudinal magnetic field. *Superlattice. Microst.* 98, 458–472 (2016)
- [130]. Masrour, R., Jabar, A., Bahmad, L., Hamedoun, M., Benyoussef, A.: Magnetic properties of mixed integer and half-integer spins in a Blume–Capel model: A Monte Carlo study. *J. Magn. Magn. Mater.* 421, 76–81 (2017) 136-140
- [131]. Kantar, E., Keskin, M.: Thermal and magnetic properties of ternary mixed Ising nanoparticles with core–shell structure: Effective-field theory approach. *J. Magn. Magn. Mater.* 349, 165–172 (2014)
- [132]. Keskin, M., Kantar, E., Canko, O.: Kinetics of a mixed spin-1 and spin-3/2 Ising system under a time-dependent oscillating magnetic field. *Phys. Rev. E.* 77(5), 051130 (2008)
- [133]. Lv, D., Wang, F., Liu, R., Xue, Q., Li, S.: Monte Carlo study of magnetic and thermodynamic properties of a ferrimagnetic mixed spin (1, 3/2) Ising nanowire with hexagonal core-shell structure. *J. Alloys Compd.* 701, 935–949 (2017)
- [134]. Kantar, E., Deviren, B., Keskin, M.: Magnetic properties of mixed Ising nanoparticles with core-shell structure. *Eur. Phys. J. B.* 86, 253 (2013)
- [135]. Masrour, R., Jabar, A., Benyoussef, A., Hamedoun, M.: Mixed spin-5/2 and spin-2 Ising ferrimagnetic system on the Bethe lattice. *J. Magn. Magn. Mater.* 393, 151–156 (2015)
- [136]. Arejidal, M., Kadiri, M., Abbassi, A., Slassi, A., Raiss, A.A., Bahmad, L., Benyoussef, A.: Magnetic properties of the double perovskite Ba₂CoUO₆: ab initio method, mean field approximation, and Monte Carlo study. *J. Supercond. Nov. Magn.* 29, 2659–2667 (2016)
- [137]. Şarlı, N., Akbudak, S., Ellialtıođlu, M.: The peak effect (PE) region of the antiferromagnetic two layer Ising nanographene. *Phys. B.* 452, 18–22 (2014).
- [138]. Peng, Z., Wang, W., Lv, D., Liu, R.J., Li, Q.: Magnetic properties of a cubic nanoisland in the longitudinal magnetic field: A Monte Carlo study. *Superlattice. Microst.* 109, 675–686 (2017),
- [139]. Dendrimer-magnetic nanoparticles as multiple stimuli responsive and enzymatic drug delivery vehicle. *J. Magn. Magn. Mater.* 380, 7–12 (2015) ,
- [140]. Wang, W., Bi, J., Liu, R., Chen, X., Liu, "Effects of the single-ion anisotropy on magnetic and thermodynamic properties of a ferrimagnetic mixed-spin (1, 3/2) cylindrical Ising nanowire.", *J. Superlattice. Microst.* 98, 433 (2016)

- [141]. Jiang, W., Lo, V., Bai, B., Yang, J.: Magnetic hysteresis loops in molecular-based magnetic materials $\text{AFeIIIFeIII}(\text{C}_2\text{O}_4)_3$. *Phys. A.* 389, 2227–2233 (2010)
- [142]. Bobák, A., Jaščur, M.: Ferrimagnetism in diluted mixed Ising spin systems. *Phys. Rev. B.* 51, 11533–11537 (1995).
- [143]. S. Mitsuda, M. Mase, K. Prokes, H. Kitazawa, H. Katori, "Field-induced magnetic phase transitions in a triangular lattice antiferromagnet CuFeO_2 up to 14.5 T.", *J. Phys. Soc. Jpn.* 69, 3513 (2000).
- [144]. R.D. Shannon, D.B. Rogers, D. Burl, C.T. Prewitt, J.L. Gillson, "Chemistry of noble metal oxides. III. Electrical transport properties and crystal chemistry of ABO_2 compounds with the delafossite structure.", *Inorg. Chem.* 10, 723 (1971).
- [145]. Seki, Shinichiro. "Magnetoelectric response in triangular lattice antiferromagnets." *Magnetoelectric Response in Low-Dimensional Frustrated Spin Systems*. Springer, Tokyo, 2012. 25-83. *Frustrated Spin Systems* (Springer, Tokyo, 2012) pp. 25–83.
- [146]. T. Takagi, M. Mekata, "Proc. 2nd. Int. Conf. Solid Surfaces Proc. 2nd. Int. Conf. Solid Surfaces 145, 1974.", *J. Phys. Soc. Jpn.* 64, 4609 (1995).
- [147]. Cristiana Di Valentin, Silvana Botti, Matteo Cococcioni (Editors), *First Principles Approaches to Spectroscopic Properties of Complex Materials*, Vol. 347 (Springer, 2014).
- [148]. R.M. Dreizler, E.K. Gross, *Density Functional Theory: An Approach to the Quantum Many-body Problem* (Springer Science & Business Media, 2012).
- [149]. R. Car, F. de Angelis, P. Giannozzi, N. Marzari, *First-principles molecular dynamics*, in *Handbook of Materials Modeling*, edited by S. Yip (Springer, Dordrecht, 2005).
- [150]. T.F. Cerqueira, R. Sarmiento-Pérez, F. Trani, M. Amsler, S. Goedecker, M.A. Marques, S. Botti, *MRS Commun.* 3, 157 (2013).
- [151]. M.A. Marquardt, N.A. Ashmore, D.P. Cann, "Crystal chemistry and electrical properties of the delafossite structure.", *Thin Solid Films* 496, 146 (2006).
- [152]. A. Kokalj, *J. Mol. Graph. Model.* 17, 176 (1999) code available from <http://www.xcrysden.org/>.
- [153]. J.P. Perdew, K. Burke, M. Ernzerhof, "Perdew, burke, and ernzerhof reply.", *Phys. Rev. Lett.* 77, 3865 (1996).
- [154]. V.I. Anisimov, O. Gunnarsson, "Density-functional calculation of effective Coulomb interactions in metals.", *Phys. Rev. B* 43, 7570 (1991).
- [155]. G.K.H. Madsen, P. Novak, "Charge order in magnetite. An LDA+ U study." *Europhys. Lett.* 69, 777 (2005).

- [156]. K. Schwarz, P. Mohn, "Itinerant metamagnetism in YCO₂." J. Phys. F 14, L129 (1984).
- [157]. F.A. Benko, F.P. Koffyberg, "Opto-electronic properties of p-and n-type delafossite, CuFeO₂.", J. Phys. Chem. Solids 48, 431 (1987).
- [158]. C.T. Crespo, Solar Energy, "Potentiality of CuFeO₂-delafossite as a solar energy converter.", 163, pp, 162-166 (2018).
- [159]. C.G. Read, Y. Park, K.-S. Choi, "Electrochemical synthesis of p-type CuFeO₂ electrodes for use in a photoelectrochemical cell.", J. Phys. Chem. Lett. 3, 1872 (2012).
- [160]. Yuemei Zhang, Erjun Kan, Myung-Hwan Whangbo, "Density Functional Investigation of the Difference in the Magnetic Structures of the Layered Triangular Antiferromagnets CuFeO₂ and AgCrO₂.", Chem. Mater. 23, 4181 (2011).
- [161]. F. Ye, J.A. Fernandez-Baca, R.S. Fishman, Y. Ren, H.J. Kang, Y. Qiu, T. Kimura, "Magnetic interactions in the geometrically frustrated triangular lattice antiferromagnet CuFeO₂.", Phys. Rev. Lett. 99, 157201 (2007).
- [162]. G. Kresse, J. Hafner, "Ab initio molecular dynamics for liquid metals.", Phys. Rev. B 47, 558(R) (1993),
- [163]. G. Kresse, J. Hafner, "Efficiency of ab-initio total energy calculations for metals and semiconductors using a plane-wave basis set.", Phys. Rev. B 49, 14251 (1994).
- [164]. Bahlagui, T., Bouda, H., El Kenz, A., Bahmad, L., Benyoussef, A. (2017). Monte Carlo simulation of compensation behaviours for a mixed spin-5/2 and spin-7/2 Ising system with crystal field interaction. Superlattices and Microstructures, 110, 90-97.
- [165]. P. Mohn, Clas Persson, P. Blaha, K. Schwarz, P. Novák, H. Eschrig, "Correlation induced paramagnetic ground state in FeAl.", Phys. Rev. Lett. 87, 196401 (2001).